ISTANBUL TECHNICAL UNIVERSITY ★ GRADUATE SCHOOL OF SCIENCE ENGINEERING AND TECHNOLOGY

AN INVESTIGATION OF HEAT TRANSFER PERFORMANCE OF RECTANGULAR CHANNEL BY USING VORTEX GENERATORS

M.Sc. THESIS

Seyfi GİRGİN

Department of Aeronautical and Astronautical Engineering

Aeronautical and Astronautical Engineering Programme

DECEMBER 2017

ISTANBUL TECHNICAL UNIVERSITY ★ GRADUATE SCHOOL OF SCIENCE ENGINEERING AND TECHNOLOGY

AN INVESTIGATION OF HEAT TRANSFER PERFORMANCE OF RECTANGULAR CHANNEL BY USING VORTEX GENERATORS

M.Sc. THESIS

Seyfi GİRGİN
511131138

Department of Aeronautical and Astronautical Engineering

Aeronautical and Astronautical Engineering Programme

Thesis Advisor: Assist. Prof. Dr. Bayram ÇELİK

DECEMBER 2017

ISTANBUL TEKNİK ÜNİVERSİTESİ ★ FEN BİLİMLERİ ENSTİTÜSÜ

GİRDAP ÜRETİCİLERİ KULLANARAK DİKDÖRTGEN KANALIN ISI TRANSFER PERFORMANSININ İNCELENMESİ

YÜKSEK LİSANS TEZİ

Seyfi GİRGİN
511131138

Uçak ve Uzay Mühendisliği Anabilim Dalı

Uçak ve Uzay Mühendisliği Programı

Tez Danışmanı: Yrd. Doç. Dr. Bayram ÇELİK

ARALIK 2017

Seyfi Girgin, a **M.Sc** student of İTU Graduate School of Science Engineering and Technology student ID **511131138**, successfully defended the **thesis** entitled "**AN INVESTIGATION OF HEAT TRANSFER PERFORMANCE OF RECTANGULAR CHANNEL BY USING VORTEX GENERATORS**", which he prepared after fulfilling the requirements specified in the associated legislations, before the jury whose signatures are below.

Thesis Advisor : **Assist. Prof. Dr. Bayram ÇELİK**
İstanbul Technical University

Jury Members : **Prof. Dr. Cihat BAYTAŞ**
İstanbul Technical University

Assist. Prof. Dr. Murat BARIŞIK
İzmir Institute of Technology

Date of Submission : 17 November 2017
Date of Defense : 19 December 2017

To my family..

FOREWORD

Firstly, I wish to express my appreciation to my advisor Assist. Prof. Dr. Bayram Çelik for his valuable and inspring support. He always kept my motivation high although having worked in Ankara. I also would like to thank Assist. Prof. Dr. Murat Barışık for contributing my thesis.

My beloved friends Tanju Ergen, İsmail Çağatay Koyuncuoğlu, and my honorable colleague Mehmet Umut Haliloğlu many many thank you for your great assists and advices, you made my life easier.

I also wish to thank my friends Orkun Ovayurt, Evren Tuna, Alinda Öykü Akar, Coşkun Yıldız, Arda Küçüksarı, Gürkan Sarıkaya for being with me in this hard times. I alwasy felt your help.

Finally, I would like to thank my family for their endless support.

December 2017

Seyfi GİRGİN
Mechanical Engineer

TABLE OF CONTENTS

Page

ABBREVIATIONS

BR	: Blockage Ratio
CFD	: Common Flow Down
CFU	: Common Flow Up
COP	: Coefficient of Performance
CPCS	: Cabin Pressure Control System
CRVG	: Curve Rectangular Vortex Generator
DWP	: Delta Winglet Pair
ECS	: Environmental Control System
FVM	: Finite Volume Method
LV	: Longitudinal Vortex
LVG	: Longitudinal Vortex Generator
QF	: Quality Factor
RWP	: Rectangular Winglet Pair
PFHE	: Plate Fin Heat Exchanger
PR	: Pitch Ratio
SIMPLE	: Semi Implicit Method for Pressure Linked Equation
SST	: Shear Stress Transport
TEF	: Thermal Enhancement Factor
TV	: Transverse Vortex
TVG	: Transverse Vortex Generator
VCCS	: Vapor Cycle Cooling System
VG	: Vortex Generator

SYMBOLS

°C	: celcius degree
A_c	: flow cross section area, [m^2]
ft	: feet
m	: meter
kW	: kilowatt
f	: friction factor
j	: colburn factor
D_h	: hydraulic diameter
L	: length of channel, [m]
α	: angle of attack of vortex generators
ρ	: density of air, [kg/m^3]
$\dot{m}$	: mass flow rate of air, [kg/s]
h	: average heat transfer coefficient, [W/m^2K]
k	: thermal conductivity of air, [W/mK]
Nu	: Nusselt number, [hD/k]
A	: heat transfer area of channel,[m^2]
T	: temperature, [K]
Re	: Reynolds number
Pr	: Prandtl number
St	: Stanton number
u_m	: mean velocity, [m/s]
μ	: dynamic viscosity of air, [kg/ms]
υ	: kinematic viscosity of air, [m^2/s]
T_w	: wall temperature, [K]
T_b	: **b**ulk temperature, [K]
C_p	: specific heat capacity of air, [J/kgK]
ΔP	: pressure drop, [Pa]
Γ	: vorticity
Q	: heat transfer rate
W_w	: wing width, [m]
W_h	: wing height, [m]
p	: pressure, [Pa]
l_p	: longitudinal pitch, [m]

LIST OF TABLES

Page

LIST OF FIGURES

Page

AN INVESTIGATION OF HEAT TRANSFER PERFORMANCE OF RECTANGULAR CHANNEL BY USING VORTEX GENERATORS

SUMMARY

The need of high performance of thermal systems in many engineering applications has increased. The convectional heat exchangers are generally improved by surface augmentation. There are two enhancement techniques of convective heat transfer for compact heat exchangers. One is to extend heat transfer surface area like a fin, the other is to increase heat transfer coefficient between solid surface and fluid such as using turbulators as vortex generators. Solution to this problem in this study is to increase the intensity of secondary flow and reduce the size of wake regions in rectangular channel so as to increase heat transfer coefficient to gain size and effectiveness.

In this study a new type of vortex generator pairs which are called common-flow-up (CFU) and common-flow-down (CFD) and their various configurations in terms of number of pairs and attack angle was reported. Rectangular winglet pairs (RWP) of vortex generator has been selected.

One rectangular channel of an air to air plate-fin cross flow compact heat exchanger has been analyzed. Before calculation process, detailed literature survey has been done about aviation application of heat transfer enhancement of plate-fin heat exchanger. Geometrical dimensions has been originated from F-16 heat exchanger and similar cross section area has been drawn. Solution approach to problem has been selected from validated benchmark problem. Boundary conditions have been applied according to TAI specification of ECS model. Model was prepared and meshed in Pointwise and computational fluid dynamics analysis was performed in ANSYS Fluent 16.

In rectangular channel, three configurations have been analyzed; CFD, CFU, and mix type (both CFD and CFU) with the number of 2 and 3 pairs by applying four different attack angle (15°, 30°, 45°, and 60°). The height of the vortex generator which is also called blockage ratio (BR) was half of the channel height.

3D computational fluid dynamics results showed that 3 pairs of CFD configuration of 30° and 45° winglet angle of attack provides the best heat transfer enhancement in the channel. At the same configuration 60° attack angle of pairs give the best thermal enhancement factor at Re = 4000. Overall results demonstrated that wings angle of attack play an important role in determining heat transfer performance.

VORTEX JENERATÖRÜ KULLANILARAK DİKDÖRTGEN KANALIN ISI TRANSFER PERFORMANSININ İNCELENMESİ

ÖZET

Gelişen teknoloji ile birlikte yüksek performans sağlayan termal sistemlere ihtiyaç artmaktadır. Bu yüzden ısı değiştiriciye ihtiyaç duyulan birçok alanda yüzey alanı diğerlerine göre çok fazla olan kompakt ısı değiştiriciler kullanılıyor. Yüzey alanının artması ısı transfer alanının artmasını, bu da ısı transfer katsayısını arttırıp daha verimli bir ısı değiştirici performansı ortaya çıkmasını sağlıyor.

Kompakt ısı değiştiricilerde ısı transfer performansını arttırmak için genelde iki yoldan biri tercih ediliyor. Birincisi akışkanın temas ettiği yüzey alanine kanatçık kullanarak arttırmak, diğeri ise girdap jeneratörü kullanarak katı yüzey ile akışkan arasındaki ısı transfer katsayısını arttırmak. Bu çalışmadaki probleme yaklaşım, ikincil akışın yoğunluğunu arttırarak, kanal içinde ısı transfer katsayısını arttırmaktır.

CFU-CFD gibi yeni kullanılmaya başlanıp termal performansının çok iyi olduğu gözlemlendiği girdap jeneratörlerinin analizi bu çalışmada yapılmıştır. Çift sayısı ve hücum açısı şekillenmesi ile toplamda 32 farklı durum ortaya çıkmıştır. 2li ve 3lü çiftlerin yanında 15°, 30°, 45° ve 60° hücum açıları ile beraber CFU ve CFD girdap üreticilerinin ısı transfer ve basınç kayıpları gözlemlenmiştir.Girdap jeneratörü olarak da dikdörtgen yapı seçilmiştir.

Dikdörtgen kanal içinde sadece açılar değişmek koşuluyla 8 farklı durum orataya çıkmıştır. Anlatımı kolaylaştırmak için her bir duruma numara verilerek ayrı ayrı incelenmesi yapılmıştır. İnceleme kriterleri ısı artım faktörü, basınç düşüşü ve vortisitedeki değişimdir. Hesaplanan değerler literatürdeki örnekleriyle karşılaştırılmış ve doğrulanmıştır.

1. durumda 2 CFD girdap üretici çiftinden oluşan kanal incelenmiştir. Yapılan analiz sonuçlarına göre ısı transfer katsayısındaki artışın en fazla olduğu açı %42.29 artış oranı ile 30°, en optimum Reynolds sayısının da 1552 olduğu görülmüştür. Bu konfigürasyonda ortalama ısı transfer katsayısı artışı ise 33.91% olarak gözlenlenmiştir. Öte yandan basınç düşüşünün 15° lik girdap üreticili durumda en fazla olduğu gözlemlenmiştir. Maximum basınç kaybı oranı %115.24 ile Reynolds'un 1552 olduğu durumda meydana gelmiştir.

2.durumda CFD-CFU konfigürasyonu ele alınmıştır.1. durumdaki gibi maximum ısı transfer katsayısındaki artış Reynolds'un 1552 olduğu durumda görülmüştür.Fakat ısı transfer artışındaki oranın en fazla olduğu açı 15° olarak hesaplanmıştır. Bu durumdaki ortalama ısı transfer artış oranı %30.08 olarak gözlemlenmiştir. Basınçtaki düşüşün en fazla olduğu açı 15°, Reynolds da 1552 iken bulunmuştur.Basınç kaybındaki oran baz duruma göre %123.79 artmıştır.

3.durumda CFU-CFD konfigürasyonu test edilmiştir. Isı transfer katsayısındaki en fazla artış bu sefer Reynolds'un 776, girdap üreticisinin 15°lik açıda olduğu durumda meydana gelmiştir. Bu durumdaki artış %51.91dir. Ortalama ısı transfer katsayısı artışı ise %32.37 olarak hesaplanmıştır. Basınç kaybındaki oranın ise %118.78 mertebelerine çıktığı görülmüştür. Vortisite değerinin baz duruma göre 2.6 kat arttığı görülmüştür.

4.durumda 2 CFU girdap üretici çiftinden oluşan konfigürasyonun değerlendirilmesi yapılmıştır. Ortalama ısı transfer katsayısındaki artışın %34.95 olduğu görülmüştür. Aynı durumda basınç kaybındaki oranın ise %133.83'e kadar çıktığı görülmüştür. Vortisite değerindeki artışın en az olduğu konfigürasyon 4. durum olarak hesaplanmıştır. Vortisitedeki artış baz duruma göre 2.16 kat daha fazladır.

5.durumda 3 çift CFD girdap üreticisinden meydana gelen durum değerlendirilmiştir. Isı transfer katsayısındaki en fazla artışın %92.23 ile 30°lik konfigürasyonda ve Reynolds'un 1552 olduğu durumda gözlemlenmiştir. Ortalama ısı transfer katsayısının %50.62ye çıktığı görülmüştür. Basınç kaybındaki oran da 2 çiftli duruma göre daha daha fazla artmıştır. Bu beklenen bir durumdur çünkü; akışın engellendiği girdap üreticisi sayısı artmıştır. Maximum artış girdap üretici açısının 15°, Reynolds'un 1552 olduğu durumda meydana gelmiştir. Bu durumdaki basınç kaybı değeri baz duruma göre %147.14 artmıştır. Fakat vortisite performansının en fazla olduğu konfigürasyon olarak da görülmüştür. Vortisite değeri baz duruma göre 2.72 kat artmıştır. Artışın en fazla olduğu durum 30°lik açıda ve Reynolds 1552 iken meydana gelmiştir.

6. durumda CFD-CFU-CFD konfigürasyonu ele alınmıştır. Isı transfer katsayısındaki artışın en fazla olduğu durum 15°lik açıda Reynolds 1552 iken %60.24 ile görülmüştür. Isı transfer katsayısındaki ortalama artış ise %39.30 olarak hesaplanmıştır. Maximum basınç kaybı ise %156.48 mertebesine ulaşmıştır. Beklendiği gibi 15°lik açıda kayıp en fazla olmuştur. Vortisitedeki artış 2.6 kat olarak görülmüştür.

7.durumda CFU-CFD-CFU konfigürasyonunun analizi yapılmıştır. Isı transfer katsayısındaki artışın en fazla olduğu durum 15°lik açıda Reynolds 1552 iken %67.15 olarak ölçülmüştür. Ortalama artış ise %42.20 olarak hesaplanmıştır. Basınç kaybındaki artış ise %174 seviyelerine yükselmiştir. Vortisitedeki artış baz duruma göre 2.6 kat daha fazladır.

8.durumda 3 çift CFU konfigürasyonu incelenmiştir. Isı transfer katsayısındaki maximum artışın %81.65 ile 30°lik konfigürasyonda oluştuğu saptanmıştır. Bu durumda ısı transfer katsayısındaki ortalama artış %47.77 olarak hesaplanmıştır. Basınç kaybındaki oran ise bu durumda maximum seviyeye ulaşmıştır. Basınç kaybındaki artış baz duruma göre %200 seviyelerine kadar çıkmıştır. Vortisitedeki artış ise baz duruma göre 2.64 kat daha fazladır.

Isı artım faktörü, basınç kaybı ve vortisitedeki artış tek tek ele alınarak en büyük değerden en küçüğe aşağıdaki gibi sıralanabilir:

Tablo 1. Isı artım faktörü

Case IV > Case I > Case III > Case V > Case II > Case VII > Case VI > Case VIII

Tablo 2. Basınç kaybı

Case VIII > Case V > Case VII > Case VI > Case II > Case IV > Case I > Case III

Tablo 3. Vortisite

Case V > Case VIII > Case VII > Case VI > Case III > Case I > Case II > Case IV

8 akış konfigürasyonu, 4 girdap üretici açısı ve 5 farklı Reynolds sayısı ölçümleri ile toplamda 160 durum Pointwise 17'de çözüm ağına kavuşup, ANSYS Fluent 16'da koşturulmuştur. 160 koşu ile birlikte hesaplanan Nu ve f faktör değerleri için objektif fonksiyonlar belirlenmiştir. Koşu sonucu bulunan nümerik değerler ile objektif fonksiyon sonucu çıkan değerler birbirleriyle karşılaştırılmıştır. Yapılan hata analizi sonuçlarına göre Nu için ortalama hata oranı %9.71, f faktör içinse %10.89 bulunmuştur. Hesaplamalarla ilgili ayrıntılı tablo Appendix A ve B'de verilmiştir.

Analiz sonuçlarına göre girdap üreticilerinin ısı transfer katsayısında önemli bir rol oynadığı görülmüştür.2li ve 3lü girdap üretici çiftler karşılaştırıldığında, beklendiği gibi 3lü çiftlerin ısı transfer oranını daha fazla arttırdığı görülmüştür. Fakat basınç düşüşündeki artış da bu çiftlerde daha fazladır. Isı transfer katsayısındaki en fazla artış Reynolds'un 1500 mertebelerinde seyrettiği durumda oluşurken, basınç kaybındaki artış da aynı Reynolds seviyesinde gerçekleştiği için bu seviyede etkili bir ısı artırım faktörü elde edilememiştir. Isı artırım faktörünün en iyi olduğu durum ise Reynols'un 4000 mertebesinde, basınç kaybının en düşük olduğu konfigürasyonlarda ortaya çıktığı görülmüştür. 4.durumda 60° lik girdap üreticili konfigürasyon ısı artım faktörü için en iyi tasarımken, 8.durum 15°lik girdap üreticili konfigürasyon ise en kötü tasarımdır. Vortisitenin maximum olduğu Reynolds'ta ve girdap üreticili açıda ısı transfer katsayısının da maximum olduğu görülmüştür. Buradan vortisite ile ısı transfer katsayısı arasında doğrudan bir bağlantı olduğu sonucuna varılmıştır.

1. INTRODUCTION

This introduction chapter aims from general to specific; the needs for aircraft cooling systems, usage of heat exchangers, their applications in aerospace industry, air to air cross flow plate-fin heat exchaners and modifications with vortex generators to enhance heat transfer coefficient and to become more compact so that to gain weight and efficiency.

The main objective of the present study is to determine the effects of the vortex generator arrangements on the flow structure and the overall heat transfer augmentation for a rectangular channel of a plate – fin heat exchanger.

1.1 Motivation of Study

Avionic heat loads are increasing with the new generation of aircraft and this influences the entire ECS design. Because ECS has a significant impact on aircraft performance such as fuel consumption, mission profile, and stealth characteristics. Overall aircraft weight, location of ram inlet and use of ram air, engine bleed air flow rate and other aircraft power source that effects the performance of the system such as radar, avionics cooling has a major impression on ECS configuration. Therefore, heat loads must be determined and accurate cooling system (liquid, vapor, air) has to be chosen in accordance with the aircraft requirements and also a compact heat exchanger that will provide very effective cooling for the ECS must be selected.

Different approaches has been considered for the avionic bay and avionic equipment cooling that effects the avionic equipment design, performance, reliablity and maintainability. These approaches are; use of direct ram air, ECS cooling with compact heat exchanger, liquid cooling (PAO, fuel). Those can be provided by naturel free convection, forced convection, air to air or air to liquid heat exchangers. Major ECS performance has been spent on the heat dissipated by avionic equipment especially radar. For representative comparison, Table 4 shows the range of cabin and avionic heat loads for military aircrafts.

Table 4. Cabin and avionic heat loads of various fighters[1]

Aircraft Type	Initial Operational Year	Cabin Heat Load (kW)	Avionic Heat Load (kW)
Bombers			
B-58	1958	12.9	35.5
B-52H	1961	16.6	18.5
B-52H (Upgrade)	1980	12.2	118.2
B-1B	1985	52.1	170.9
Cargo			
KC-135A	1957	22.7	10.1
C-5A	1968	69.0	21.6
C-17	1991	44.4	14.4
Fighter			
F-105D	1959	6.4	8.9
F-111A	1966	10.8	14.1
F-14A	1970	14.1	25.6
F-15A/D	1973	3.0	26.2
F-15E	1986	4.8	46.3
F-16	1975	5.4	15.9
F/A-18A	1980	7.3	18.8
F/A-18E		7.3	28

The subject of heat transfer is of serious interest in heat exchanger applications. The process industries call for more and more compact designs of heat exchanger. Flow interruption created in flow at periodic intervals is a popular means for heat transfer enhancement in compact heat exchangers. One relevant application using such flow configurations is the heat transfer between the flowing fluid and plates in the case of plate-fin heat exchangers[2]. Since global energy consumption is starting to impact negatively on the environment, as well as causing depletion of the existing fuel stocks, energy utilization has come under close scrutiny. Energy, cost and environmental considerations continue to motivate attempts to derive better performance over the existing designs[3].

Heat transfer enhancement by vortex generator is one passive method to generate streamwise vortices that create high turbulence in fluid flow over heat transfer surfaces. It was founded that the only effective way to increase the heat transfer coefficient is to to decrease the thermal resistance of sublayer adjacent to the wall immediately where the viscous effects of the sublayer are dominant. This can be done by increasing the turbulence of the fluid flow in the main stream so that the turbulent eddies can penetrate deeper into this layer. The thermal resistance can be reduced and the heat transfer can be augmented by using vortex generator that can be punched or attached to the internal surface of the channel wall. The vortex generator can be regarded as a special kind of extended surface, which can be stamped on or punched out from the fin. Vortex generator not only disturbs the flow field, disrupt the growth of the boundary layer, but also makes fluid swirling and causes a heavy exchange of core and wall fluid, leading to the enhancement of heat transfer between the flowing fluid and the channel walls.

Vortex induced heat transfer enhancement is a passive augmentation method that relies on the intentional generation of secondary, streamwise vortices to enhance heat transfer. The method may be utilized in many liquid-to-air and refrigerant-to-air heat exchanger applications. Streamwise vortices can be introduced using small flow manipulators. Vortex generator is used with the flat-plate compact heat exchangers to improve their thermal performance[4].

In the development of recent industrial world, the reduction in the heat exchanger volume and augmentation in their performance for heat transfer had a great interest of many researchers. In addition, there are always economical factors need to be considered to reduce the costs of heat transfer process. The need for high performance thermal systems due to increase in the pressure drop associated with the augmentation in heat transfer becomes necessary[5].

Motivation of this thesis is to enhance heat transfer coefficient of a compact heat exchanger by using new type of vortex generators which is called common-flow-up and common-flow-down.

2. LITERATURE SURVEY

Heat exchangers are widely used in many industrial areas such as chemical engineering, radiators of cars, locomotive powered by internal combustion engine, geothermal, fossil, process plant, power system, air-conditioning, refrigeration, internally cooled gas turbine blades, air-cooled solar collectors, electronic chip cooling, wastewater aeration tanks, chemical mixers, nuclear reactor cores, aerospace, and other engineering applications. An efficient heat exchanger in such system could result in the lesser consumption of the energy resource, which provides both economical and environmental benefits. Increasing demands are being placed on heat exchanger performance for reasons of compactness, economy in manufacturing and operating costs, energy conservation and even for ecological reasons. The importance of these issues continues to motivate the study of enhancement techniques[6].

2.1 Compact Heat Exchangers

Generally, a compact heat exchanger is defined as its surface area density greater than about 700 m^2/m^3. If surface area density is above 10,000 m^2/m^3, it is called as microheat exchanger. In heat exchangers, in order to increase heat transfer rate per unit volume, heat transfer surface area is increased by using fins and there are couple of configurations and different designs to do it[7].

With the higher rate of heat transfer, compact heat exchangers become popular in industry like aerospace and automotive especially gas-to-gas and liquid-to-gas ones. They are also used in cryogenic process, electronics and other industries. For example; condensers, evaporators, aircraft coolers, automotive radiators, oil coolers, intercoolers of compressors.

Currently there are many engineering approaches available in order to enhance heat transfer performance of the compact heat exchangers in both gas-gas and gas-liquid side. Concentration of surface augmentation is one method to improve heat transfer enhancement seen in the traditional heat exchangers. Higher performance of a heat exchanger specifications require smaller size, light weight, low cost and better heat transfer rate. With the vortex generators, the augmentation of heat transfer rate can be done by increasing turbulence intensity, and generating secondary flows.

One of the earliest and comprehensive works on compact heat exchangers was carried out by Kays and London at Stanford University in late 1940. They studied experimentally and published report in 1948 about methodology in non dimensional heat transfer coefficient and friction factor. Based on this report many empirical correlations were done[8].

Plate-fin heat exchangers are one of the main categories of compact heat exchangers. They are designed to pack a high heat transfer capacity into a small volume. Heat transfer is mainly function of surface area; therefore high performance can be obtained with a small size heat exchanger by increasing surface area per unit volume[9].

2.2 Plate-Fin Heat Exchangers

Plate-fin heat exchanger is a type of compact heat exchanger where the heat transfer surface area is enhanced by providing extended metal surface. Two fluids are interfaced by fins. Out of the various compact heat exchangers, plate fin heat exchangers are unique due to their superior construction and performance[10].They are characterized by high effectiveness, compactness, low weight, and moderate cost. As the name suggests, a plate fin heat exchanger (PFHE) is a type of compact heat exchanger that consists of a stack of alternate flat plates[11].

Early development of plate-fin compact heat exchangers were stimulated by their applications in the automobile and aircraft industries. Development of compact heat exchangers in the automobile and air conditioning industries has been reviewed by Mori et al.[12] and Cowell et al.[13].

2.3 Vortex Generators

The need of high performance of thermal systems in many engineering applications has stimulated enormous interesting to find various methods to improve heat transfer rate in the system. The convectional heat exchangers are generally improved by various augmentation techniques which focus on many types of surface augmentation.

There are two enhancement technologies of convective heat transfer for compact heat exchangers. One is to extend heat transfer surface area like a fin, the other is to increase heat transfer coefficients between solid surface and fluid such as using turbulators as vortex generators. In cooling channel and channel heat exchanger design, rib, fin, wing turbulators are often employed in order to increase the convective heat transfer rate. The use of wing turbulators completely results in the change of the flow field and hence the variation of the local convective heat transfer coefficient. Winglets have been successfully used for enhancement of heat transfer of modern thermal systems because they can generate longitudinal vortices and help to disrupt the main flow with less penalty of pressure loss[14].

The generated vortices may be classified as transverse vortex (TV) and longitudinal vortex (LV) according to its rotation axis direction. The axis of TVs lie perpendicular to the main flow direction, while LVs have their axes parallel to the main flow direction, thus they are also called streamwise vortices. In general, the LVs have been reported to be more effective than TVs for heat transfer enhancement[15]. A transverse vortices TV and longitudinal vortices LV are generated as a mainstream flows across the vortex generator.(VG) The axis of the longitudinal vortices is parallel to the main flow direction whereas the axis of the transverse vortices is normal to the flow direction. Generally, the effect of longitudinal vortices is more effective than transverse vortices on heat transfer performance[16].

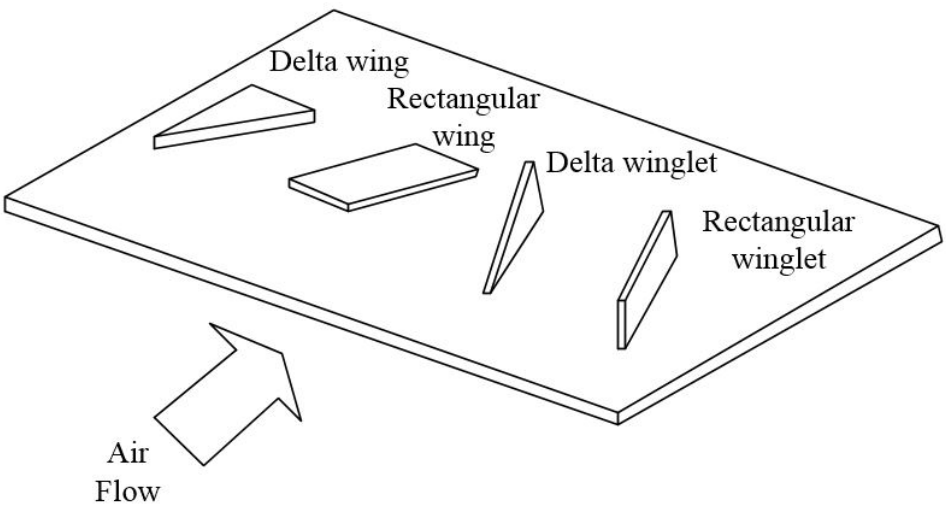

Figure 1. Common types of vortex generators[6]

Figure 1 shows the common types of vortex generators. They are delta wing, rectangular wing, delta winglet and rectangular winglet vortex generators.

Henze and Wolfersdorf examined the effects of longitudinal vortices induced by tetrahedral vortex generator. They highlighted that the tallest vortex generator shows the highest heat transfer enhancement. The convection heat transfer coefficient increases as Reynolds number increase while the heat transfer enhancement related to the smooth channel flow is decreasing. They found that the effect of turbulence is less remarked for regions which are affected by vortices[17].

The enhancement of heat transfer by using vortex generators depends on many parameters such as their shape, geometries, position from leading edge of the test duct, and angles of attack. The geometrical parameters of vortex generators have more effects on the heat transport. Four basic configurations of vortex generators are; delta wing, rectangular wing, delta-winglet and rectangular winglet[18].

Wu and Tao [19] and He et al. [20] used punched rectangular and triangular VGs to study the effects of the positions, surface area over the heat transfer augmentation. Due to the positioning of the winglets, the in-line tube arrangement was having better heat transfer in comparison to the staggered arrangement.

The vortex generators usually take configurations of tiny protrusions which may be incorporated into the main surface of the channel by punching, stamping, attaching, mounting and embossing. Although the heat transfer surface area may be not changed before and after the set up of vortex generator, the fluid flow can be significantly disturbed because of the longitudinal vortices generated by vortex generator. Winglets have been successfully used in order to improve the convective heat transfer rate of modern thermal systems because they can generate intensive longitudinal vortices with less penalties in pressure drop.

Yonggang Lei[21] investigates that delta-winglet vortex generators play an important role on the flow structure and temperature distribution in circular tube. According to study, the delta winglet vortex generators significantly improve the thermal hydraulic performance of circular tube with modest pressure drop penalty. The Nusselt number increases with the increase of the attack angle and the increase tendency decrease with the increase of attack angle. Also, compared with the smooth tube, the Nusselt number for the circular tube with delta-winglet vortex generators at 15°, 30°, 45°, and 60° are increased by 32.3-85.3%, 43.9-96.0%, 53.1-108.4%, and 60.2-117.2%, and the corresponding pressure drop are increased by 43-156%, 102-264%, 186-374%, and 251-466%.

It is well known that in turbulent flow, although the main flow region is in turbulent state, the viscous sublayer is near a laminar state, which is called laminar sublayer. The heat transfer modes outside laminar sublayer are conduction and convection. However the heat transfer mode inside viscous sublayer is usually dominated by conduction. As a result, the thermal resistance is mainly occupied in the viscous sublayer.

Wrobleski and Eibeck showed that the longitudinal vortices imbedded into turbulent boundary layers enhanced the heat transfer[22]. Fiebig had studied the influences of different types of vortex generators on heat transfer performance; such as delta wing, rectangular winglet, and delta winglet[23]. Fiebig also used a vortex-induced device in finned-tube banks and found that the heat transfer coefficient increased by 55-65% for in-line tube arrangement and 9% for staggered arrangement. The corresponding pressure drop was increased by 20-45% and 3%, respectively[24]. Kwak also studied the heat transfer and pressure loss penalty of staggered finned-tube bundles with delta winglet pairs set in the front of the tube bundle at a low Reynolds number (350 – 2100), and better performance was observed[25].

Xiaoze Du found that the location of the longitudinal vortex generators on fin surface has a great impact on the heat transfer performance. It is also found that the delta winglet pairs located in the middle of the fin surface is more effective than located ahead and rear of the fin surface for the heat transfer augmentation[26].

Bao Gong investigated the curve rectangular vortex generators (CRVG) in terms of circumferential and radial position and base length. He reported that height of the VGs play an important role in determining heat transfer characteristics. For the studied cases, the height of the VGs is about 0.8 times of fin spacing can obtain better heat transfer performance. Gong also studied the effect of fn spacing and found that when Re ranges from 800 to 3000 and the ratio of the fin spacing to tube outside diameter is 0.239, a better heat transfer performance can be obtained[27].

Jin-Sheng Leu analyzed the fluid flow and heat transfer over 3-row plate fin and tube heat exchangers with and without a pair of inclined block shape vortex generators.

Results shows that 45° attack angle of VG arrangement provides the best relative heat transfer enhancement with 8-30% increase of Colburn factor across the Re range, while the Fanning friction factor is only increased by 11 – 15%.This arrangement also gives the greatest area reduction ratio up to 25%. Furthermore, the heat transfer enhancement by using inclined block vortex generator is more useful for low and moderate Reynolds number[28].

It was shown experimentally by Jacobi and Shah [29] and Tiggelbeck et al [30] that the longitudinal vortices generated by surface-mounted delta-wings and winglet pairs are very effective for heat transfer enhancement.

Over the years, researchers had shown that VGs are capable to increase heat transfer for both fin-tube and plate-fin heat exchangers. In case of plate-fin heat exchangers, protrusions can be mounted on the channel surfaces to enhance heat transfer between flowing fluid and parallel plate ducts[31-33]. The two most commonly and developing type VGs are common flow down (CFD) and common flow up (CFU).

In this thesis study, rectangular vortex generator with common flow up and common flow down configurations were examined. During the investigation, different attack angles were applied with various Reynolds numbers. The number of pairs of the vortex generators were choosen as 2 and 3.

2.4 Common Flow Up and Common Flow Down Type Vortex Generators

Common flow up means the VGs on the working fluid side are placed in such a way that the resulting vortices move the fluid between them away from the surface on which they are located. Common flow down means the flow stream between the two vortices is directed toward the surface on which they are located[34].

Figure 2(a) shows the schematic diagram of common flow down configuration. Figure 2(b) represents the common flow up configuration. In the figure, α represents the attack angle of vortex generators.

The earlier investigations reported in the literature [35-37] reveal that in a CFD arrangement, the VGs are placed as a pair downstream of the tube in the near-wake region. This provides high-momentum fluid behind the tube and remove the zone of poor heat transfer from the wake region. In CFU approach[38-40] the VGs are usually located slightly upstream contiguous to the tube such that the winglet forms a narrow passage with the tube. This leads the fluid to accelerate in the near-tube region. The reason for this arrangement is to cause separation delay and narrow the wake. The heat transfer enhancement due to vortex generation is usually accompanied by additional pressure loss related to the form drag associated with VG. Joardar and Jacobi [41] studied the performance of leading edge delta-wings in a flat tube, louvered-fin compact heat exchanger. They reported an average heat transfer (j-factor) increase over the baseline configuration of 21%, with a pressure drop penalty smaller than 7%. Biswas and Chattopadhyay [33] analyzed the the flow structure and heat transfer in a fin tube heat exchanger with delta winglet pairs. The two rows were arranged in a staggered design and a punched-out delta winglet pair with an aspect ratio of 2 was located behind each tube at an attack angle of 45. At a Reynolds number of 500, heat transfer enhancement occurs about 240% reported at a location about 12 times the channel height downstream of the inlet.

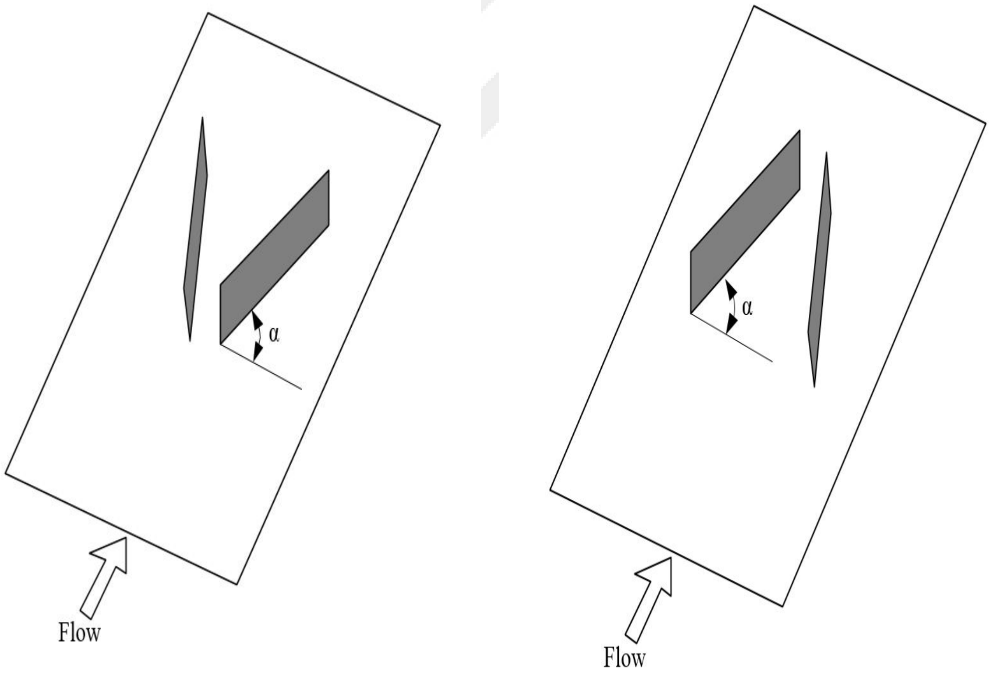

(a) (b)

Figure 2.(a) Common Flow Down, (b) Common Flow Up

Sinha et al. [42] studied the effects of different combinations of CFD and CFU orientations of winglet arrays on the performance of plate-fin type heat exchanger. Tian et al.[43] compared the performances of plate-fin type heat exchangers with both delta winglet pairs (DWP) and rectangular winglet pairs (RWP) for Re up to 1200 and it was shown that RWP performs better than DWP when only the heat transfer enhancement considered. Similar studies by Saha [34] with very low Re, demonstrated that compared to DWP, RWP produces higher heat transfer enhancement and the difference increases with increase in Reynolds number. However, the RWP develops slightly higher pressure drop than DWP.

Pankaj Saha and Gautam Biswas has studied two types of winglet geometry, rectangular winglet pair (RWP) and delta winglet pair (DWP), along with two types of configurations of CFD and CFU. Namely four different cases have been investigated. The cases are RWP-CFD, RWP-CFU, DWP-CFD, and DWP-CFU. The angle of attack is set at 45°. They found that compared to DWP, RWP produces more heat transfer enhancement and the difference increases with increasing Reynolds number. The CFD configurations provide better heat transfer enhancement compared to CFU configurations. However, pressure loss penalty is as high as 1.7-3.8 times the baseline case. The RWP develops slightly higher pressure drop than DWP. The performance analysis shows that RWP performs better than the DWP and that the CFD configurations are more beneficial[34].

Pongjet Promvonge examined airflow friction and heat transfer characteristics in a square duct inserted diagonally with a 30° finned tape at different fin blockage and pitch ratios for the turbulent flow. Reynolds number varies from 4000 to 23000 and it was found that at BR=0.3 and PR=1 causes a much higher pressure drop increase, f/f_0=67-109 but also provides a considerable heat transfer augmentation in the duct, Nu/Nu_0=5.9-6.3. The study shows that the Nusselt number of the finned tape insert has an increasing trend with the rise in BR and Re values. In addition, the 30° finned tape insert of BR=0.2 and PR=1 yields the highest thermal enhancement factor of about 1.8 at lower Reynolds number[44].

Amnart Boonloi[45] investigated turbulent forced convection, heat transfer and thermal performance in the heat exchanger square channel with wavy ribs inserted diagonally. Influences of BR=0.05-0.25, attack angle of 30° and 45° for Reynolds number 3000-20000 investigated and found that the enhancement of the Nusselt number is around 1.97 – 5.14 and 2.04 – 5.27 times over the smooth square channel for 30° and 45°, respectively. According to the study, the 45° wavy ribs give higher heat transfer rate than the 30° wavy ribs, while the 30° wavy ribs can help to save friction loss in the channel.

3. GOVERNING EQUATIONS AND PARAMETERS

In this chapter, basic heat transfer equations will be outlined for the thermal analysis of a rectangular channel.

3.1 Parameters

One of the present objectives is to use a common treatment of basic heat transfer and flow – friction data for all the surfaces considered.

Reynolds number is based on a hydraulic diameter defined as

$$\frac{D_h}{L} = 4\frac{A_c}{A} \tag{3.1}$$

where L is the flow length of the heat exchanger, A_c is the flow cross – section area, and A is the total heat transfer area.

The Nusselt number, Nu is one of the dimensionless representations of the heat transfer coefficient. Nu is a ratio of the convective conductance to pure thermal conductance over the hydraulic diameter. It is defined as

$$Nu = \frac{hD_h}{k} \tag{3.2}$$

Here k is the thermal conductivity of the fluid.

The Reynolds number, Re is interpreted as a flow characteristic proportional to the ratio of flow momentum rate to viscous force for a specified geometry. Re is also called as flow modulus and defined for internal flow as

$$\mathrm{Re} = \frac{\rho u_m D_h}{\mu} \tag{3.3}$$

where, μ_m is the mean fluid velocity, and μ is the viscosity of the fluid. For internal flows, if Re < 2300 then the flow is laminar.

Friction factor is defined as

$$f = \frac{2\Delta P}{\rho u^2} \frac{D_h}{L_d} \tag{3.4}$$

Where ρ is the fluid density, u is the mean velocity of the minimum transverse area, D_h is the hydraulic diameter, L_d is the channel length, and ΔP is the pressure drop of inlet and outlet of the heat exchanger.

Colburn factor is defined as

$$j = \frac{h}{\rho u C_p} \mathrm{Pr}^{2/3} \tag{3.5}$$

where C_p is the specific heat of working fluid, Pr is the Prandtl number, h is the convective heat transfer coefficient.

The Stanton number, St is the ratio of convection heat transfer to the enthalpy rate change of the fluid reaching the wall temperature. St does not depend on any geometrical characteristic dimesion. It is defined as

$$St = \frac{h}{\rho u_m C_p} \tag{3.6}$$

The Prandtl number, Pr is the fluid property modulus representing the ratio of momentum diffusivity to thermal diffusivity of the fluid. Pr is expressed as

$$\mathrm{Pr} = \frac{\upsilon}{\alpha} = \frac{\mu C_p}{k} \tag{3.7}$$

$$h = \frac{Q_{conv}}{A_t (T_{w-T_b}) LMTD} \tag{3.8}$$

where Q_{conv} is the convective heat transfer rate which the fluid flowing through the channel absorbs from the hot surfaces. The absorbed heat by the fluid can be expressed as follows,

$$Q_{conv} = mC_p(T_{b,out} - T_{b,in}) \tag{3.9}$$

where, m is the mass flow rate, and $T_{b,in}$ and $T_{b,out}$ are the average temperature of fluid at the inlet and outlet of the channel, respectively. A_t the total heat transfer area, and $(T_w\text{-}T_b)_{LMTD}$ is the log mean temperature difference, as follows,

$$(T_w - T_b)_{LMTD} = \frac{\Delta T_{w-b,in} - \Delta T_{w-b,out}}{\log(\Delta T_{w-b,in} / \Delta T_{w-b,out})} \tag{3.10}$$

where, $\Delta T_{w\text{-}b,in}$ and $\Delta T_{w\text{-}b,out}$ denote the differences between the wall temperature and the bulk fluid temperature at the inlet and outlet of heat transfer section.

The ΔP is the pressure difference between inlet and outlet as

$$\Delta P = P_{av,in} - P_{av,out} \tag{3.11}$$

where, subscripts '$_{av,in}$' and '$_{av,out}$' refer to the average pressure values at the inlet and outlet cross sections.

3.2 Governing Equations

The following assumptions were made:

- Newtonian fluids in single phase and incompressible,
- Continuous, steady state,
- Negligible viscous dissipation, radiation, and natural convection,

Under the above assumptions, the governing equations for the mathematical model were as follows.

- Conservation of mass for fluid

$$\frac{\partial}{\partial x_i}(\rho u_i)=0 \tag{3.12}$$

- Conservation of momentum for fluid

$$\frac{\partial}{\partial x_i}(\rho u_i u_k)=\frac{\partial}{\partial x_i}\left(\mu\frac{\partial u_k}{\partial x_i}\right)-\frac{\partial P}{\partial x_k} \tag{3.13}$$

- Conservation of energy for fluid

$$\frac{\partial}{\partial x_i}(\rho u_i T)=\frac{\partial}{\partial x_i}\left(\frac{k}{C_p}\frac{\partial T}{\partial x_i}\right) \tag{3.14}$$

- Transport Equations for the SST k-ω Model

$$\frac{\partial}{\partial t}(\rho k)+\frac{\partial}{\partial x_i}(\rho k u_i)=\frac{\partial}{\partial x_j}\left(\Gamma_k\frac{\partial k}{\partial x_j}\right)+G_k-Y_k \tag{3.15}$$

and

$$\frac{\partial}{\partial t}(\rho\omega)+\frac{\partial}{\partial x_i}(\rho\omega u_i)=\frac{\partial}{\partial x_j}\left(\Gamma_\omega\frac{\partial \omega}{\partial x_j}\right)+G_\omega-Y_\omega+D_\omega \tag{3.16}$$

In these equations, G_k represents the generation of turbulent kinetic energy due to mean velocity gradients,

$$G_k=-\rho\overline{u_i u_j}\frac{\partial u_j}{\partial x_i} \tag{3.17}$$

G_ω represents the generation of ω,

$$G_\omega = \alpha \frac{\omega}{k} G_k \tag{3.18}$$

The coefficient α is given by

$$\alpha = \frac{\alpha_\infty}{\alpha^*}\left(\frac{\alpha_0 + \mathrm{Re}_t / \mathrm{Re}_\omega}{1 + \mathrm{Re}_t / \mathrm{Re}_\omega}\right) \tag{3.19}$$

where $R_\omega = 2.95$.

$$\alpha_\infty = F_1 \alpha_{\infty,1} + (1 - F_1)\alpha_{\infty,2} \tag{3.20}$$

where

$$\alpha_{\infty,1} = \frac{\beta_{i,1}}{\beta_\infty^*} - \frac{\kappa^2}{\sigma_{\omega,1}\sqrt{\beta_\infty^*}} \tag{3.21}$$

$$\alpha_{\infty,2} = \frac{\beta_{i,2}}{\beta_\infty^*} - \frac{\kappa^2}{\sigma_{\omega,2}\sqrt{\beta_\infty^*}} \tag{3.22}$$

where κ is 0.41. $\beta_{i,1}$ and $\beta_{i,2}$ are 0.075 and 0.0828 respectively.

$$\alpha^* = \alpha_\infty^* \left(\frac{\alpha_0^* + \mathrm{Re}_t / R_k}{1 + \mathrm{Re}_t / R_k}\right) \tag{3.23}$$

where

$$\mathrm{Re}_t = \frac{\rho k}{\mu \omega} \tag{3.24}$$

$R_k = 6$

$$\alpha_0^* = \frac{\beta_i}{3} \tag{3.25}$$

β_i = 0.072

Γ_k and Γ_ω represent the effective diffusivity of k and ω, respectively.

$$\Gamma_k = \mu + \frac{\mu_t}{\sigma_k} \quad (3.26)$$

$$\Gamma_\omega = \mu + \frac{\mu_t}{\sigma_\omega} \quad (3.27)$$

Where σ_k and σ_ω are the turbulent Prandtl numbers for k and ω, respectively. The turbulent viscosity, μ_t, is computed as follows:

$$\mu_t = \frac{\rho k}{\omega} \frac{1}{\max\left[\frac{1}{\alpha^*}, \frac{\Omega F_2}{\alpha_1 \omega}\right]} \quad (3.28)$$

where

$$\Omega = \sqrt{2\Omega_{ij}\Omega_{ij}} \quad (3.29)$$

$$\sigma_k = \frac{1}{F_1/\sigma_{k,1} + (1-F_1)/\sigma_{k,2}} \quad (3.30)$$

$$\sigma_\omega = \frac{1}{F_1/\sigma_{\omega,1} + (1-F_1)/\sigma_{\omega,2}} \quad (3.31)$$

Ω_{ij} is the mean rate of rotation tensor. The blending functions, F_1 and F_2, are given by

$$F_1 = \tanh\left(\Phi_1^4\right) \tag{3.32}$$

$$\Phi_1 = \min\left[\max\left(\frac{\sqrt{k}}{0.09\omega y}, \frac{500\mu}{\rho y^2 \omega}\right), \frac{4\rho k}{\sigma_{\omega,2} D_\omega^+ y^2}\right] \tag{3.33}$$

$$D_\omega^+ = \max\left[2\rho \frac{1}{\sigma_{\omega,2}} \frac{1}{\omega} \frac{\partial k}{\partial x_j} \frac{\partial \omega}{\partial x_j}, 10^{-20}\right] \tag{3.34}$$

$$F_2 = \tanh\left(\Phi_2^2\right) \tag{3.35}$$

$$\Phi_2 = \max\left[2\frac{\sqrt{k}}{0.09\omega y}, \frac{500\mu}{\rho y^2 \omega}\right] \tag{3.36}$$

Where y is the distance to the next surface and D^+_ω is the positive portion of the cross-diffusion term.

The term Y_k represents the dissipation of turbulence kinetic energy.

$$Y_k = \rho \beta^* k \omega \tag{3.37}$$

The term Y_ω represent the dissipation of ω.

$$Y_{\omega} = \rho \beta \omega^{2} \tag{3.38}$$

The cross diffusion term D_{ω} is defined as,

$$D_{\omega} = 2(1 - F_{1}) \rho \sigma_{\omega,2} \frac{1}{\omega} \frac{\partial k}{\partial x_{j}} \frac{\partial \omega}{\partial x_{j}} \tag{3.39}$$

Model Constants:

$\sigma_{k,1} = 1.176$, $\sigma_{\omega,1} = 2.0$, $\sigma_{k,2} = 1.0$, $\sigma_{\omega,2} = 1.168$, $\alpha_{1} = 0.3$

4. COMPUTATIONAL DETAILS

In this chapter; dimensions of the channel and the vortex generator pairs and the boundary conditions of the studied cases are represented.

Schematic diagram of the problem is shown in Figure 3. In the figure channel with vortex generator pairs is shown. The vortex generator pairs are placed in the middle section of the channel. In order to get rid of outlet effect and provide fully developed flow, upstream and downstream regions are extended. Channel length, height and widht are 150, 5, 5 mm respectively. The distance between the vortex generators represented as t_p and 1 mm. l_p shows the distance between the pairs and is equal to 10 mm. Length of the vortex generators, l_v is 1.5 mm. Blockage ratio is defined as the ratio of vortex generator height over channel height. This ratio is 0.5 for all cases. Wings attack angle, α is 15°, 30°, 45° and 60°. Corresponding transverse distances, d, are 0.55 mm, 0.70 mm, 0.94 mm and 1.25 mm. These dimensions are constant for all cases as shown in Table 5. The vortex generator flow configurations; CFD and CFU and the number of vortex generator pairs are variable for all cases. Combining vortex generator configuraitons and the number of pairs, studied cases are described in section 5.4.

Boundary Conditions:

At the inlet boundary (1-2-3-4)

$$u_x = u_z = 0 \tag{4.1}$$

$$u_y = u_{in} = const \tag{4.2}$$

$$T = T_{in} = const \tag{4.3}$$

In the middle region at upper and lower boundaries (1-2-7-8 and 3-4-5-6)

$$u_x = u_y = u_z = 0 \tag{4.4}$$

$$T = T_{wall} = const \tag{4.5}$$

In the middle region at the left and right boundaries (2-3-6-7 and 1-4-5-8)

$$T = T_{wall} = const \tag{4.6}$$

$$\frac{\partial u_y}{\partial x} = \frac{\partial u_z}{\partial x} = 0 \tag{4.7}$$

$$\frac{\partial T}{\partial x} = 0 \tag{4.8}$$

At the outlet boundary (5-6-7-8)

$$\frac{\partial u_x}{\partial y} = \frac{\partial u_y}{\partial y} = \frac{\partial u_z}{\partial y} = 0 \tag{4.9}$$

$$\frac{\partial T}{\partial y} = 0 \tag{4.10}$$

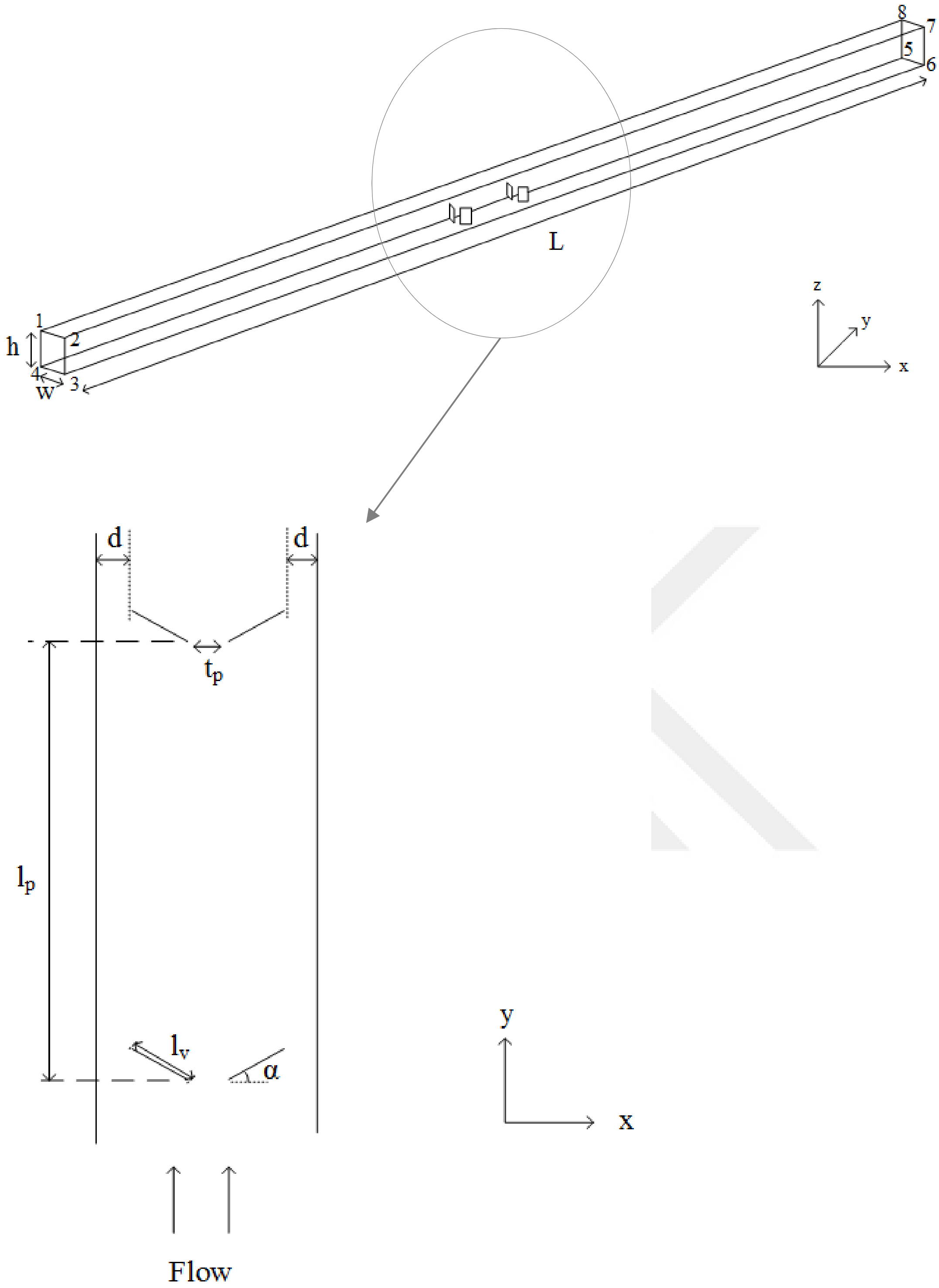

Figure 3. Schematic diagram of the problem

Table 5. Dimensions for all cases

Parameter	Symbol	Value
Wings attack angle	α [°]	15, 30, 45, 60
Transverse distance	d [mm]	0.55, 0.70, 0.94, 1.25
Channel length	L [mm]	150
Channel height	h [mm]	5
Channel width	w [mm]	5
Vortex generator length	l_v [mm]	1.5
Longitudinal wing pitch	l_p [mm]	10
Transverse wing pitch	t_p [mm]	1
Number of VG pairs	n	2, 3

4.1 Numerical Method

Pointwise 17 was used in order to create the computational domain and commercial CFD program ANSYS Fluent 16 was used to solve the governing equations in conjunction with the boundary conditions. A multi-block structural mesh was used to control the mesh quality and density as shown in Figure 4. In order to control the number of mesh volumes, graded mesh was used in the direction normal to the walls as shown in Figure 5(a), (b) and (c).

The governing equations were discretized by the finite volume method (FVM). The standard scheme was used for the pressure discretization, and the semi implicit method for pressure linked equation (SIMPLE) algorithm was applied to deal with the coupling of pressure and velocity. The diffusion term in the momentum and energy equations was approximated by second – order central difference which gives a stable solution. In addition, a second – order upwind scheme was adopted for the discretization of convection terms. The aforesaid governing equations were solved by a segregated implicit iterative scheme. To ensure the computational convergence, the under relaxation factors were 0.3, 0.7 and 0.8 for the pressure, momentum and energy respectively. Before proceeding with computations, the appropriate convergence criteria were obtained. It was done by taking continuity and momentum equations as 10^{-3} and energy equation as 10^{-6}. The governing equations were iteratively solved until the set residuals were obtained or when they stabilized at constant values. In order to satisfy the SST k-ω turbulence model, y^+ kept under 1. Due to using structural mesh and having non-complex geometry skewness kept no bigger than 0.7.

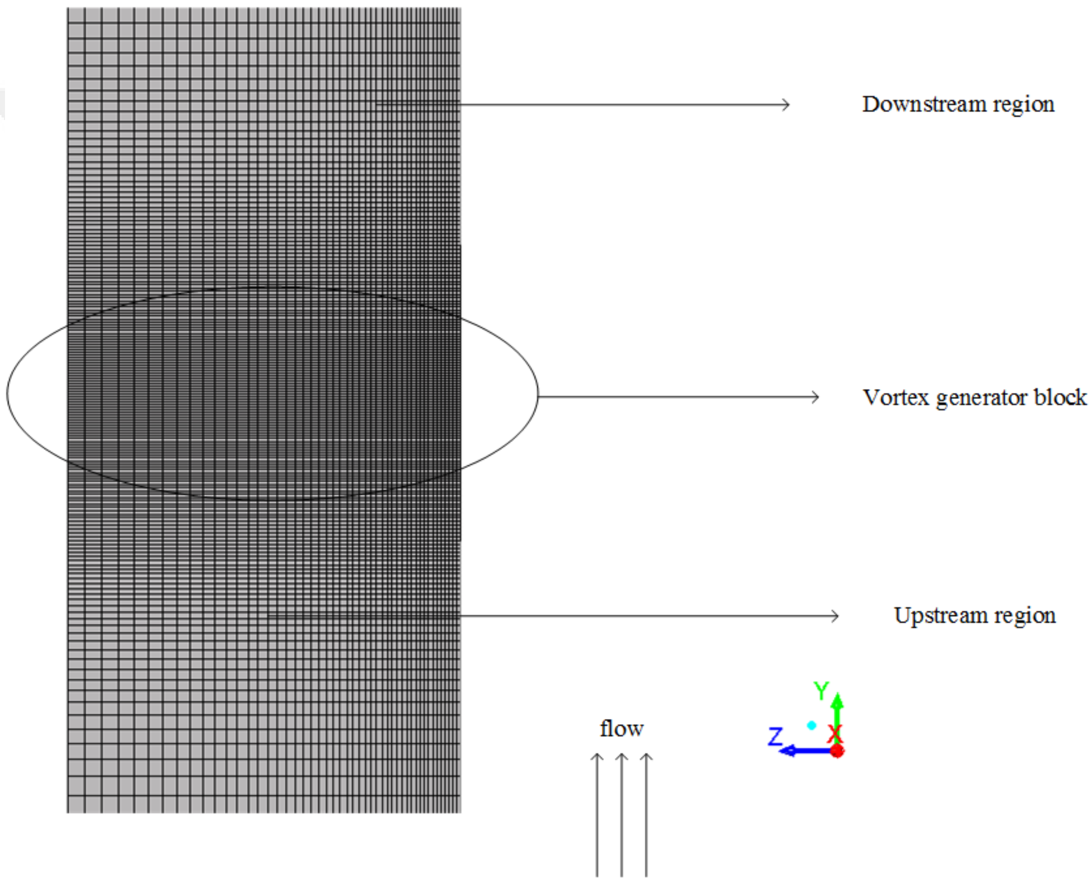

Figure 4. Mesh generation in blocks

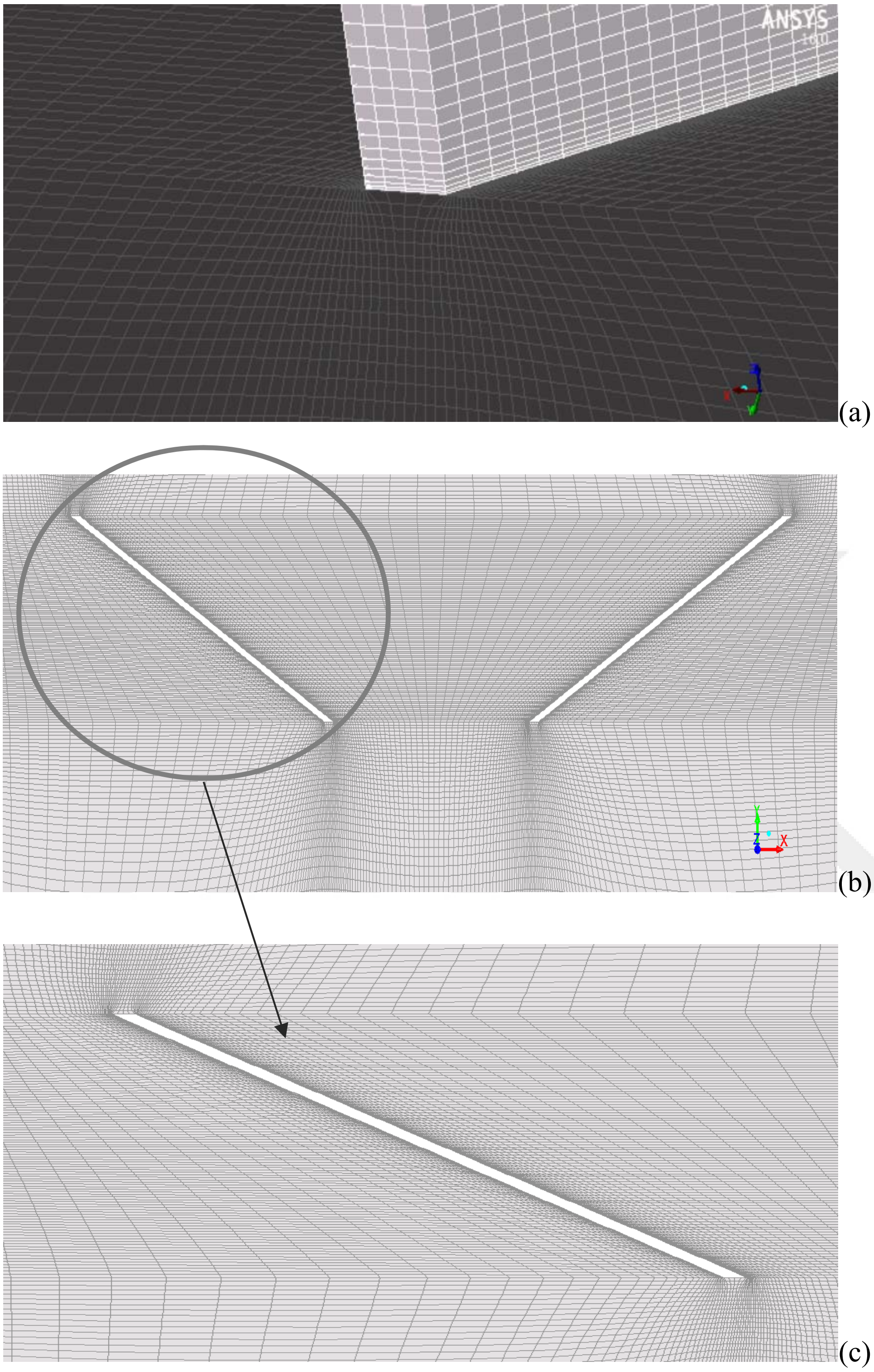

Figure 5. Mesh generation around vortex generators

5. RESULTS AND DISCUSSION

In this chapter; grid independence test, validation of benchmark problem and smooth square duct, studied vortex generator configurations analysis and correlation of Nu and friction factors are presented.

5.1 Grid Independency

A careful check for the grid – independence of the numerical solution has been carried out to ensure the accuracy and validity of the numerical results. In the process of check, seven grid systems: 100×50×140, 110×70×160, 120×90×150, 130×110×130, 140×130×125, 150×150×130, 160×170×125 are selected and examined at a Reynolds number of 3000 for the case of rectangular winglet vortex generator with attack angle of 30 deg for common flow up configuration. The calculation results of the Nu and the friction factor f with different grid system are shown in Table 6.

Table 6. Grid system test

Grid	Nu	f
100×50×140	26.867	0.1138
110×70×160	27.821	0.1124
120×90×150	28.036	0.1105
130×110×130	28.140	0.1094
140×130×125	27.961	0.1113
150×150×130	27.765	0.1122
160×170×125	28.019	0.1100

Figure 6 indicates the grid independence test results. Left vertical axis shows Nu, right vertical axis shows friction factor,f. In horizontal axis, grid cell number is shown. The difference of the calculated data between 100×50×140 and 160×170×125 is less than 3.5% for Nusselt number and within 4.28% for friction factor. Also 0.7% for Nusselt number and 2.14% for friction factor for the grid number of 110×70×160 and 120×90×150. The deflection in Nusselt number is much less because of having most homogeneous temperature profile rather than velocity profile. Simulations by Saha[22] for a similar flow configuration revealed that 1.5% and 2.5% discrepancy of Nusselt number and friction coefficient. Therefore, the final grid system was adopted as 110×70×160 considering both the reasonable computational time and solution precision for the rest of the study.

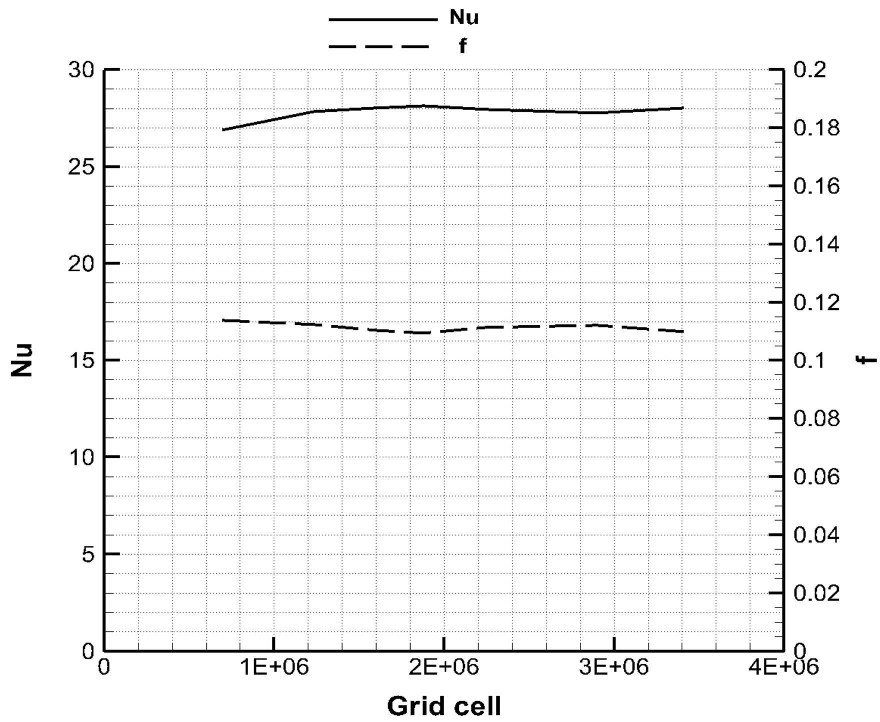

Figure 6. Grid independent test

5.2 Validation of Benchmark Problem

Performance of a plate fin heat exchanger with vortex generator channels by M.Khoshvaght-Aliabadi [46] is selected as benchmark problem for validation process. The model validation was conducted to verify the reliability of the numerical algorithm used in the present investigation.

5.2.1 Description of the problem

The computational domain consists of the inlet fluid block, core part of the computational domain, and outlet fluid block as shown in Figure 7. The applied boundary conditions in these regions are described as follows.

- In the upstream extended region (inlet fluid block):
    - At the inlet boundary (1-9-16-8)

$$u_x = u_y = 0 \tag{5.1}$$

$$u_z = u_{in} = const \tag{5.2}$$

$$T = T_{in} = const \tag{12}$$

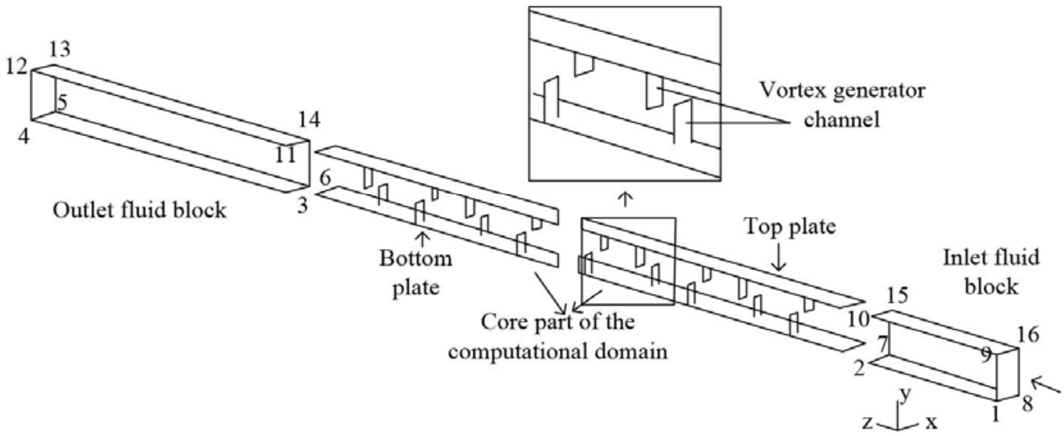

Figure 7. Computational domain and applied boundary conditions [11]

- At the left and right boundaries (1-2-10-9 and 8-7-15-16)

$$u_x = u_y = u_z = 0 \tag{5.4}$$

$$\frac{\partial T}{\partial z} = 0 \tag{13}$$

- At the lower and upper boundaries (1-2-7-8 and 9-10-15-16)

$$u_x = u_y = u_z = 0 \tag{5.6}$$

$$\frac{\partial T}{\partial y} = 0 \tag{5.7}$$

- In the middle region (core part of the computational domain):
  - At lower and upper boundaries (2-3-6-7 and 10-11-14-15)

$$u_x = u_y = u_z = 0 \tag{5.8}$$

$$T = T_{wall} = const \tag{5.9}$$

  - At the left and right boundaries (2-3-11-10 and 7-6-14-15)

$$u_x = 0 \tag{5.10}$$

$$\frac{\partial u_y}{\partial x} = \frac{\partial u_z}{\partial x} = 0 \tag{5.11}$$

$$\frac{\partial T}{\partial x} = 0 \tag{5.12}$$

- In the downstream extended region (outlet fluid block):
  - At the left and right boundaries (3-4-12-11 and 6-5-13-14)

$$u_x = u_y = u_z = 0 \tag{5.13}$$

$$\frac{\partial T}{\partial x} = 0 \tag{5.14}$$

- At the lower and upper boundaries (3-4-5-6 and 11-12-13-14)

$$u_x = u_y = u_z = 0 \tag{5.15}$$

$$\frac{\partial T}{\partial y} = 0 \tag{5.16}$$

- At the outlet boundary (4-12-13-5)

$$\frac{\partial u_x}{\partial z} = \frac{\partial u_y}{\partial z} = \frac{\partial u_z}{\partial z} \tag{5.17}$$

$$\frac{\partial T}{\partial z} = 0 \tag{5.18}$$

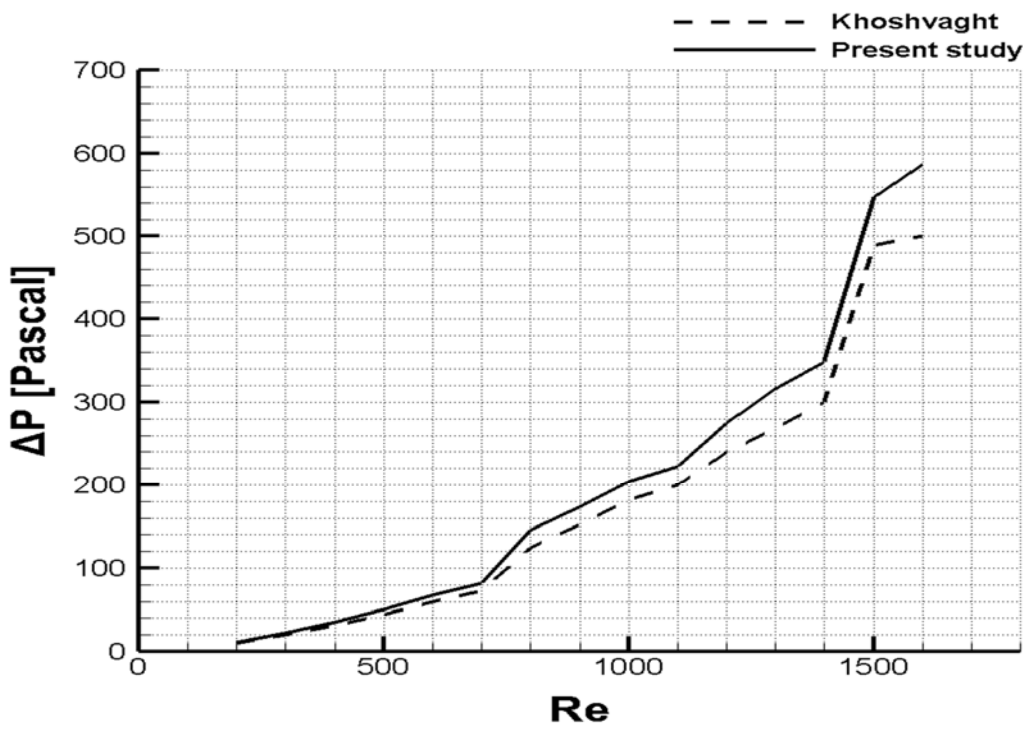

Figure 8. Pressure drop - Reynolds number relation

Figure 8 and 9 shows pressure drop and heat transfer coefficient over Reynolds number respectively. Dashed line indicates the results from benchmark problem. Solid line represents the present study.

Reynolds number values are from 200 to 1600. Therefore, the inlet velocities of each model were changed based on its geometrical parameters at different Reynolds number.

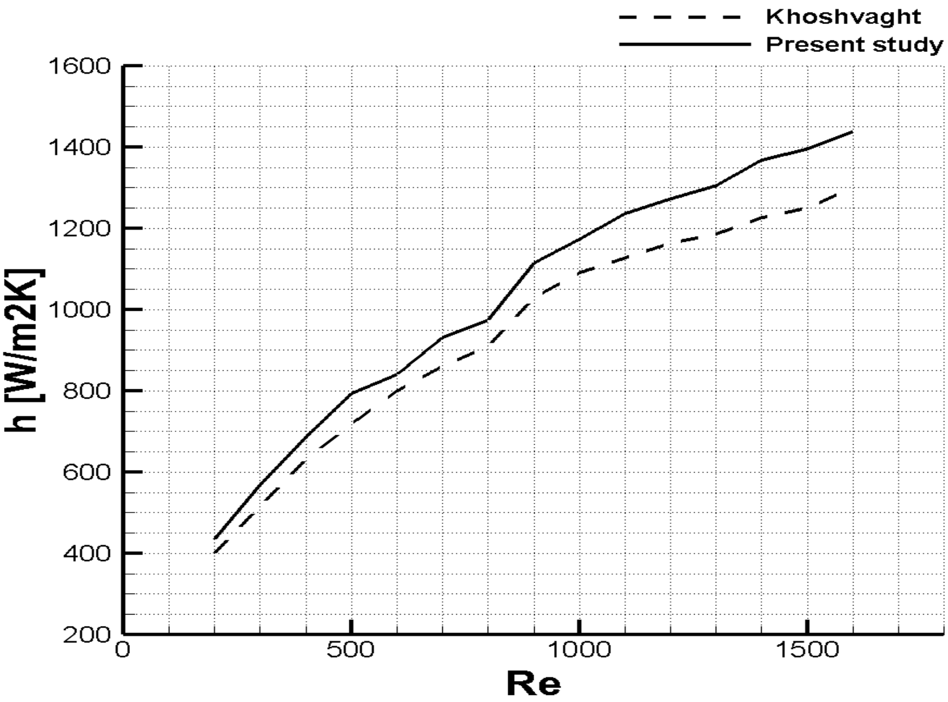

Figure 9. Heat transfer coefficient - Reynolds number relation

In order to validate the computational fluid dynamics study, simulation was carried out at the same geometry, dimensions, and operating conditions, as presented in the current benchmark problem by Khoshvaght[46]. Wing width was held constant and 5 mm for various wing height (2,5 mm – 5 mm – 7,5 mm). For the validation process wing height was selected as 5 mm. Channel length was 0,01 m in order to simplify the solution. Wing attach angle and wing attack angle was 90. Also the thickness of the channel and vortex generators were 0,7 and 0,4 mm respectively. Reynolds number is based on the velocity in the minimum cross sectional flow area and hydraulic diameter.In order to ensure the accuracy of the numerical simulations, structured hexahedral meshes were employed for the upstream extended and downstream extended regions. In the present study, the vicinity of the channel wall and the inserted fin were mashed into a smaller control volumes to solve the near wall gradients.

The region of the rectangular winglet vortex generators was meshed by using structured hexahedral cells and meshes were highly concentrated around the rectangular winglet vortex generators to capture the structure of the fluid flow where high gradients are expected. To confirm the quality of meshes in the computational domain and the accuracy of simulation solution, a very large difference between adjacent cells was avoided and the skewness were ensured less than 0.7. As presented in Figure 8 and 9, the obtained computational fluid dynamics results show a good agreement with the benchmark problem. It can be observed that the numerically predicted pressure drop is about 3.26% higher than that of the benchmark problem with 5 mm wing height and 5 mm wing width. Heat transfer coefficient is also make a good fit in the same geometrical conditions. Deviations in terms of percentage are presented in Table 7.

Table 7. ΔP and h errors of selected benchmark problem

Wing width(mm)	Wing height(mm)	Pressure drop(Pa)	Heat transfer coefficient (W/m2K)
5	5	3.26	4.87

The agreement between the numercal results and the selected benchmark problem indicates the reliability of present numerical procedure.

It can be concluded that the present numerical model is reliable to predict heat transfer characteristics.

5.3 Validation of Smooth Square Duct

The present results on friction characteristics in a smooth wall square duct are validated in terms of friction factor. Friction factor obtained from the present smooth square duct are compared with the correlations of Blasius and Petukhov for turbulent flow in ducts.

Correlation of Blasius,

$$f = 0.316 \mathrm{Re}^{-0.25} \qquad \text{for } 3000 < \mathrm{Re} < 20{,}000 \qquad (5.19)$$

Correlation of Petukhov,

$$f = \left(0.79 In \mathrm{Re} - 1.64\right)^{-2} \qquad \text{for } 3000 < \mathrm{Re} < 5 \times 10^{6} \qquad (5.20)$$

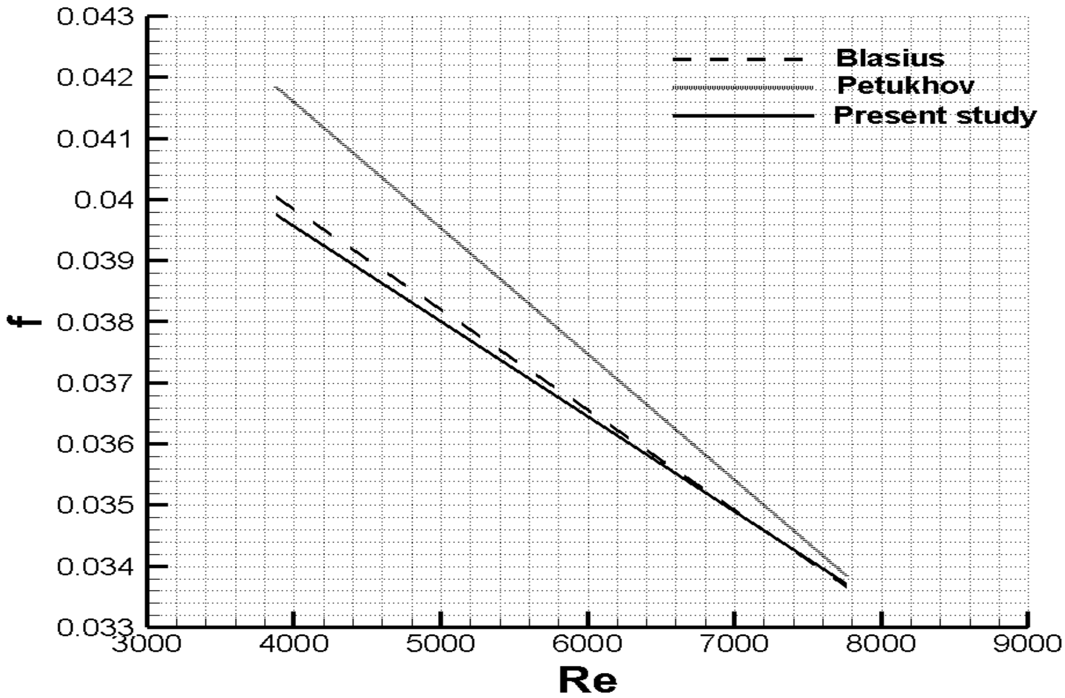

Figure 10. Validation of friction factor for smooth square duct

Figure 10 shows a comparison of friction factor obtained from the present work with those from correlations of equations. In the figure the present smooth duct results are in excellent agreement within the ±0,427745% with the Blasius correlation and ±2,6974% with the Petukhov correlation.

5.4 Vortex Generator Configurations

For the present study, eight rectangular channel of the same dimension were evaluated. These eight channels have rectangular block vortex generator pairs along the stream-wise direction, but with different configurations and attack angles as shown in Table 8. In order to simplify the expression and avoid repetition, these configurations have been named as cases from one to eight. The first four cases have 2 pairs of vortex generator, the rest of the cases have 3 pairs of vortex generators. Each case has been evaluated individually.

Table 8. Cases

Cases	Configurations	Schematic Diagram
Case I	CFD-CFD	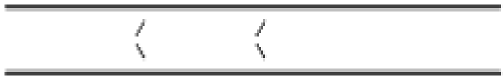
Case II	CFD-CFU	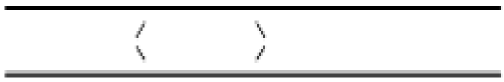
Case III	CFU-CFD	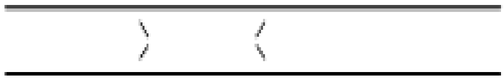
Case IV	CFU-CFU	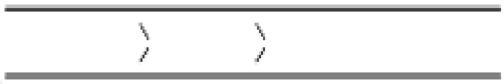
Case V	CFD-CFD-CFD	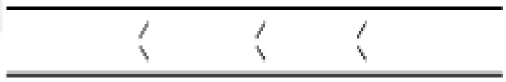
Case VI	CFD-CFU-CFD	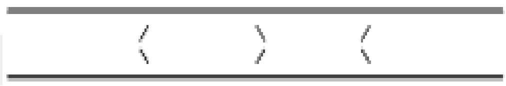
Case VII	CFU-CFD-CFU	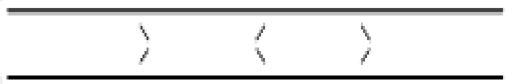
Case VIII	CFU-CFU-CFU	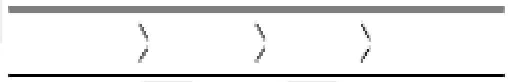

5.4.1 Case I

Figure 12(a) shows the heat transfer characteristics for various attack angle of vortex generators. Solid line represents the duct without vortex generator. Heat transfer coefficient is gradually increasing with Reynolds number. In the figure lowest Re is 385 and at that point corresponding heat transfer coefficient is 67.3. When Re reaches 7762, heat transfer coefficient becomes 291.5. This is due to increasing inlet velocity which cause decrease of temperature difference between inlet and outlet of the channel. In the figure, dashed line represents the 15° attack angle of vortex generator configuration. Heat transfer coefficient is on the increase by 22.19%, 31.47%, 30.28%, 30.82%, and 30.61% at Re equals to 385, 776, 1552, 3881, and 7762 respectively. The dash dot line illustrates the 30° attack angle of vortex generator behavior. From the figure, it was calculated that h is increasing by 37.41%, 40.85%, 42.29%, 37.96%, and 39.49% at the same Re values. Dotted shows 45° attack angle configuration and the increament depends between 33.26% and 38.28%. Dash dot dot line demonstrates 60° attack angle of vortex generator pairs. Heat transfer coefficient is increasing relative to the smooth duct configuration.However increament is not so high. It depends between 25.83% and 34.55%. This is due to the increase of the angle between the vortex generator and transverse line. Because, at that circumstance, flow is not disrupted effectively which cause less swirl motion.

Figure 12(b) shows the pressure drop behavior of the channel with vortex generator with different attack angle and without vortex generator pairs. In the figure, solid line shows the duct without vortex generator. Pressure drop is increasing with increasing Reynolds number. It is 9.99 Pa when Re at 385, and 999.89 Pa when Re at 7762. It can be said that at 15° attack angle pairs, pressure drop reaches its highest values for all Re numbers. Because at 15° vortex generator pairs, flow is obstructed too much compared to the other attack angle of VG pairs. The pressure drop increament reaches up to 115.44% at Re equals to 1552. For 30°, 45°, and 60° attack angle of VG pairs, maximum increament occurs at the same Re number by 97.33%, 72.91%, and 42.03% respectively. It can be said that for Case I, pressure drop penalty reaches its maximum values for all attack angles when Re equals to 1552.

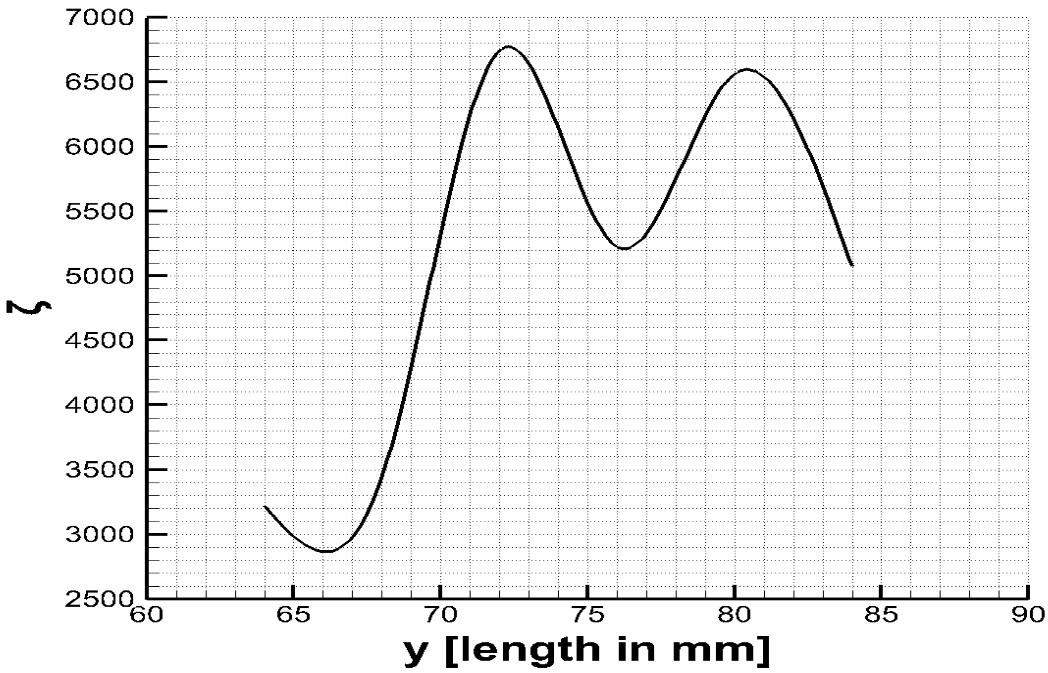

Figure 11. Vorticity for Case I

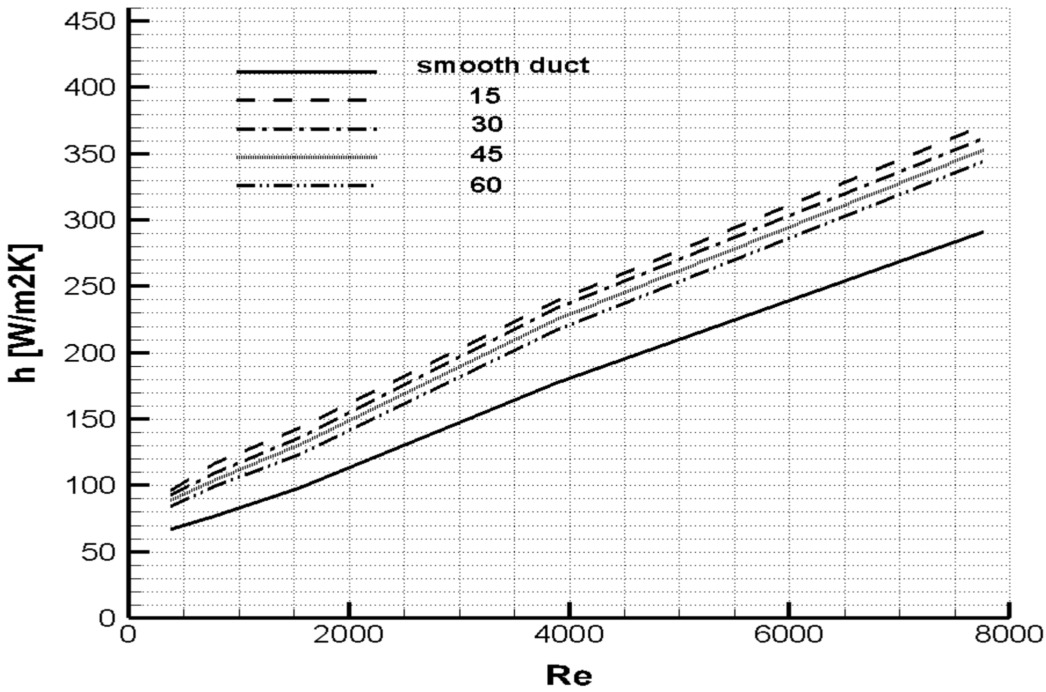

(a)

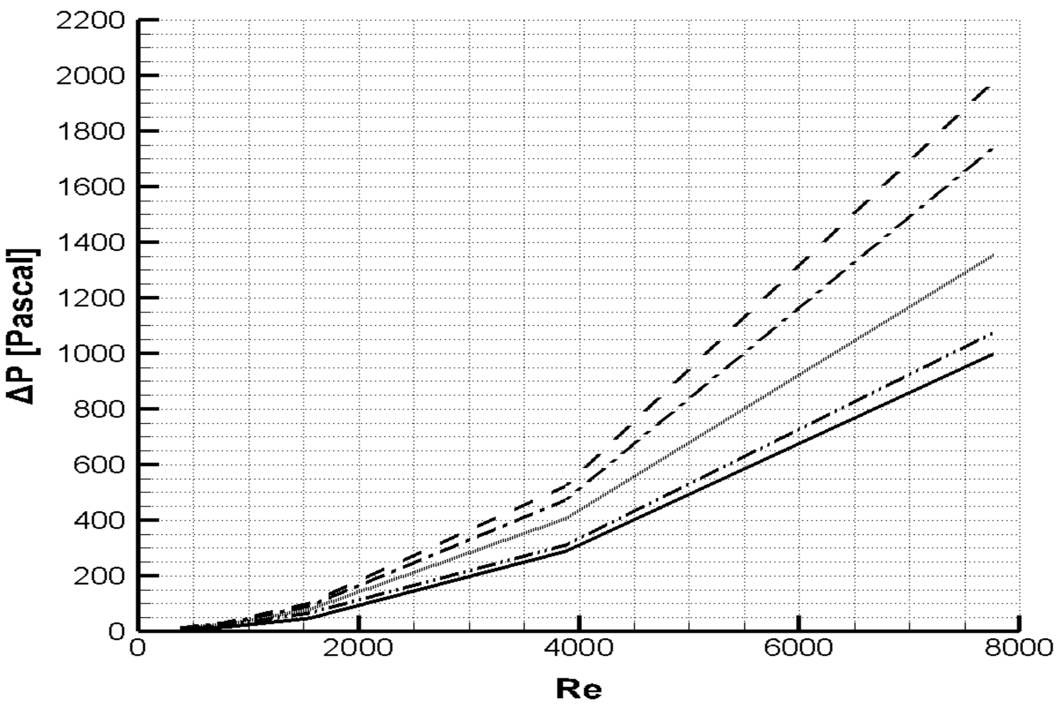

(b)

Figure 12. Comparison of (a) h and (b) pressure drop for Case I

Figure 11 shows vorticity magnitude for Case I configuration. In the figure, vertical axis represents the magnitude of vorticity for 30° attack angle of vortex generator pairs. Horizontal axis indicates the direction of the flow that vortex generators placed. It is shown that vorticity mangitude has two maximum points where vortex generator pairs located. Vortex generators almost double the magnitude of vorticity. After the first pair of vortex generator, magnitude of vorticity slightly decreases at the second pair.

5.4.2 Case II

Heat transfer coefficient for different attack angle of vortex generator over Reynolds number relation is shown in Figure 13(a). Solid line represents the duct without vortex generator analysis results. Dashed line indicates 15° attack angle of vortex generator pair placed in the duct. Enhancement of heat transfer coefficient in that case is better at that angle. The best heat transfer enhancement is shown at Re equals to 1552 by 43.98%. Heat transfer increament at calculated Re range from 300 to 8000 peaks at Re equals to 1552. For Re > 1552, increament rate starts to decrease. Dash dot represents 30° attack angle case. Increament rate almost the same for the entire Re range for this angle. It depends between 32% and 33%. Dotted and dash dot dot indicates 45° and 60° respectively. Average heat transfer enhancement is 27.45%, and 22.67% for these angles.

Figure 13(b) shows the pressure drop values for smooth duct and vortex generator pairs over Re. Solid line demonstrates the base configuration without vortex generator. It is obvious that pressure drop penalty occurs with vortex generator pairs. As expected, 15° gives the highest pressure drop for the whole Re. Pressure drop increase peaks at Re = 1552 by 123.79%. It again peaks for 30°, 45°, and 60° attack angle cases by 107.42%, 72.62%, and 38.95% respectively. The highest pressure drop penalty occurs at Re = 1552 independent from the attack angle.

Figure 14 illustrates the vorticity magnitude along positions of flow direction. The figure shows behavior of vorticity magnitude for 30° attack angle of vortex generator pairs. It is found that first pair doubles the vorticity magnitude. The second pair also boosts the magnitude of vorticity relative to the first one. The reason for this increase is to place different flow configurations(CFD-CFU). Due to non-symmetric flow, longitudinal vortices create more effective corner vortices.

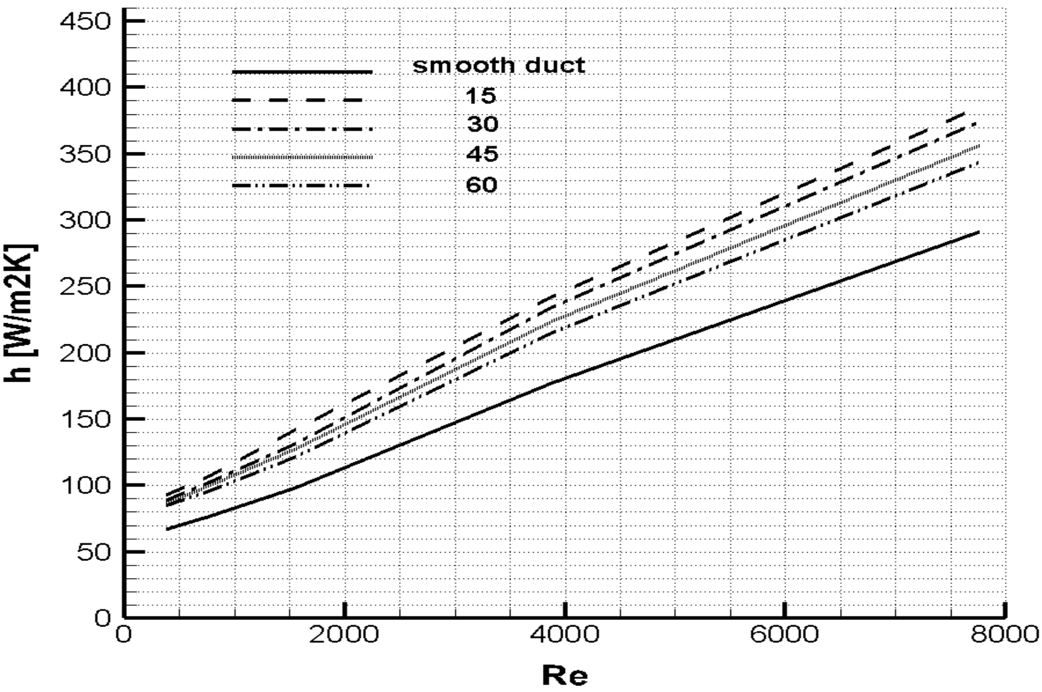

(a)

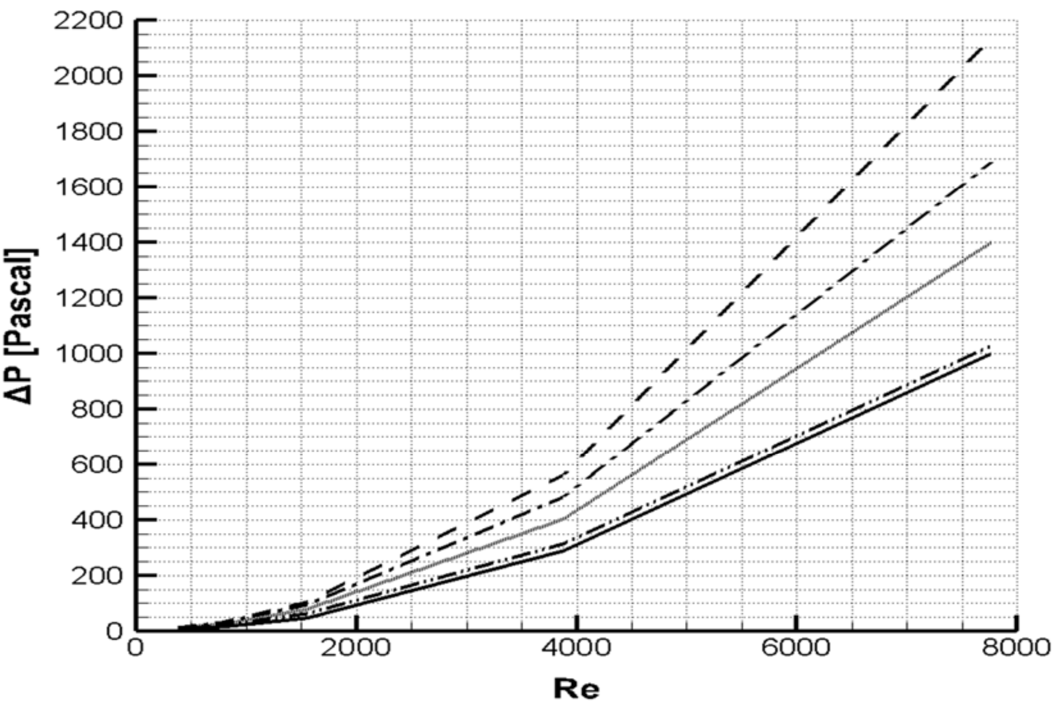

(b)

Figure 13.Comparison of (a) h and (b) pressure drop for Case II

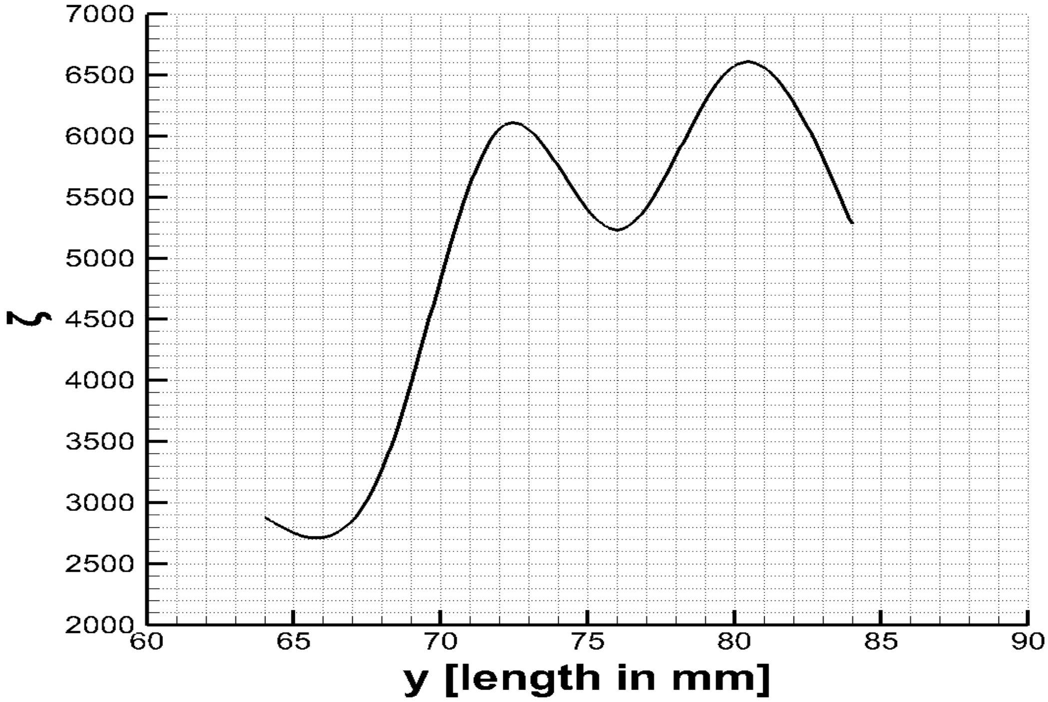

Figure 14.Vorticity for Case II

5.4.3 Case III

Figure 15(a) shows the heat transfer coefficient versus Re for calculated attack angle of vortex generator and smooth duct case. Solid line indicates the duct without vortex generator case. Compared to smooth duct, 15° attack angle of vortex generator pairs gives the highest increament along the entire Re. The best heat transfer enhancement occurs at Re = 776 by 51.91%. Increase in heat transfer coefficient is almost the same for Re numbers 385 and 1552 by 43.13% and 45.86% respectively. After Re > 1552, heat transfer increament rate significantly decreases. The dash dot illustrates 30° attack angle of vortex generator pairs. Enhancement trend is similar but less than 15°. Similar to 15°, the highest increament occurs at Re = 776 by 42.07%. In Re numbers 385 and 1552, heat transfer characteristics shows common performance by 38.32% and 38.46%. Again after Re > 1552, increament rate is decreasing. 45° and 60° attack angle of vortex generator pairs demonstrate the similar performance. The best results occurs at Re = 776 by 35.44% and 29.85% respectively.

Pressure drop and Re number relation with different attack angles of VG pairs and smooth duct case is shown in Figure 15(b). Compared to duct without vortex generator

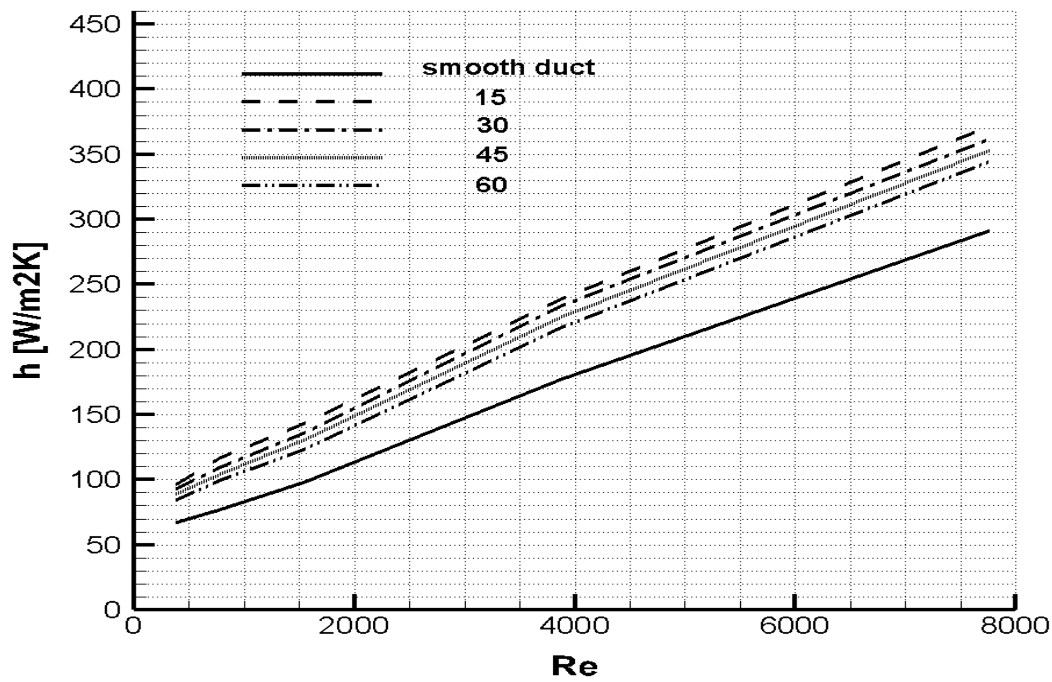

(a)

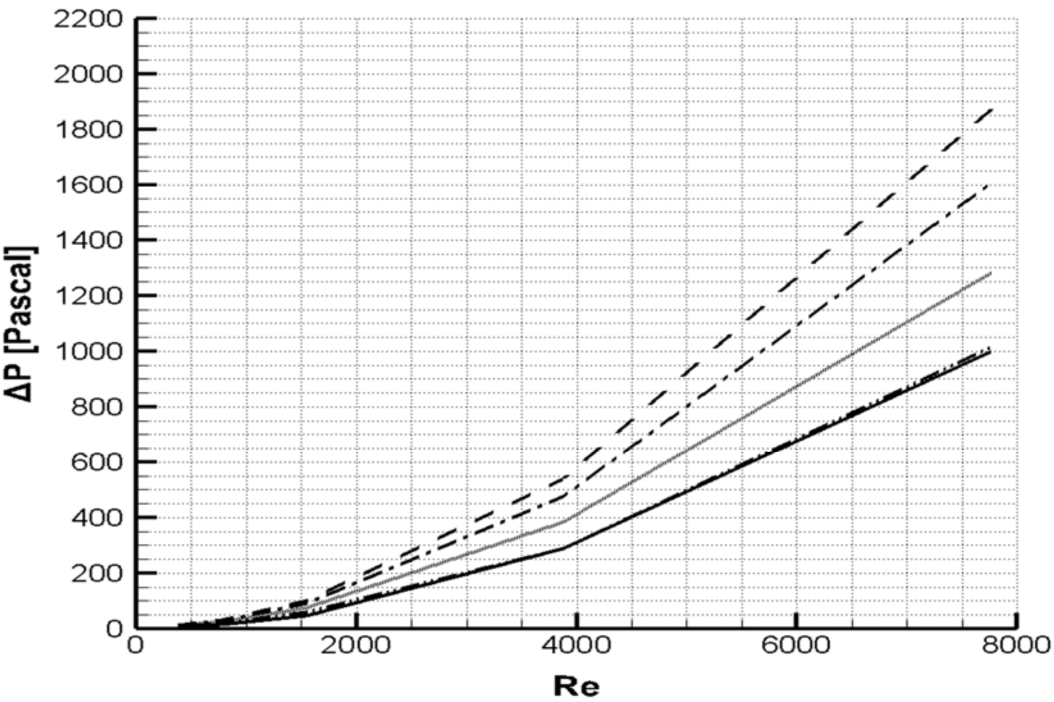

(b)

Figure 15. Comparison of (a) h and (b) pressure drop for Case III

configuration, 15° gives the highest pressure drop penalty for the entire Re. From the figure, it can be understood that increase of pressure drop relative to smooth duct is growing with Re number. The highest increase in pressure drop is observed at Re = 1552 by 118.78%. In 30°, 45° and 60° attack of angle, again highest pressure drop penalty occurs at the same Re number by 95.80%, 63.03% and 26.54% respectively. However 60° attack angle of VG pairs show similar trend like the smooth duct. The lowest pressure drop penalty observed in 60° attack of angle pairs as expecte

Effects of vorticity is shown in Figure 16. For this case, vorticity is 2.6 times higher than the base configuration. Although having different flow configurations(CFU-CFD), the impact of the first and the second pair is almost the same. As shown in the figure, magnitude of vorticity decreases between the vortex generator pairs. After that it equalizes at the second pair.

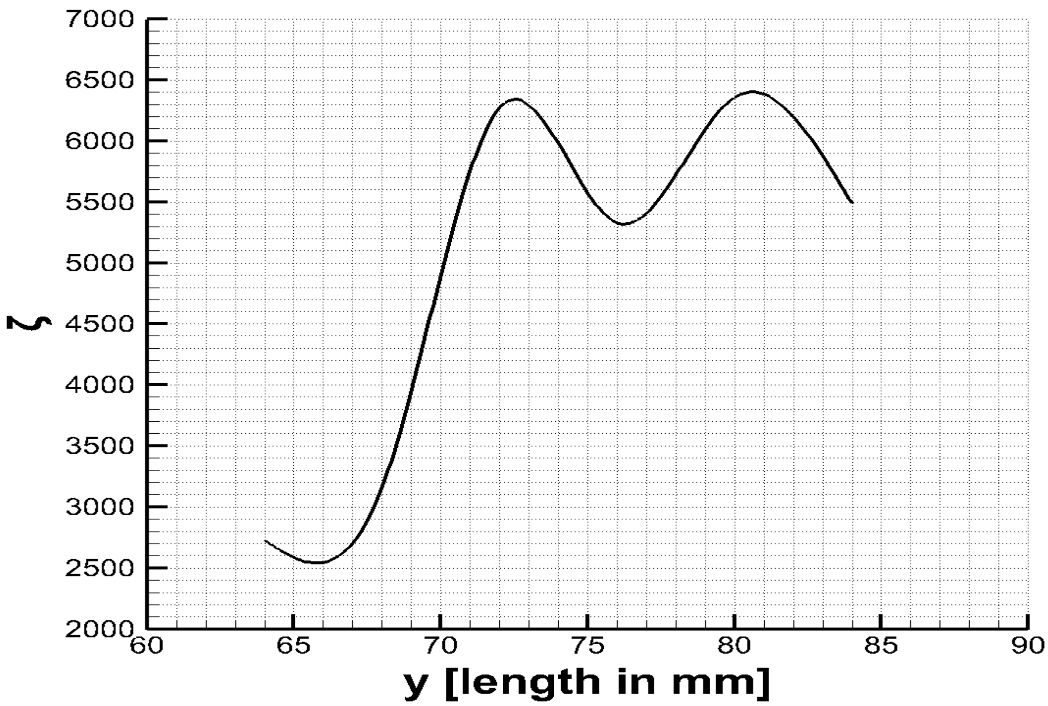

Figure 16. Vorticity for Case III

5.4.4 Case IV

Heat transfer coefficient and Re number relation with base configuration and attack angle of vortex generator pairs is shown in Figure 17(a). From the figure, it can be said that attack angles effects on heat transfer coefficient is close to each other. Solid line represents the base configuration of the duct. Dashed line represent 15° attack angle of vortex generator pairs. Increase on heat transfer coefficient is 33.52%, 35.13%, 35.64%, 34.39% and 28.60% for Re equals to 385, 776, 1552, 3881 and 7762 respectively. Heat transfer enhancement for 15° attack angle of VG pairs has similar performance on different Re numbers. The figure shows that 30° gives the highest heat transfer increament rate. Enhancement on this angle peaks at Re = 1552 by 44.36%. Average heat transfer enhancement for different Re number is 40.06% relative to smooth duct case. Unlike 30°, 45° gives its best performance on Re = 776 by 40.19% increment rate. Less increamant occurs at 60° vortex generator configuration as expected. Average increment rate in 60° is 30.73%.

Figure17(b) shows pressure drop and Re number relation for different attack angle of vortex generators and smooth duct configuration. In 15° attack angle of vortex generator pairs, pressure drop penalty reaches the highest value on Re = 1552 by 133.83% compared to baseline configuration. At low Re numbers (Re < 400) pressure drop penalty is also low which is 38.76%. When attack angle is 30°, pressure drop doubles the baseline configuration only at Re = 1552 by 108.27%. Pressure drop characteristics at Re equals to 776, 3881 and 7762 shows similar increment rate by 76.03%, 74.05% and 76.64%. In 45° and 60° attack angle of vortex generator pairs, the highest pressure drop is observed at Re = 1552 by 68.97% and 36.68% respectively.

Figure 18 illustrates the vorticity magnitude along positions of flow direction. For this case, vorticity is 2.16 times higher than the base configuration. Magnitude of vorticity peaks at the first pair and then slightly decreases at the second pair. If the flow is symmetric (CFU-CFU), the highest value of vorticity is seen at the first pair and it starts to decrease for the following vortex generators. Case IV has the lowest increment in vorticity magnitude.

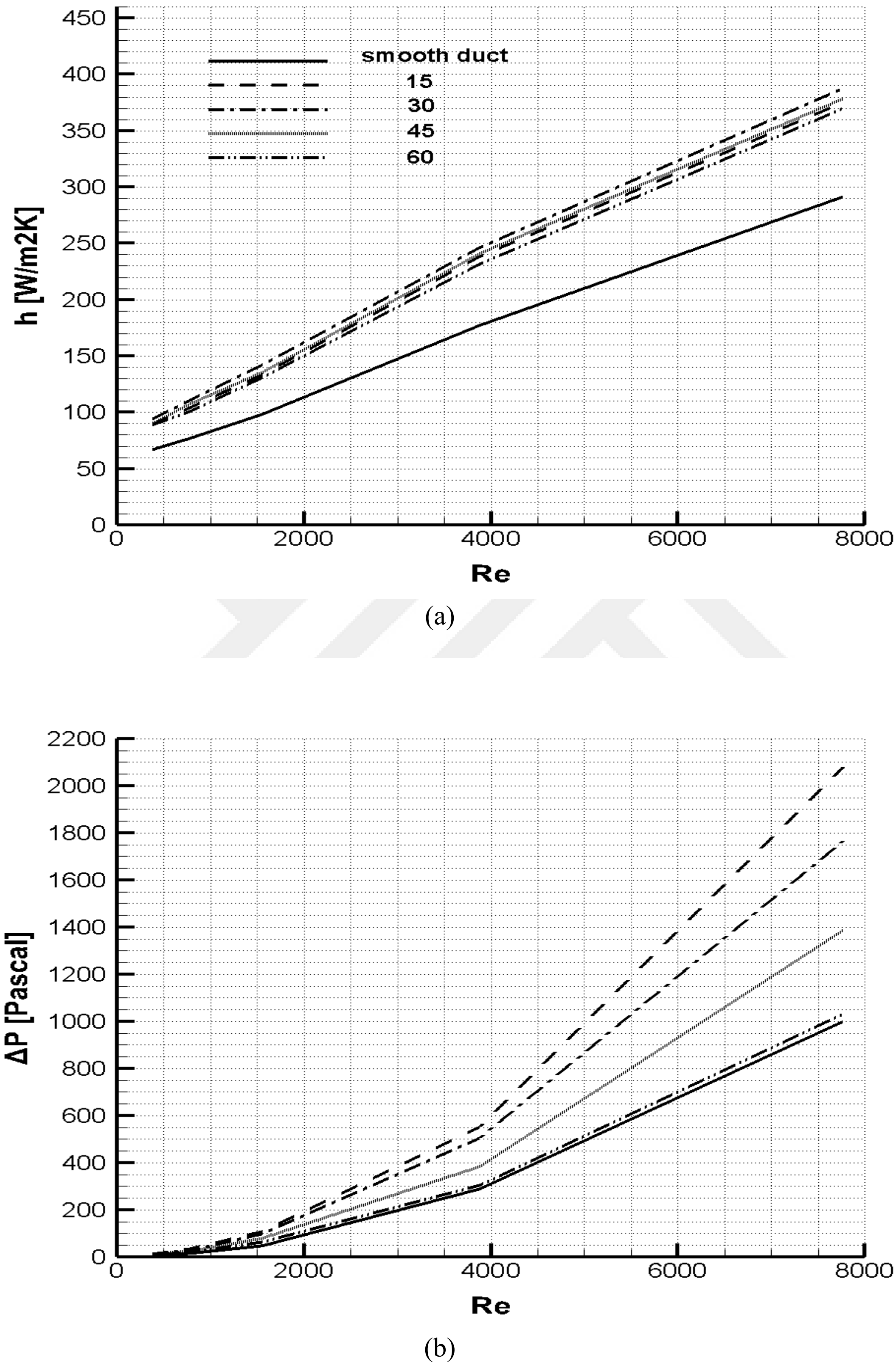

Figure 17. Comparison of (a) h and (b) pressure drop for Case IV

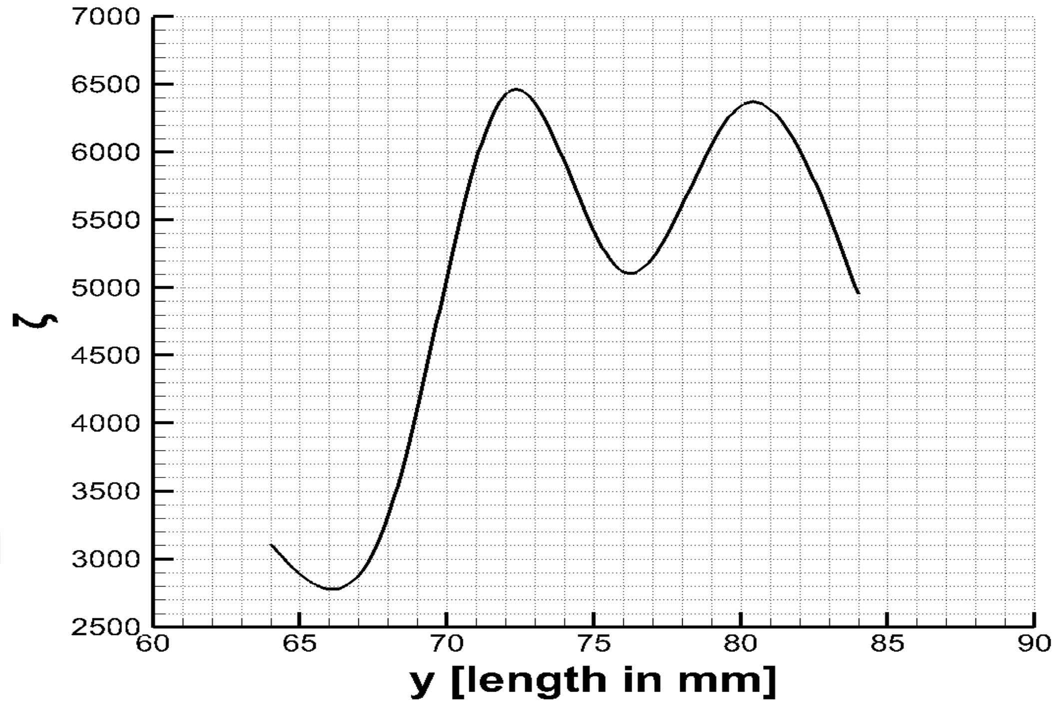

Figure 18.Vorticity for Case IV

5.4.5 Case V

Figure 19(a) shows the relation between heat transfer coefficient and Re numbers for different attack angle of vortex generator pairs. Solid line indicates the duct without vortex generator characteristics. The best heat transfer enhancement is observed in 30° attack angle of pairs for the entire Re number range. Heat transfer increment rate is 46.93%, 66.56%, 92.23%, 68.16% and 51.17% at Re equals to 385, 776, 1552, 3881 and 7762. The highest increase occurs at Re = 1552. From the figure it can be said that the slope of increment decreases after Re = 1500. Dotted line shows 45° attack angle of vortex generator behaviour. Heat transfer enhancement rate is 38.75%, 54.90%, 77.94%, 58.51% and 44.48% for given Re numbers. Increase in heat transfer coefficient is higher at Re = 1552. Dashed line indicates 15° and dash dot dot indicates 60° attack angle of vortex generator pairs. Similar to previous ones, best increment occurs at Re = 1552 by 60.15% and 52.18% respectively.

Pressure drop and Re number relation for different attack angle of vortex generator pairs is shown in Figure 19(b). For Re > 400, increment rate is dramatically rising. 15° gives the highest pressure drop difference. Pressure drop penalties compared to smooth duct case are 114.21%, 147.14%, 114.75% and 126.16% for Re equals to 776, 1552,

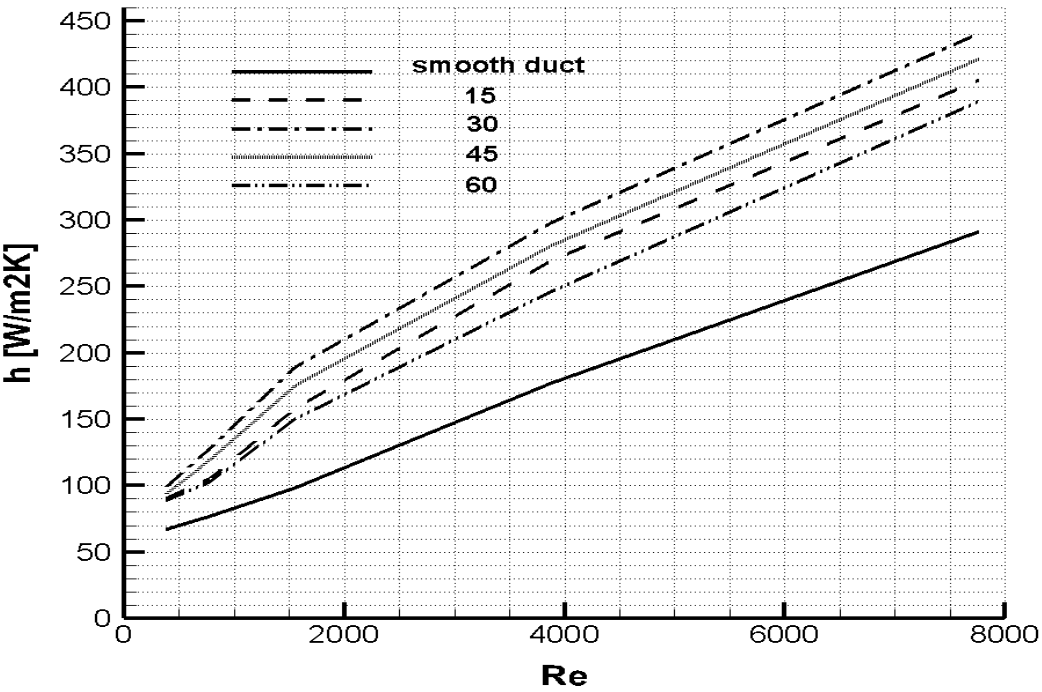

(a)

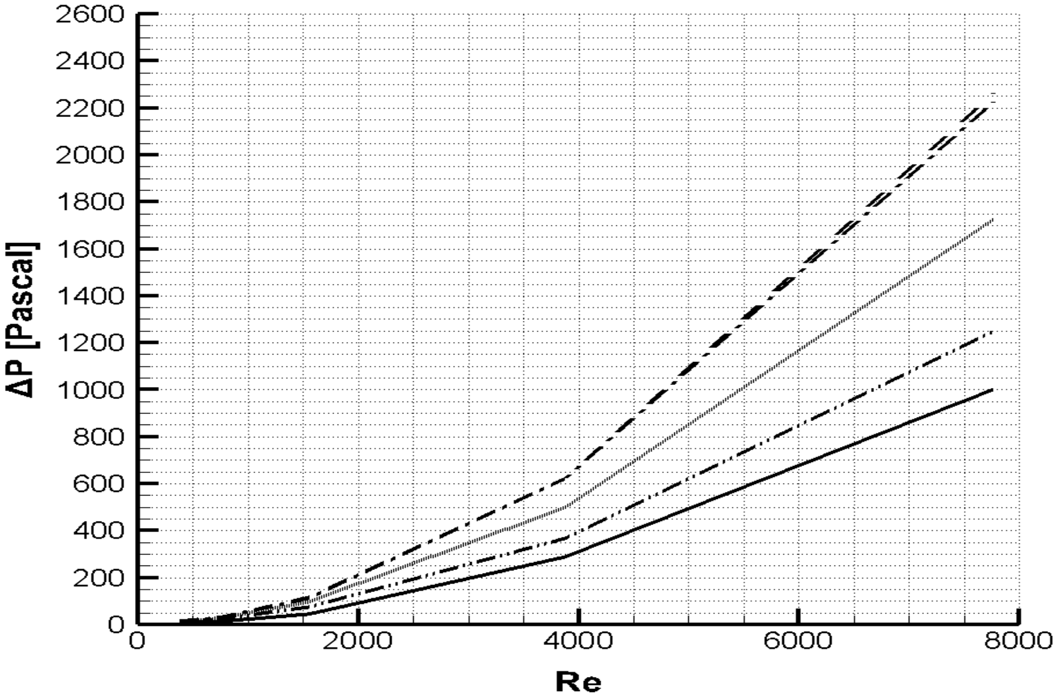

(b)

Figure 19. Comparison of (a) h and (b) pressure drop for case V

3881 and 7762. However, 30° also shows the similar performance. Pressure drop rates are 111.14%, 146.02%, 114.46% and 122.32% for the same Re numbers. For Re < 400 pressure drop is very low compared to Re > 400. Dotted line represent 45° and dash dot dot represent 60° attack angle of vortex generator configuration. Pressure drop is higher at Re = 1552 by 110.54% and 62.68 respectively. For Re > 4000, pressure drop increment slope is significantly rising for 15° and 30° and slightly rising for 45° and 60° attack angle of vortex generator pairs.

Figure 20 shows the vorticity magnitude for Case V configuration. In the figure three peaks indicates three pairs of vortex generators. For this case, magnitude of vorticity is 2.72 times higher than the base configuration. Case V performs the best vorticity magnitude increase among other configurations. In the figure there occurs sharp decrease after the second pair of vortex generator. However, third pair stabilizes the magnitude of the vorticity.

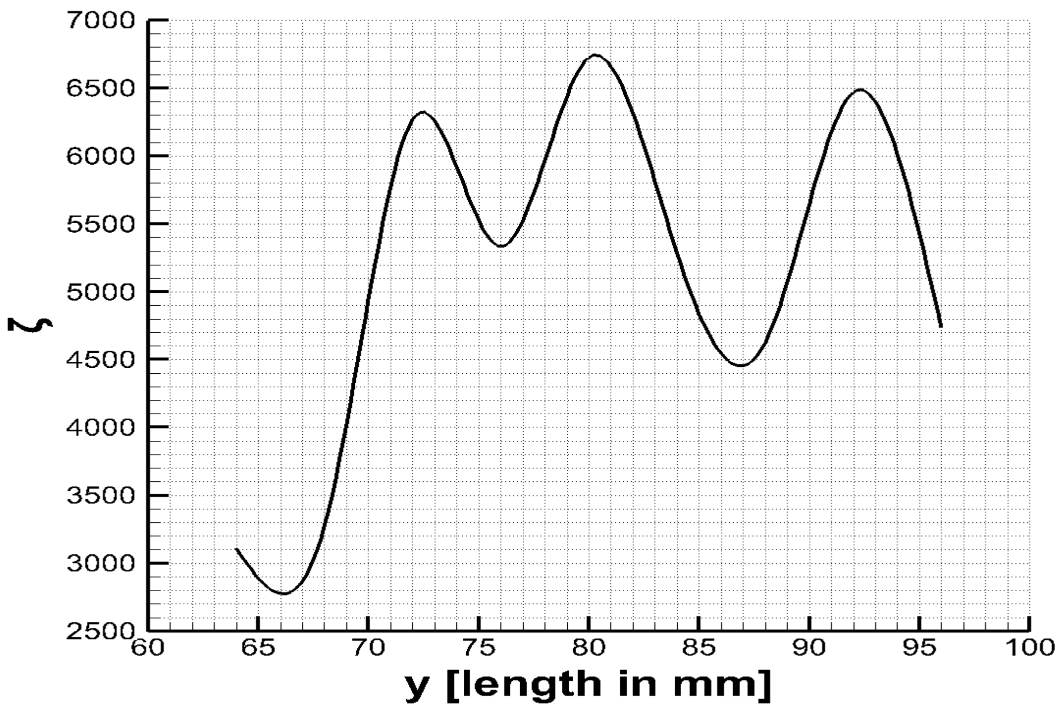

Figure 20. Vorticity for Case V

5.4.6 Case VI

Figure 21(a) shows the relation between heat transfer coefficient and Re numbers for various attack angle of vortex generator pairs. Figure demonstares that all attack angle pairs have a similar trend. Dashed line indicates 15° attack angle of VG pairs. Heat transfer enhancement at this angle is the highest for case V. Increase in heat transfer rate is 42.69%, 50.74%, 60.24%, 55.71% and 46.48% for Re numbers 385, 776, 1552, 3881 and 7762 respectively.Dash dot line represent 30° attack angle of vortex generator pairs. Heat transfer rate increment at this angle is 36.16%, 42.10%, 45.65%, 46.92% and 40.80% respectively. At Re = 3881, heat transfer enhancement is bigger than the others. Increment in 30° angle is almost linear. Dotted line indicates 45° angle attack of vortex generator pairs. Increment rate at this angle does not fluctuate more than 7%. Minimum and maximum increment increase depends between 30.82% and 37.32%. The highest heat transfer coefficient occurs at Re = 3881 by 37.32%. Dash dot dot line demonstrates 60° attack angle of vortex generator pairs. Increment at this angle for the entire Re number range is almost the same. Average heat transfer enhancement is 28.84%.

Relation between pressure drop and Re number for various attack angle of vortex generator is shown in Figure 21(b). Solid line represents the configuration without vortex generator. As expected, 15° gives the highest pressure drop penalty rate. Except for the lowest Re number (Re = 385) pressure drop penalty rates remain between 119.63% and 156.48%. The greatest value occurs at Re = 1552. For 30° attack angle pressure drop penalty peaks at Re = 1552 by 142.96%. 45° and 60° attack angle of vortex generator pairs also gives the similar results. Increase in pressure drop is 96.34% and 54.36% respectively. As expected pressure drop penalty decreases with increasing attack angle of vortex generator.

Figure 22 represent the magnitude of vorticity versus positions of flow directions for case VI. At this case, second vortex generator pair performs the best increment in magnitude of vorticity. Vorticity magnitude is 2.6 times higher than the base configuration.

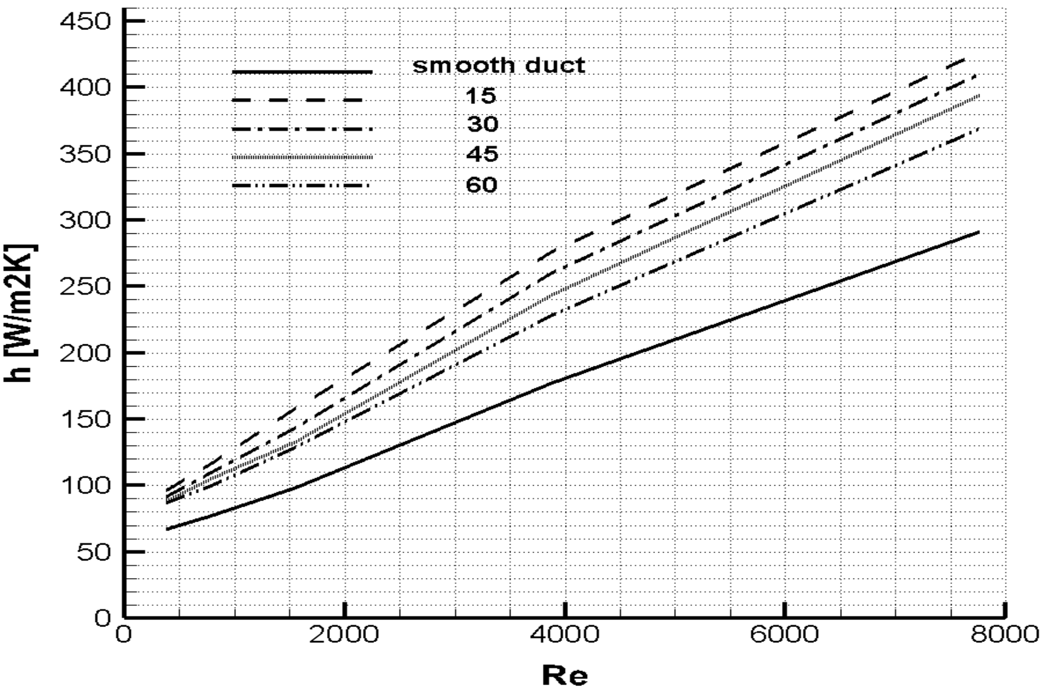

(a)

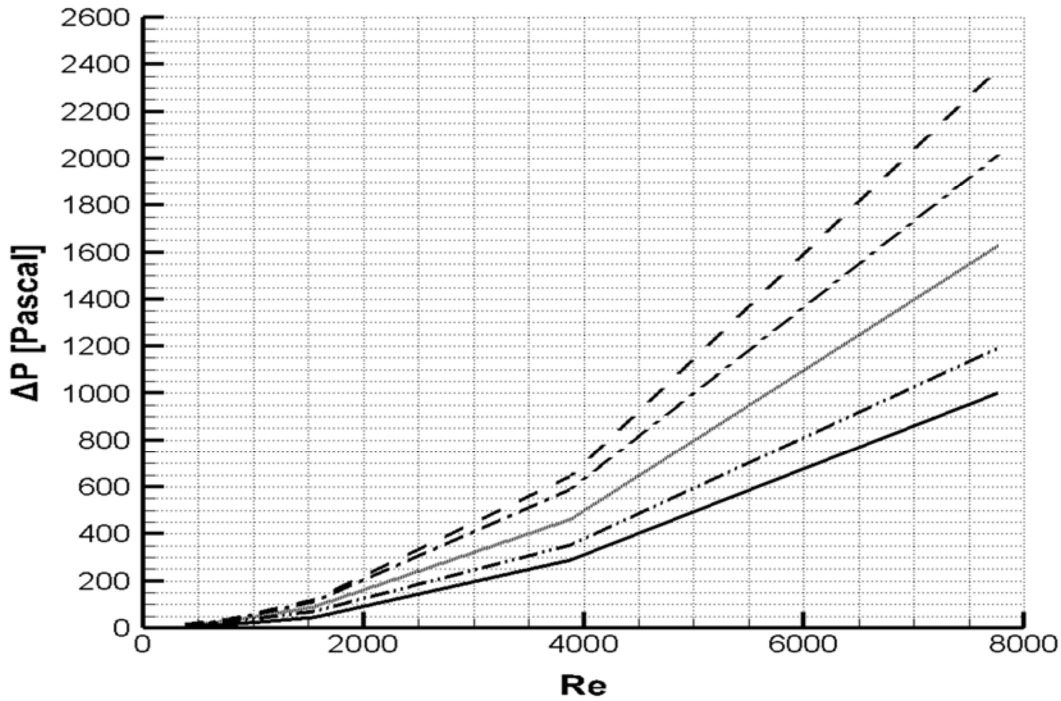

(b)

Figure 21. Comparison of (a) h and (b) pressure drop for Case VI

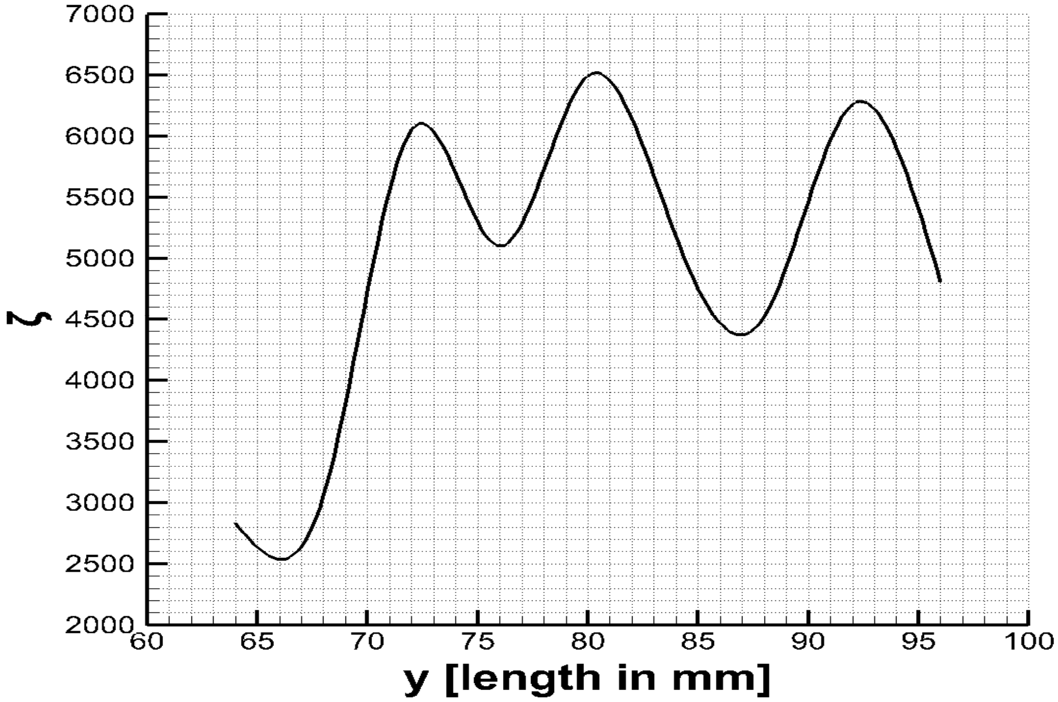

Figure 22. Vorticity for Case VI

5.4.7 Case VII

Figure 23(a) demonstrates the relation between heat transfer coefficient and Re number for various attack angle of vortex generators. Dashed line shows heat transfer behavior of 15° attack angle vortex generator pairs. Increase on heat transfer rate is 46.46%, 56.23%, 67.15%, 57.36% and 45.43% for Re equals to 385, 776, 1552, 3881, and 7762 respectively. The highest increase occurs at Re = 1552 for this angle. Dashed dot line represent heat transfer characteristics of 30° attack angle of vortex generator pairs. Enhancement on heat transfer rate is 40.93%, 44.80%, 53.11%, 49.05% and 41.49% percent for given Re numbers. Again highest increment on heat transfer can be seen at Re = 1552 by 53.11%. 45° attack angle of vortex generator pairs perform similar increment rate for the entire Re numbers. Increment rate for all Re number is approximately 38%. 60° attack angle of vortex generator pairs also have similar performance but less than 45° attack angle of pairs. The average heat transfer rate on 60° attack angle of vortex generator pair is 30.37%.

Pressure drop and Re number relation for different attack angle of vortex generator pair is shown in Figure 23(b). As expected, 15° gives the highest pressure drop for the entire Re numbers. Pressure drop increase is 30.33%, 139.56%, 174.03%, 135.86%

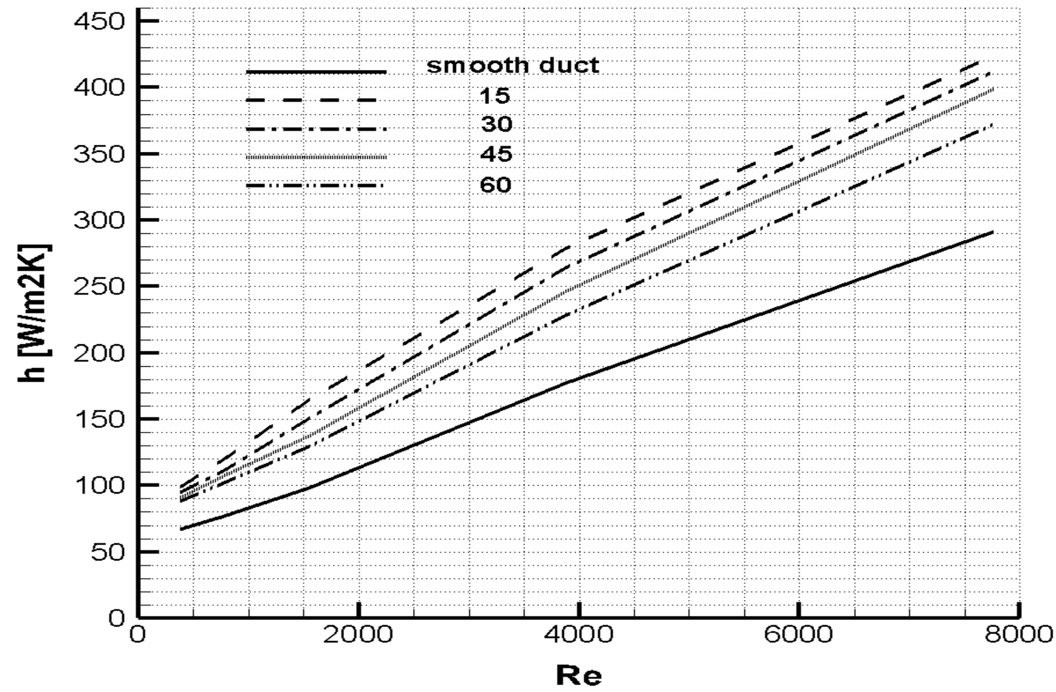

(a)

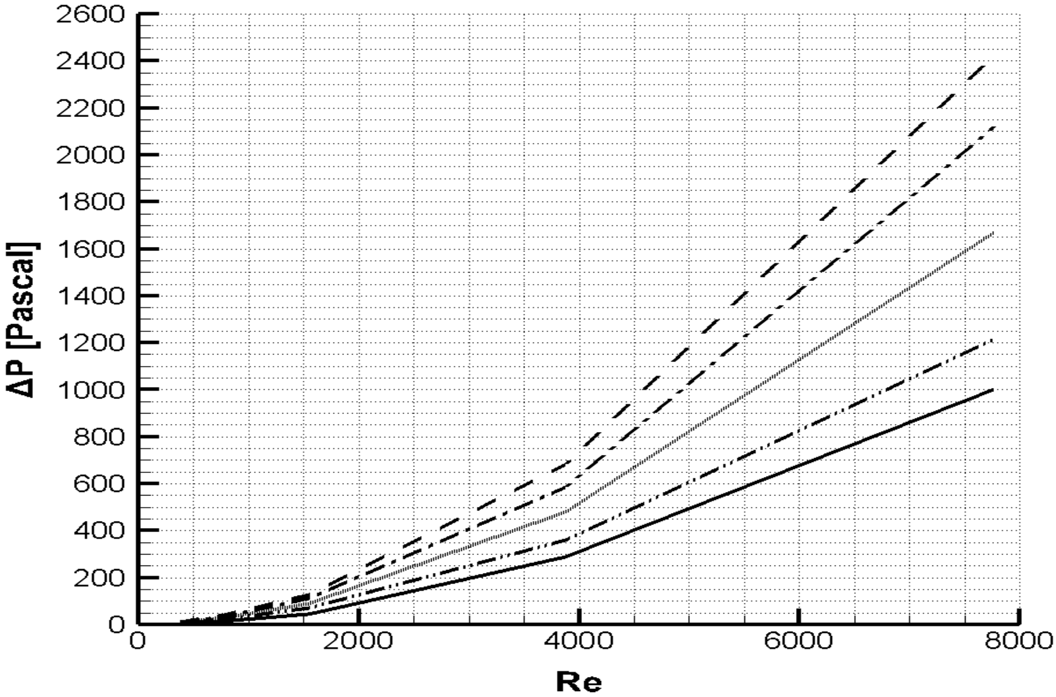

(b)

Figure 23. Comparison of (a) h and (b) pressure drop for Case VII

and 142.46% for Re equals to 385, 776, 1552, 3881 and 7762 respectively. At 15° angle attack of VG pairs, Re = 1552 gives the highest pressure drop penalty. Pressure drop increase is 29.84%, 109.23%, 142.83%, 102.24% and 111.82% for given Re numbers. Presure drop penalty peaks at Re = 1552 for 30°, 45° and 60° attack of angles by 142.83%, 97.33% and 56.39%. From the figure, increment rate of pressure drop is growing after Re = 4000.

Figure 24 indicates the magnitude of vorticity change along positions of flow directions. The magnitude of vorticity is around 2.6 times higher than the base configuration.

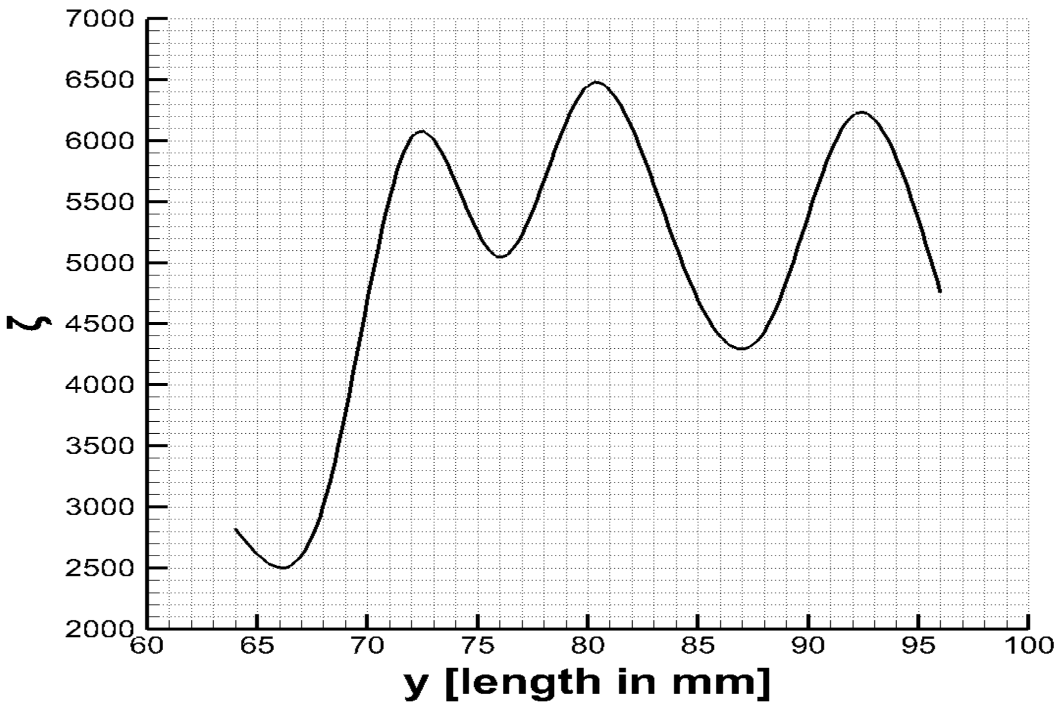

Figure 24. Vorticity for Case VII

5.4.8 Case VIII

Heat transfer increment and Re number relation for various attack angle of vortex generator pairs is shown in Figure 26(a). Dashed line shows 15° attack angle of vortex generator pairs configuration. Heat transfer enhancement at this angle is 34.78%, 45.83%, 58.78%, 46.52% and 37.68% compared to smooth duct case. The best increment occurs at Re = 1552. Dash dot line represent 30° attack angle of vortex generator pairs. The highest enhancement ocurs at this angle. Increase on heat transfer increase coefficient is 42.66%, 66.16%, 81.65%, 60.87% and 50.42% for Re equals to 385, 776, 1552, 3881 and 7762. The best performance is observed at Re = 1552. 45° and 60° attack angle of vortex generator pairs also show similar effects. Heat transfer increment for these angles at Re = 1552 is 72.29% and 35.38% respectively. Figure also indicates that increment rate on heat transfer performance is almost linear for the entire Re numbers.

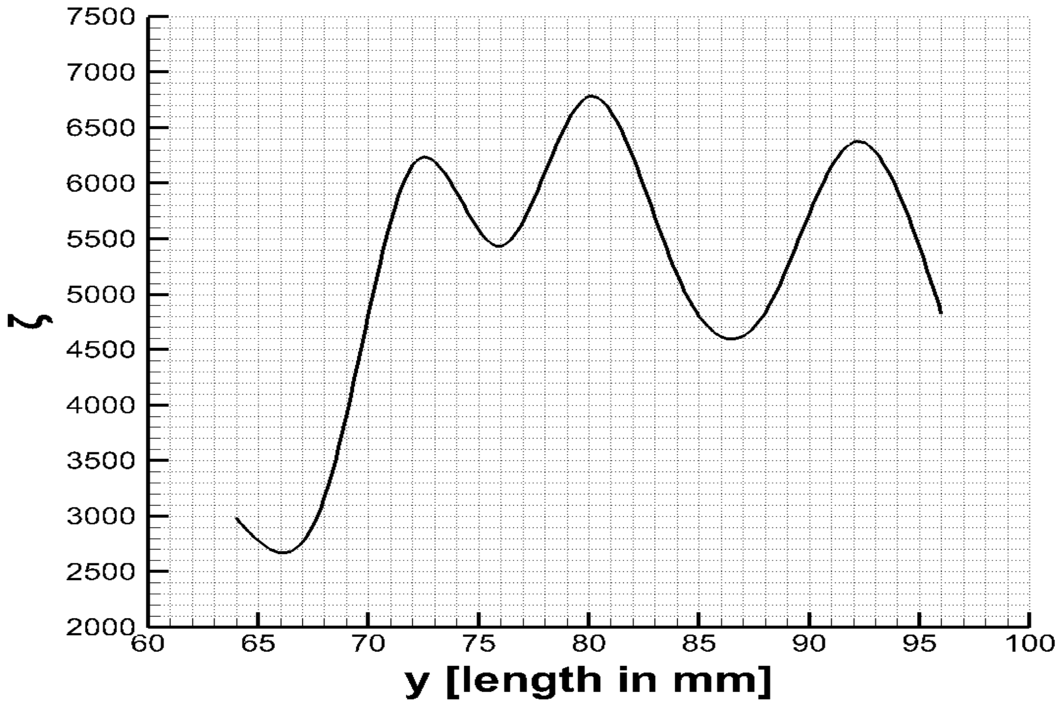

Figure 25. Vorticity for Case VIII

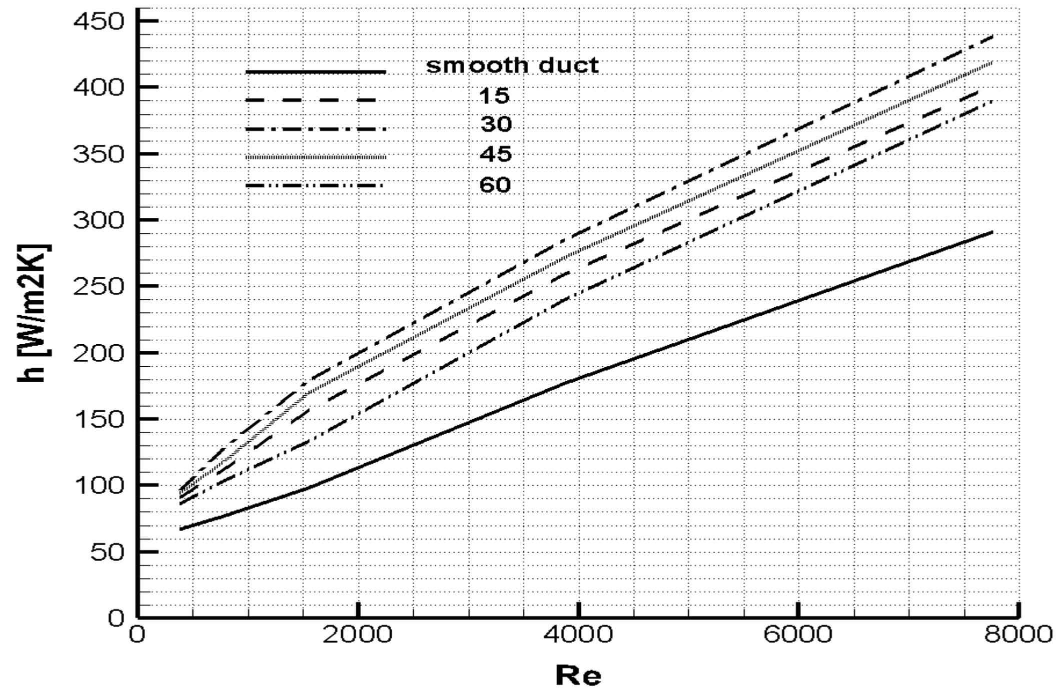

(a)

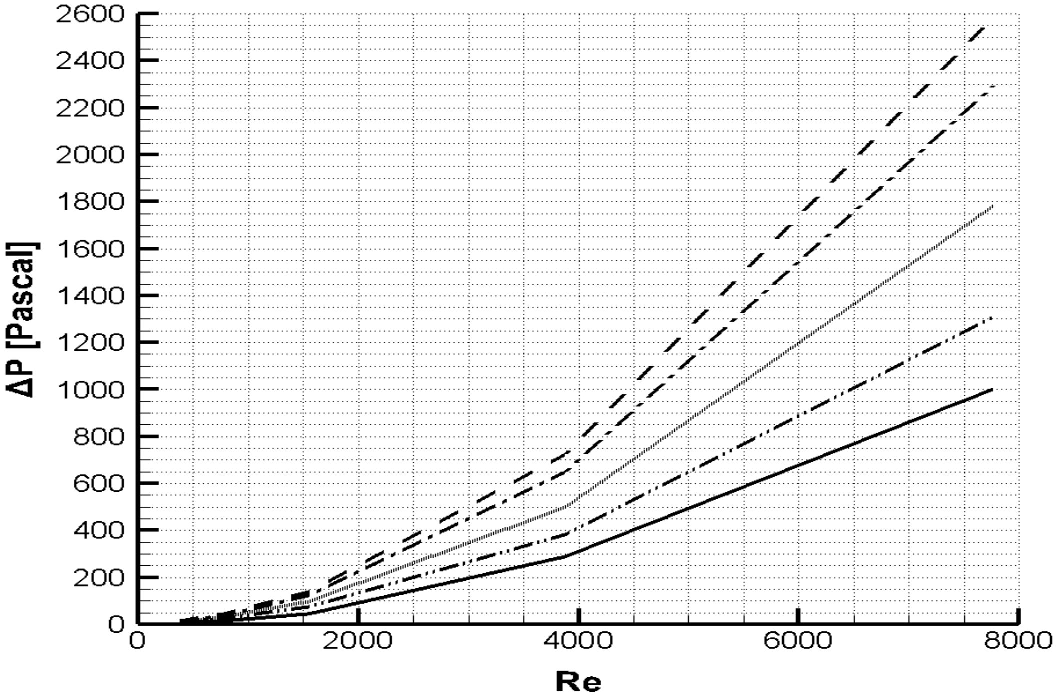

(b)

Figure 26. Comparison of (a) h and (b) pressure drop for Case VIII

Figure 26(b) shows relation between pressure drop and Re numbers for various attack angle of vortex generator configurations. 15° gives the higher pressure drop penalty among them. Increase on pressure drop is 48.31%, 167.19%, 200.66%, 149.50% and 158.68% for the given Re numbers. Pressure drop penalty peaks at Re = 1552. For 30°, 45° and 60° attack angle of vortex generator pairs, pressure drop peaks at the same Re. Increase rate is 169.10%, 112.73% and 64.76% respectively.

Figure 25 represent the magnitude of vorticity versus positions of flow directions for case VIII. At this case, second vortex generator pair performs the best increment in magnitude of vorticity. Vorticity magnitude is 2.64 times higher than the base configuration.

5.5 General Discussion

Rectangular channel with different flow configurations of vortex generator and baseline case has been compared. Effects of heat transfer coefficient, pressure drop and vorticity field has been discussed.

Investigations with eight different configurations and four different angle of attack for each configurations with five different mass flow rate inlet, overall 32 different cases and over 160 simulations have been conducted. The angle of attack for each cases are kept as 15°, 30°, 45°, and 60°. The number of vortex generator pairs are 2 and 3 depending on the flow configuration. The vortex generator types (CFD - CFU) formed the 8 different configurations. The Reynolds number, based on the average axial velocity and channel height varies in the range of 300 – 8000.
Channel length is 150 mm and channel height and width is 5 x 5 mm rectangular channel. Vortex generator pairs are placed at 70 mm from entrance and the distance of the one pair to another is kept as 10 mm which is equal to two times of the hydraulic diameter. This is done in order to provide the flow to be fully developed.
Comparing eight cases in terms of heat transfer enhancement, it is found that 2 pairs of vortex generators can give 42.29%, 43.98%, 51.91% and 44.36% increase for Case I, II, III and IV respectively. For Case I and IV maximum enhancement rate occurs at 30° attack angle of vortex generator pair and Re = 1552. Moreover, heat transfer increment for case II is maximum at 15° attack angle of vortex generator pairs at the same Reynolds number. For Case III, maximum enhancement can be seen at Re = 776

and 15° attack angle of vortex generator pairs. However, 3 pairs of vortex generators can give 92.23%, 60.24%, 67.15% and 81.65% increase for Case V, VI, VII and VIII respectively. Case V and VIII have similar heat transfer characteristics with I and IV. Maximum enhancement can be observed at 30° attack angle of vortex generator pairs at Re = 1552. Case VI and VII perform the best heat transfer increment at 15° attack angle of vortex generator pairs. It can be said that increasing the number of vortex generator pairs can enhance the heat transfer coefficient. Symmetric flow configurations can perform their best at 30° attack angle of vortex generator and Re around 1500. Y. L. He [47] studied the heat transfer characteristics of fin-and-oval-tube heat exchanger with attack angles of 15°, 30°, 45° and 60°. He also found that the average heat transfer coefficient reaches the maximum at 30°.

Considering pressure drop penalties, it is found that the numbers of vortex generator pair play an important role. Xiaoze Du [26] investigated that pressure drop increase rapidly when the more number of winglet pairs used.

The rectangular winglets generate longitudinal vortices behind them due to the pressure gradient set by the pressure surface of the winglets. The longitudinal stream-wise vortices swirl the fluid downstream entraining fluid from periphery to the centre of the vortices. This mechanism culminates in disruption of thermal boundary layer and the heat transfer from the confining solid surface is enhanced.

The generation of longitudinal vortices and subsequent disruption of thermal boundary layers are the prime movers of heat transfer augmentation.

5.5.1 Thermal enhancement factor

The efficiency of different flow arrangement of vortex generators in augmenting heat transfer requires an analysis based on a performance evaluation criterion that covers both the heat transfer and pressure drop simultaneously. The thermal enhancement factor[48], η, defined as the ratio of the heat transfer coefficient of an inserted duct, h to that of a smooth duct, h_0, at equal pumping power is given by:

$$\eta = \left.\frac{h}{h_0}\right|_{pp} = \left.\frac{Nu}{Nu_0}\right|_{pp} = \left(\frac{Nu}{Nu_0}\right)\left(\frac{f_0}{f}\right)^{1/3} \tag{5.23}$$

where Nu_0 and f_0 are the Nusselt number and friction factor for the smooth channel, respectively.

Figure 27(a) and (b) illustrates the thermal enhancement factor, η, with the Reynolds number. The thermal enhancement factor is found to be optimum at Re < 500 for laminar flow and Re = 4000 for turbulent flow. For all cases, heat transfer enhancement at Re < 500 region is not too effective. However, the reason for being greater thermal enhancement factor at this region is having relatively very low pressure drop. Figure 27(a) represent the thermal enhancement factor behavior of Case IV for 60° attack angle of vortex generator pairs. This case gives the best thermal enhancement factor among 160 cases. For this configuration, pressure drop penalty at Re < 500 region is 3.24%, but heat transfer enhancement rate is 32.07%. Thats why enhancement factor peaks in this region. Pressure drop penalty and heat transfer enhancement rate is 5.31% and 30.85% respectively at Re = 4000. At this configuration, thermal enhancement factor for Re < 500 and Re = 4000 is found to be 1.53 and 1.41 respectively.For Re > 4000, the increase in the Re number leads to the decrease in the η for all cases.

Figure 27(b) indicates the thermal enhancement factor of Case VIII for 15° attack angle of vortex generator pairs. At Re < 500 region, thermal enhancement factor is almost 1.30. Heat transfer enhancement is 34.78% and pressure drop is 48.31%. Increasing Re number gives more pressure drop penalty that thermal enhancement factor becomes almost 1 at Re = 8000. This configuration demonstrates the worst performance among all cases. This behavior is related to the difference in the local flow structures generated by the VG pairs at the different Reynolds regions.

P. Promvonge and C.Thianpong [49] also investigates the thermal enhancement factor for rectangular ribs in rectangular channel. He found that the best enhancement occurs at Reynolds number around 4000. Another study from Promvonge [44] shows that the highest thermal enhancement factor occurs at Re = 4130 for 60° attack angle of vortex generator pairs.

Oneissi[50] studied the effect of delta winglet vortex generator in a rectangular channel. According to the results given by Oneissi, the optimum thermal enhancement factor has been found at Reynolds between 4000 and 4500. Results showed that thermal enhancement factor can be found above 1.33 at this range.

It is observed that for almost all cases heat transfer enhancement is better at Re = 1552. However, also pressure drop penalty peaks at this Re number. For this reason effect of enhancement factor is not clearly seen at this region. Increasing the number of vortex

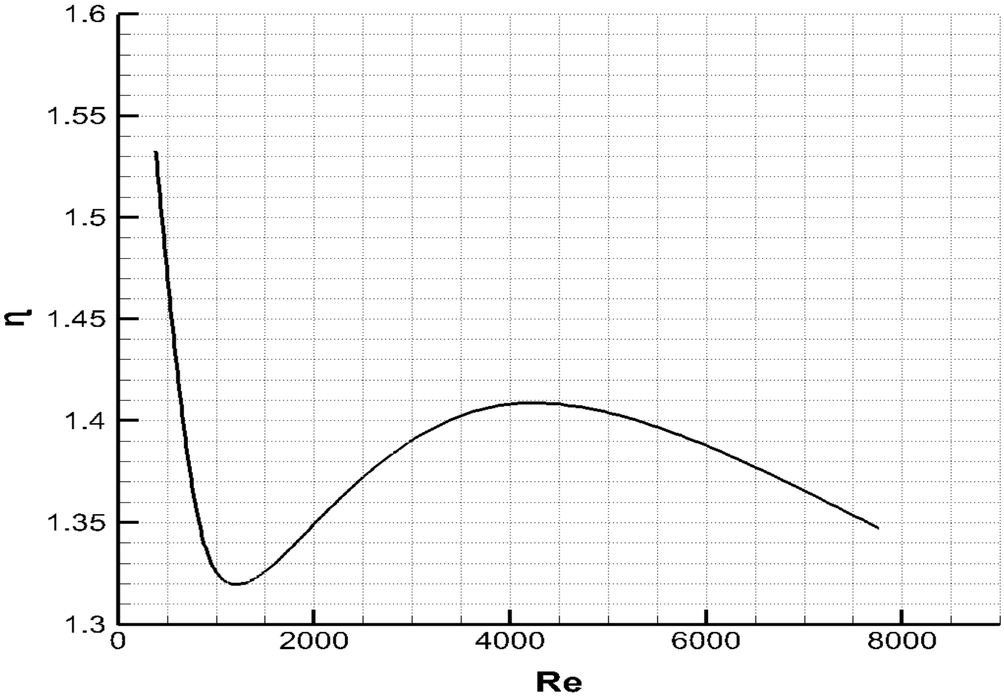

(a)

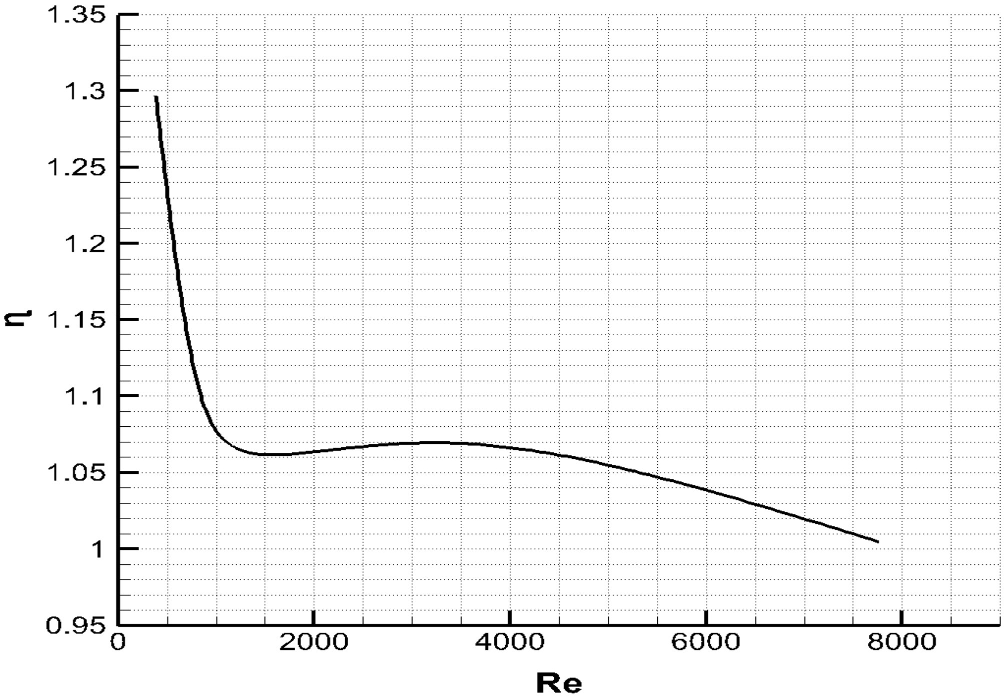

(b)

Figure 27. Thermal enhancement factor (a)Case IV (b)Case VIII

generator pair is also increase the pressure drop penalty. For Case VIII, pressure drop penalty at Re = 1552 reaches 200.66%. Although there occurs an increase in heat transfer coefficient, increase in pressure drop penalty is higher. That's why increasing the number of pairs decreases the thermal enhancement factor. It can be said that effect of pressure drop on thermal enhancement factor is bigger than heat transfer enhancement.

5.5.2 Pressure drop

Figure 28(a) and (b) demonstrates the pressure drop penalty with the Reynolds number. Solid line represents the duct without vortex generator configuration. For all cases pressure drop difference is increasing after Re > 4000. Due to the flow blockage area, increasing angle attack of vortex generator decreases the pressure drop. For this reason the lowest pressure drop values occur at 60° attack angle of vortex generator pairs. On the contrary, the highest pressure drop values can be seen at 15° attack angle of vortex generator pairs. Figure 28(a) indicates pressure drop characteristics of Case III with 60° attack angle of vortex generator. Compared to smooth duct configuration, pressure drop increase is 8.44%, 23.51%, 26.53%, 0.11% and 1.71% for corresponding Reynolds numbers of 385, 776, 1552, 3881 and 7762. It is clear that Case III with 60° attack angle of vortex generator pair is the best case in terms of pressure drop. It is observed that the less pressure drop penalty occurs at Re = 4000 for all cases. On the other hand, the largest pressure drop penalty occurs at Re = 1552 for the entire cases.

Pressure drop penalty at Re = 1552 can be seen up to %200.66 as shown in Figure 28(b). The figure represents the Case VIII with 15° attack angle of vortex generator pair and it is the largest pressure drop penalty case. Pressure drop increase for the given Reynolds number are 48.31%, 167.19%, 200.66%, 149.50% and 158.68%.

F. Hormozi [51] investigated the effect of vortex generators in rectangular channel and found that increase in pressure drop was 116.3% higher than the base configuration. Another reason for giving greater pressure drop penalty for Case VIII is having 3 number of vortex generator pairs. Average increase in pressure drop has been found in 2 and 3 pairs of vortex generator configurations as 89.08% and 122.93% respectively. It is expected that increasing number of vortex generator pairs also casuses an increase in pressure drop.

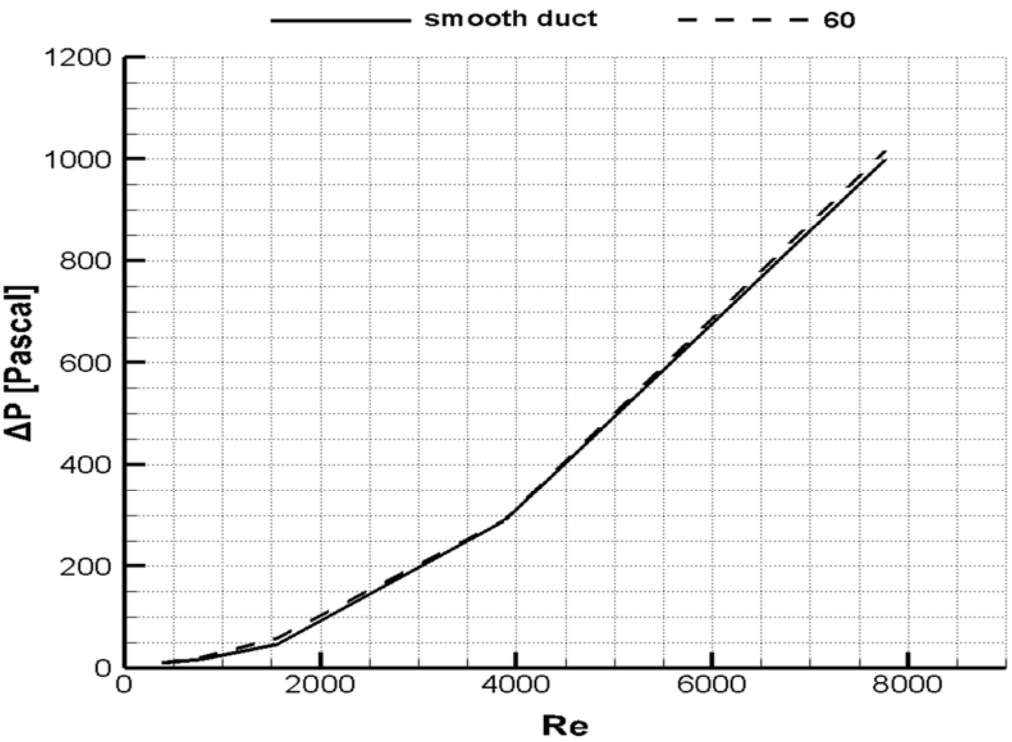

(a)

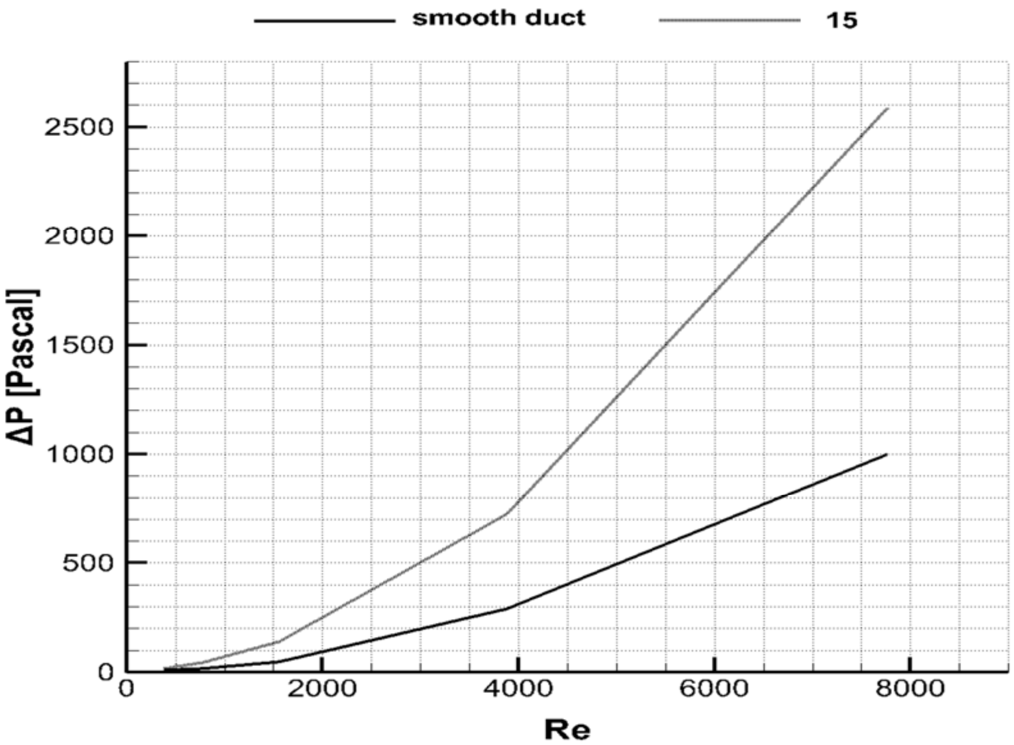

(b)

Figure 28. Pressure drop (a)Case III (b)Case VIII

5.5.3 Vorticity field

It is found that rectangular winglet vortex generator pairs have enhanced the magnitude of vorticity. Case V has the maximum enhancement rate. It is 2.72 times higher than the base configuration. It is observed that the maximum enhancement in magnitude of vorticity occurs at 30° attack angle of vortex generator pairs and Re = 1552. Sinha [52] also studied the effect of vorticity by using rectangular winglet type vortex generator. According to the results given by Sinha, it is seen that magnitude of vorticity has been enhanced 3.2 times at Re = 1500. However, it is also observed that increase in magnitude of vorticity does not direct effect on thermal enhancement factor. It is obviously clear that there is a direct relation between heat transfer enhancement and increase in vorticity magnitude. When the Re = 1552 and $\alpha = 30°$, where the magnitude of vorticity maximum, it is also seen that the maximum heat transfer enhacement occurs for all cases.

Case IV has the lowest effect on magnitude of vorticity. It enhanced the magnitude of vorticity 2.16 times the base configuration. Figure 29 indicates the vorticity contours at the top and bottom plates. Figure 29(a) represents case IV. On the bottom plate where the vortex generator pairs placed, it can be seen that resulting vortices move the fluid away from the surface. That's why, surface heat transfer augmentation is relatively low compared to other cases. Figure 29(b) represents Case V. It is seen that resulting vortices is directed towards the surface. It explains why the surface heat transfer augmentaion is high in Case V.

Table 9 shows the location of the vortices inside the channel in vortex generator region. Case V generates more streamwise vortical flow structures than Case IV. In the table also location of the vortices are highlighted. The increase in the number of streamwise vortices explains the increase in heat transfer coeeficient for Case V. In Case IV, a main (a),(b) and corner (c),(d) counter clock-wise and clock-wise vortices are generated from the fluid flow over the angle of vortex generator pairs. When moving downstream, it is shown that the effect of corner vortices (c), (d) disappears. In Case V, two main (a), (b) and corner (c), (d) counter clock-wise and clock-wise vortices are indicated. When moving downstream, at the top edge of the VG, four corner vortices (e),(f),(g),(h) are generated due to the induced viscous force of the previous vortices.

Table 9. Developing vortices for Case IV and V

y [mm]	Case IV	Case V
76	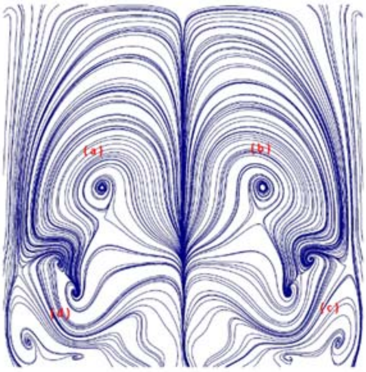	
81	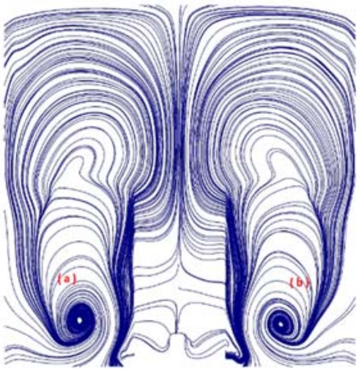	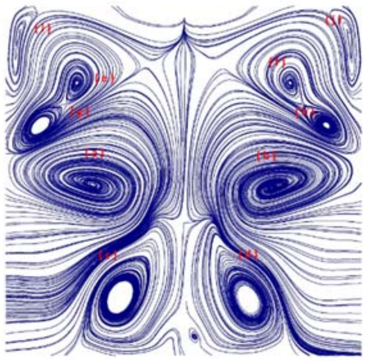
88	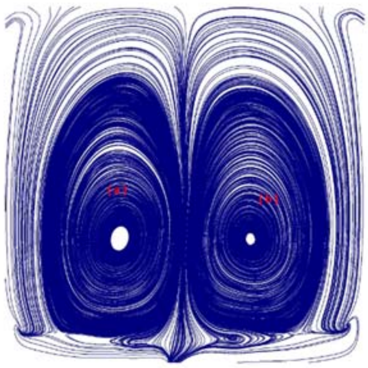	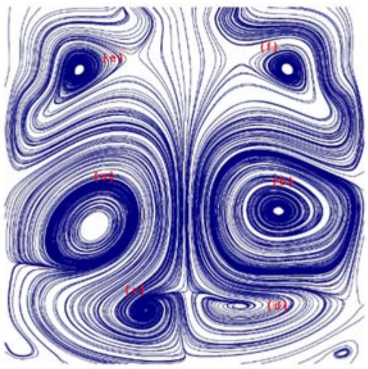
93	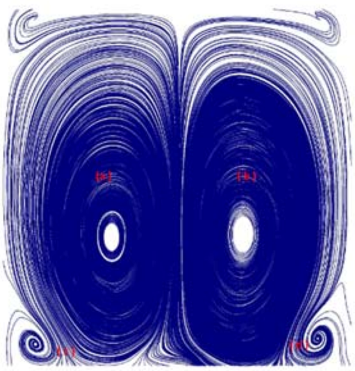	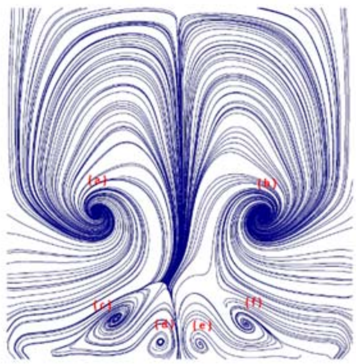

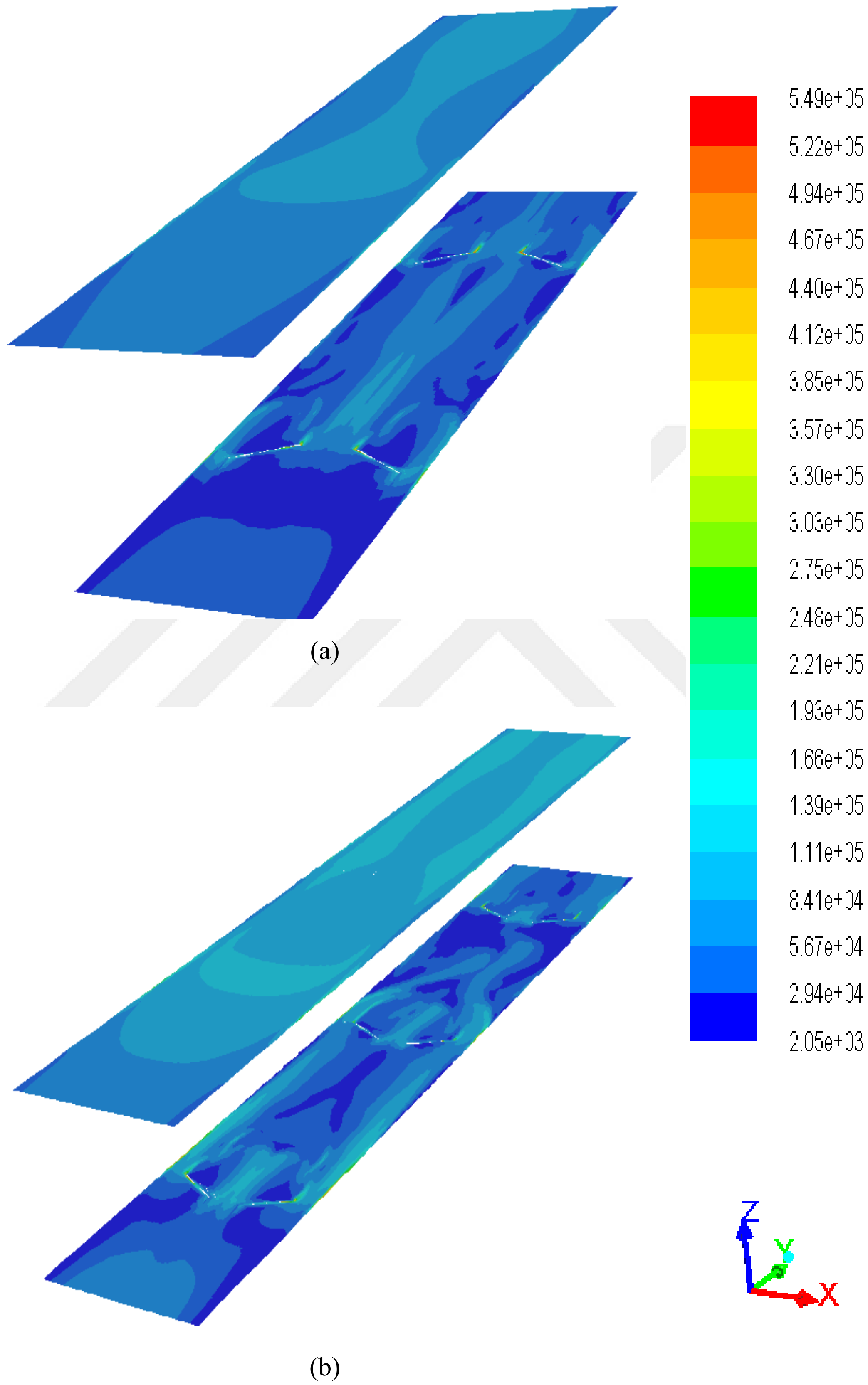

Figure 29.Vorticity contours at the top and bottom plates

5.6 Correlation

The Nusselt number and friction factor values for using the attack angles of vortex generators are correlated as functions of Reynolds number (Re), Prandtl number (Pr), number of winglet pairs (n) and attack angle α (°). Objective function for Nusselt number and friction factor is determined as follows:

$$Nu = A\,\mathrm{Re}^{B}\,\mathrm{Pr}^{C}\,n^{D}\left(\frac{\alpha}{180}\right)^{E} \tag{5.24}$$

$$f = F\,\mathrm{Re}^{G}\,n^{H}\left(\frac{\alpha}{180}\right)^{J} \tag{5.25}$$

Here; A,B,C,D,E,F,G,H, and J are coefficients to be found.
Correlations for Nusselt number and friction factor of using the all configurations for Re ranging from 300 to 8000 are written as:

$$Nu = 0.6161\,\mathrm{Re}^{0.5364}\,\mathrm{Pr}^{1.2316}\,n^{0.0766}\left(\frac{\alpha}{180}\right)^{0.0001} \tag{5.26}$$

$$f = 0.5767\,\mathrm{Re}^{-0.3649}\,n^{0.4064}\left(\frac{\alpha}{180}\right)^{-0.2676} \tag{5.27}$$

Here angle α is in degree form. The plots of the Nusselt number and friction factor of the rectangular vortex generator channel including all 160 cases predicted by equations 5.24 and 5.25 and data are illustrated in Figure 30(a) and (b), respectively. In Figure 30(a), the majority of the data falls with ±12%, for the numerical and predicted Nusselt number with average error of 9.71%. Lin and Wang[53] also used similar objective function and came up with ±10 error. In Figure 30(b), the majority of the data falls with ±18%, for the numerical and predicted f factor with average error of 10.89%. Correlated results show good agreement with the numerical results. Numerical and predicted results of Nusselt number and friction factor are given in Appendix.

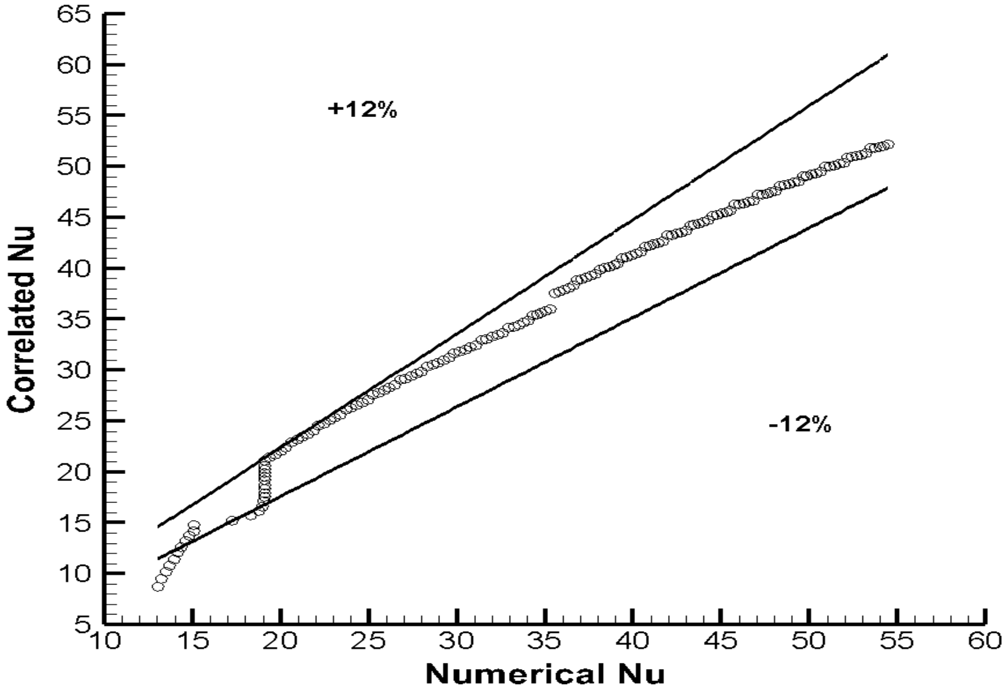

(a)

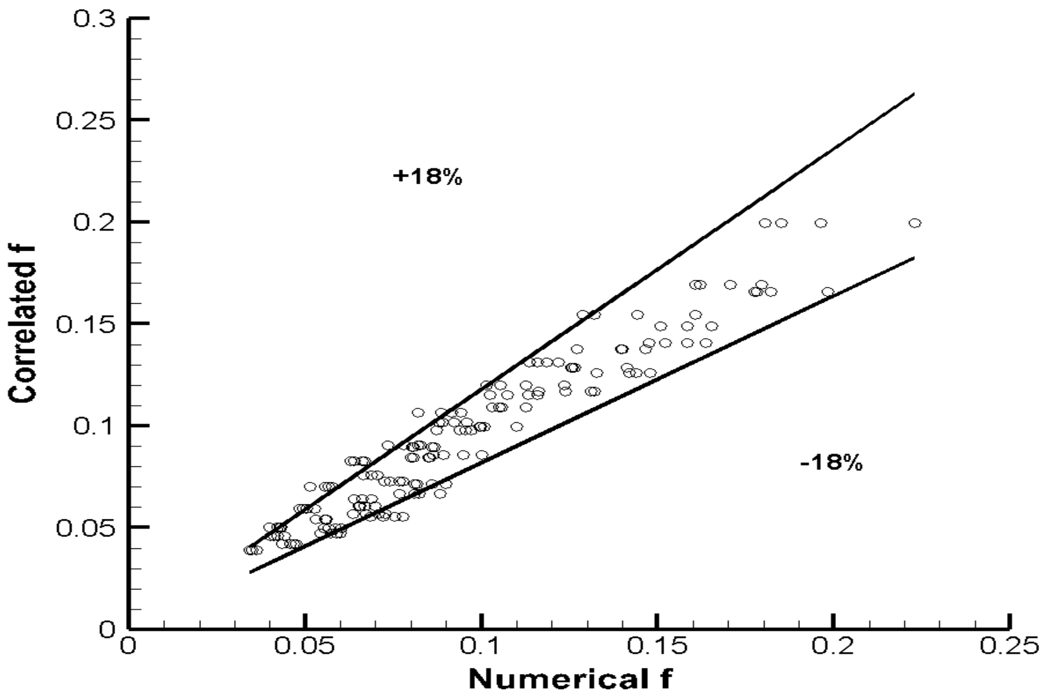

(b)

Figure 30. Predicted data of (a)Nusselt number, (b)friction factor versus numerical data

6. CONCLUSION

The present study has been carried out with the objective of assessing the effects of the new type of flow arrangements with four different (15°,30°,45°,60°) attack angle of vortex generators. Eight different flow configurations, four vortex generator attack angles with the five different Reynolds number, totally 160 cases have been meshed in Pointwise 17 and run in ANSYS Fluent 16. Objective functions for Nu and f factor have been determined and compared with the numerical results. According to the analysis, average error for Nu and f factor have been found as 9.71% and 10.89% respectively.

Analysis show that vortex generator pairs play an important role on determining heat transfer enhancement. Comparing 2 and 3 pairs of vortex generator configurations, increase in heat transfer enhancement rate is more in 3 pairs of vortex generators, as expected. Average heat transfer enhancement for 2 and 3 pairs of vortex generators is found 39.62% and 57.77% respectively compared to base configuration. However, pressure drop penalty is also much bigger in these configurations. According to the results, enhancement in heat transfer rate occurs better at Reynolds around 1500. On the other hand, pressure drop is also high at the same Reynolds range, surprisingly. Therefore, thermal enhancement factor shows inadequate performance at Reynolds 1500. It can be observed that thermal enhancement factor peaks at Re = 4000. This due to having relatively low pressure drop penalty at that Reynolds. Case IV with 60° attack angle of vortex generator pairs performs the best result in terms of thermal enhancement factor. On the other side, Case VIII with 15° attack angle of vortex generator pairs makes it with relatively low difference compared to base configuration. It is found that lower and higher pressure drop penalties occur at Re = 4000 and Re = 1500 respectively. For all cases 15° attack angle of vortex generator pairs give the highest pressure drop difference while 60° pairs do the less. This is due to increase in flow blockage area in 15° attack angle of pairs. It is found that Ccase III with 60°

vortex generator pairs has the lowest pressure drop penalty. However, Ccase VIII with 15 ° vortex generator pairs show the opposite results.

It is also found that increase in vorticity magnitude results in increase in heat transfer enhancement. Magnitude of vorticity peaks at Re = 1552 and 30° attack angle of vortex generator pairs for all cases. In this Reynolds number, heat transfer enhancement is also higher. Therefore it can be concluded that heat transfer enhancement and vorticity are directly proportional to each other.

Considering heat transfer enhancement and pressure drop, in order to satisfy the best thermal enhancement factor, flow blockage area must be decreased. For this study 60° attack angle of pairs in Case IV(CFU-CFU configuration) with Reynolds number 4000 gives the optimum result.

6.1 Future Works

Further studies can be based on the effects of length, height and placement of the rectangular vortex generators. Also, other types of vortex generators such as delta winglet, trapezoidal wing, or curvy rectangular or triangular types can be studied.

REFERENCES

[1] SAE Aerospace Information Report, **AIR1277A** (2015). Cooling of Military Avionic Equipment

[2] Kotcioglu I, Ayhan T, Olgun H, Ayhan B. (1998). Heat transfer and flow structure in a rectangular channel with winglet type vortex generator, Journal of Engineering Environmental Science, p.185-195

[3] Allison CB, Dally BB. (2007). Effect of a delta winglet vortex pair on the performance of a tube fin heat exchanger, International Journal of Heat and Mass Transfer, p.5065-5072

[4] H. E. Ahmed, H. A. Mohammed, M. Z. Yusoff (2012). Heat transfer enhancement of laminar nanofluids flow in a triangular duct using vortex generator, Superlattices and Microstructures, p.398-415

[5] Henze M, Wolfersdorf J von. (2011). Influence of approach flow conditions on heat transfer behind vortex generators, International Journal of Heat and Mass Transfer, p.279-287.

[6] M. Khoshvaght-Aliabadi, S. Zangouei, F. Hormozi. (2015). Performance of a plate fin heat exchanger with vortex generator channels: 3D-CFD simulation and experimental validation, International Journal of Thermal Science, p.180-192

[7] S. Kakaç, H.Liu, A. Pramuanjaroenkij. (2012). Heat Exchangers, CRC Press, p. 427-439.

[8] W.M. Kays, A.L.London. (1964). Compact Heat Exchangers, New York, McGraw-Hill Book Company, p.1-3.

[9] M. Thirumarimurugan, T. Kannadasan and E. Ramasamy. (2008). Simulation Studies on A Cross Flow Plate Fin Heat Exchanger, American Journal of Applied Sciences 5, ISSN 1546-9239, p.1318-1321

[10] S. Alur. (2012). Experimental Studies on Plate Fin Heat Exchangers.

[11] R. Barron. (1985). Cryogenic Systems, Oxford University Press

[12] Mori, Y. Nakayama, W. (1980)**.** Recent Advances in Compact Heat Exchangers in Japan, History, Technological Advancement and Mechanical Design Problems, 10, p.5-16

[13] Cowel, T., Achaichia,N. (1997). Compact Heat Exchangers in the Automobile Industry Proceedings of the International Conference on Compact Heat Exchangers in the Process Industries, p.11-28

[14] Yoo S, Park D, Chung M. (2002**).** Heat transfer enhancement for fin–tube heat exchanger using vortex generators, International Journal of KSME, p. 109-115

[15] M. Fiebig. (1997). Vortices and heat transfer, p.3-18

[16] Wang C, Lo J, Lin Y, Liu M. (2002). Flow visualization of wave–type vortex generators having inline fin–tube arrangement, International Journal of Heat and Mass Transfer, p.1933-1944

[17] Henze M,Wolfersdorf J von. (2011). Influence of approach flow conditions on heat transfer behind vortex generators, International Journal of Heat and Mass Transfer, p.279-287

[18] Depaiwa N, Chompookham T, Promvonge P. (2010). Thermal enhancement in a solar air heater channel using rectangular winglet vortex generators, International conference on energy and sustainable development, p.1-7

[19] J.M.Wu, W.Q.Tao. (2008). Numerical study on laminar convection heat transfer in a rectangular channel with longitudinal vortex generator, International Journal of Heat and Mass Transfer 51, p.1179-1191

[20] Y.L.He. (2012). Numerical study on heat transfer enhancement by punched winglet type vortex generator arrays in fin and tube heat exchangers, International Journal of Heat and Mass Transfer 55, p.5449-5458

[21] Yonggang Lei. (2017). Improving the thermal hydraulic performance of a circular tube by using punched delta-winglet vortex generators, International Journal of Heat and Mass Transfer 111, p.299-311

[22] Wroblewski DE, Eibeck PA. (1991). Measurements of turbulent heat transfer in a boundary layer with an embedded streamwise vortex, International Journal of Heat and Mass Transfer, p.1617-1631

[23] Fiebig M., Kallweit P., Mitra N.K. (1986). Wing type vortex generators for heat transfer enhancement, 8th International Heat Transfer Conference, San Francisco, California

[24] Fiebig M., Valencia A., Mitra N.K. (1993). Wing type vortex generators for fin-and-tube heat exchangers, Experimental Thermal Fluid Science 7, p.287-295

[25] Kwak K.M., Torii K., Nishino K. (2003). Heat transfer and pressure loss penalty for the number of tube rows of staggered finned-tube bundles with a single transverse row of winglets, International Journal of Heat and Mass Transfer, 46, p.175-180

[26] Xiaoze Du. (2014). Heat transfer enhancement of wavy finned flat tube by punched longitudinal vortex generators, International Journal of Heat and Mass Transfer 75, p.368-380

[27] Bao Gong. (2014). Heat transfer characteristics of a circular tube bank fin heat exchanger with fins punched curve rectangular vortex generators in the wake regions of the tubes, Applied Thermal Engineering

[28] Jin-Sheng Leu. (2004). Heat transfer and fluid flow analysis in plate-fin and tube heat exchangers with a pair of block shape vortex generators, International Journal of Heat and Mass Transfer 47, p.4327-4338

[29] A.M. Jacobi, R.K. Shah. (1995). Heat transfer surface enhancement through the use of longitudinal vortices: a review of recent progress, Exp. Therm. Fluid Sci. 11, p. 295-309

[30] Tiggelbeck S., Mitra N.K., Fiebig M. (1994). Comparison of wing-type vortex generators for heat transfer enhancement in channel flows, Journal of Heat Transfer 116, p.880-885

[31] G.Biswas, N.K.Mitra, M.Fiebig. (1994). Heat transfer enhancement in fin-tube heat exchangers by winglet type vortex generators, International Journal of Heat and Mass Transfer 37, p.283-291

[32] M.Fiebig, N.K.Mitra. (1998). Vortices and Heat Transfer, Vieweg Verlag, Germany

[33] G.Biswas, H.Chattopadhyay. (1992). Heat transfer in a channel flow with built in wing type vortex generators, International Journal of Heat and Mass Transfer 35, p.803-814

[34] Pankaj Saha, Gautam Biswas, Subrata Sarkar. (2014). Comparison of winglet type vortex generators periodically deployed in a plate-fin heat exchanger, A Synergy Based Analysis, International Journal of Heat and Mass Transfer 74, p.292-305

[35] R. Vasudevan, V.Eswaran, G.Biswas. (2000). Winglet type vortex generators for plate fin heat exchangers using triangular fins, Heat Transfer Part A 38, p.533-555

[36] A.Sohankar, L.Davidson. (2001). Effect of inclined vortex generators on heat transfer enhancement in a three-dimensional channel, Heat Transfer Part A 39, p.433-448

[37] M.C. Gentry, A.M.Jacobi. (2002). Heat transfer enhancement by delta wing generated tip vortices in flat plate and developing channel flows, Journal of Heat Transfer (ASME) 124, p.1158-1168

[38] K. Torii, K.M. Kwak, K. Nishino. (2002). Heat transfer enhancement accompanying pressure loss reduction with winglet type vortex generators for fin-tube heat exchanger, International Journal of Heat and Mass Transfer 45, p.3795-3801

[39] A. Jain, G. Biswas, D. Maurya. (2003). Winglet-type vortex generators with common flow up configuration for fin-tube heat exchangers, Heat Transfer Part A 43, p.201-219

[40] G. Biswas, K. Torii, D. Fujii, K. Nishino. (1996). Numerical and experimental determination of flow structure and heat transfer effects of longitudinal vortices in a channel flow, International Journal of Heat and Mass Transfer 38, p.3441-3445

[41] A. Joardar, A.M. Jacobi. (2007). A numerical study of flow and heat transfer enhancement using an array of delta-winglet vortex generators in a fin and tube heat exchangers, Journal of Heat Transfer (ASME) 129, p.1156-1167

[42] A. Sinha, K. Ashoke Raman, H. Chattopadhyay. (2013). Effects of different orientations of winglet arrays on the performance of plate-fin heat exchangers, International Journal of Heat and Mass Transfer 57, p.202-214

[43] Li-Ting Tian, Ya-Ling He, Yong-Gang Lei, Wen-Quan Tao. (2009). Numerical study of fluid flow and heat transfer in a flat plate channel with longitudinal vortex generators by applying field synergy principle analysis, International Communications in Heat and Mass Transfer 36, p.111-120

[44] P. Promvonge, S. Skullong, S. Kwankaomeng, C. Thiangpong. (2012). Heat transfer in square duct fitted diagonally with angle-finned tape-part 1:experimental study, International Communications in Heat and Mass Transfer 39, p.617-624

[45] Amnart Boonloi. (2015). Turbulent forced convection in a heat exchanger square channel with wavy-ribs vortex generator, Chinese Journal of Chemical Engineering 23, p.1256-1265

[46] M. Khoshvaght-Aliabadi. (2015). Performance of a plate-fin heat exchanger with vortex generator channels: 3D-CFD simulation and experimental validation, International Journal of Thermal Science 88, p.180-192

[47] P. Chu, Y.L.He, Y.G.Lei, L.T.Tian, R.Li. (2009). Three-dimensional numerical study on fin-and-oval –tube heat exchanger with longitudinal vortex generators, Applied Thermal Engineering 29, p.859-876

[48] M.Rahimi, S.R. Shabanian, A.A.Alsairafi. (2009). Experimental and CFD studies on heat transfer and friction factor characteristics of a tube equipped with modified twisted tape inserts, Chemical Engineering and Processing: Process Intensification 48, p.762-770

[49] P.Promvonge, C.Thianpong. (2008). Thermal performance assessment of turbulent channel flows over different shaped ribs, International Communications in Heat and Mass Transfer 35, p.1327-1334

[50] M. Oneissi, C. Habchi, S. Russeil, D. Bougeard, T. Lemenand (2016). Novel design of delta winglet pair vortex generator for heat transfer enhancement, International Journal of Thermal Science 109, p.1-9

[51] F. Hormozi. (2014). Role of channel shape on performance of plate-fin heat exchangers: Experimental assessment, International Journal of Thermal Sciences 79, p.183-193

[52] A.Sinha, H.Chattopadhyay. (2016). Enhancement of heat transfer in a fin-tube heat exchanger using rectangular winglet type vortex generators, International Journal of Heat and Mass Transfer 101, p.667-681

[53] Zhi-Min Lin, Liang-Bi Wang. (2016). Numerical study of the laminar flow and heat transfer characteristics in a tube inserting a twisted tape having parallelogram winglet vortex generators, Applied Thermal Engineering

APPENDICES

APPENDIX A: Correlation Data for Nu
APPENDIX B: Correlation Data for f

APPENDIX A

numerical Nu	Re	Pr	alfa	n	correlated Nu	%error
13,4151709	385	0,689268	15	2	10,00719417	25,40390098
15,16317771	776	0,687383	15	2	14,52510911	4,208013721
19,09146594	1552	0,686429	15	2	21,0300934	10,15441909
33,41665479	3881	0,685777	15	2	34,34288372	2,771758399
53,25733133	7762	0,685241	15	2	49,76023536	6,566412322
13,42788589	385	0,689132	30	2	10,00552921	25,48693595
15,16914168	776	0,687318	30	2	14,52454992	4,249362128
19,33631834	1552	0,686397	30	2	21,03047412	8,76152198
33,64432789	3881	0,685772	30	2	34,3451778	2,083114608
55,59044375	7762	0,685242	30	2	49,76414574	10,48075463
13,48824806	385	0,689134	45	2	10,00600033	25,8169016
15,19998378	776	0,687318	45	2	14,52519775	4,439386512
19,16968892	1552	0,686329	45	2	21,02887042	9,698548072
33,13848414	3881	0,685698	45	2	34,34217804	3,63231429
53,05927483	7762	0,685116	45	2	49,75509722	6,227332774
13,38606121	385	0,689229	60	2	10,00802426	25,23548112
14,89211026	776	0,687278	60	2	14,52461155	2,467740991
18,76601802	1552	0,686278	60	2	21,02760146	12,0514828
32,3593576	3881	0,685647	60	2	34,34011523	6,121127785
50,42497098	7762	0,685059	60	2	49,75159793	1,335396012
13,59189943	385	0,689402	15	2	10,00958305	26,35626021
15,19104035	776	0,687454	15	2	14,52697373	4,371436069
19,48384169	1552	0,686532	15	2	21,03398967	7,956069476
33,70833679	3881	0,685865	15	2	34,34834241	1,898656784
51,69333013	7762	0,685287	15	2	49,76435299	3,731578412
13,75462369	385	0,689261	30	2	10,00782514	27,24028393
15,59487269	776	0,687383	30	2	14,52623319	6,852505416
19,65724849	1552	0,686466	30	2	21,03310271	6,999220781
34,19138041	3881	0,685839	30	2	34,34930224	0,461876139
52,8196798	7762	0,685242	30	2	49,76411146	5,784905071
13,53426176	385	0,689198	45	2	10,00714343	26,06066291
15,41301645	776	0,687319	45	2	14,52520762	5,760123809
19,35721627	1552	0,686383	45	2	21,03090946	8,646352674
33,72042461	3881	0,685749	45	2	34,34529007	1,85307709

52,66834449	7762	0,68516	45	2	49,75904652	5,523807526
13,27112184	385	0,689236	60	2	10,00814443	24,58705036
14,73118024	776	0,68728	60	2	14,52464911	1,401999881
18,66217452	1552	0,686292	60	2	21,02812921	12,67780821
32,66278137	3881	0,685669	60	2	34,34144348	5,139372816
51,04400657	7762	0,685092	60	2	49,75449964	2,526265113
13,47288685	385	0,690028	15	2	10,02078428	25,62259007
15,22778088	776	0,687678	15	2	14,53280632	4,563859687
19,13511518	1552	0,686673	15	2	21,03928395	9,951174874
33,60871667	3881	0,685899	15	2	34,35039485	2,206803037
51,94305545	7762	0,685291	15	2	49,76471767	4,193703592
13,47297051	385	0,689931	30	2	10,01981644	25,63023554
15,09936216	776	0,68764	30	2	14,53291362	3,751473329
18,71698648	1552	0,686561	30	2	21,03667547	12,39349607
32,05054473	3881	0,685877	30	2	34,35168821	7,17973282
51,6683715	7762	0,685241	30	2	49,7640437	3,685674123
13,23919326	385	0,689598	45	2	10,01429727	24,3587047
14,6425559	776	0,687455	45	2	14,5287423	0,777279634
18,13339126	1552	0,686436	45	2	21,03288166	15,98978568
31,00456756	3881	0,685775	45	2	34,34693661	10,78024729
49,11322714	7762	0,685165	45	2	49,75947026	1,315822954
13,06375744	385	0,6895	60	2	10,01287542	23,35378648
14,30533657	776	0,687364	60	2	14,52683596	1,548368948
17,64511894	1552	0,686343	60	2	21,03004738	19,1833699
30,25099482	3881	0,685667	60	2	34,34133546	13,52134255
47,57034668	7762	0,685083	60	2	49,75372543	4,589789452
13,51800495	385	0,68948	15	2	10,01097634	25,94338906
15,46631566	776	0,687503	15	2	14,5282561	6,065177947
19,34597566	1552	0,686569	15	2	21,03536676	8,732519478
32,87364578	3881	0,685837	15	2	34,34660355	4,480664482
50,77160494	7762	0,685287	15	2	49,76438017	1,983834788
13,51844358	385	0,689516	30	2	10,01239232	25,93531745
15,33868259	776	0,687511	30	2	14,52955565	5,275074521
19,1231207	1552	0,686486	30	2	21,03384069	9,991674604
32,42935099	3881	0,685847	30	2	34,34983813	5,922064673
49,85039695	7762	0,685247	30	2	49,76457062	0,172167801
13,2393861	385	0,689488	45	2	10,01233059	24,37466125
14,69026476	776	0,687433	45	2	14,52818671	1,103302405
18,54620974	1552	0,686424	45	2	21,03245726	13,40569075
31,41444227	3881	0,685774	45	2	34,34688228	9,334687478
48,63560474	7762	0,685195	45	2	49,76220641	2,31641341
13,03571117	385	0,689507	60	2	10,01298694	23,18802708
14,46743819	776	0,687376	60	2	14,52715831	0,41278986
17,96017925	1552	0,686327	60	2	21,02945027	17,08931174
30,77936447	3881	0,685672	60	2	34,34164244	11,57359172
47,70780199	7762	0,685092	60	2	49,75451446	4,290100102

13,56925293	385	0,688036	15	3	10,30010696	24,09230625
15,42981533	776	0,687146	15	3	14,97689608	2,935351075
19,62822214	1552	0,686266	15	3	21,68706634	10,48920371
34,97051812	3881	0,685667	15	3	35,41911782	1,282793957
54,83144556	7762	0,685155	15	3	51,32186465	6,400671875
13,66152582	385	0,689121	30	3	10,32091049	24,45272492
15,59904107	776	0,687402	30	3	14,98493015	3,936850449
20,10670187	1552	0,686478	30	3	21,69695981	7,909093938
35,31406116	3881	0,685788	30	3	35,42949665	0,326882516
55,04568579	7762	0,685185	30	3	51,32853142	6,752853222
13,72491528	385	0,688714	45	3	10,31386617	24,85297024
15,57787015	776	0,687267	45	3	14,98195144	3,825418417
20,05462917	1552	0,686358	45	3	21,69324747	8,170773346
35,08124873	3881	0,685718	45	3	35,42664438	0,984559177
54,8678807	7762	0,685139	45	3	51,32655772	6,454273318
13,64277857	385	0,688572	60	3	10,3115789	24,41731098
15,35038581	776	0,687173	60	3	14,97991338	2,413440512
19,53166502	1552	0,686308	60	3	21,69201168	11,06073985
34,3247611	3881	0,685714	60	3	35,42753575	3,212767154
53,61006596	7762	0,685132	60	3	51,3275232	4,257675723
13,66477297	385	0,689559	15	3	10,32820595	24,41728841
15,35450914	776	0,68758	15	3	14,98855132	2,383389913
19,45123764	1552	0,686671	15	3	21,7028373	11,57561131
33,08805062	3881	0,685895	15	3	35,43359994	7,088810851
51,85765462	7762	0,685321	15	3	51,33717679	1,003666338
13,80159002	385	0,690069	30	3	10,33840027	25,09268675
15,68834806	776	0,687529	30	3	14,98831393	4,462127705
19,7507882	1552	0,686599	30	3	21,70168754	9,877577113
34,33239817	3881	0,685889	30	3	35,43596017	3,214345805
53,81122826	7762	0,685275	30	3	51,33684658	4,598262779
13,75962166	385	0,689145	45	3	10,32181492	24,98474762
15,68385317	776	0,687445	45	3	14,98674257	4,444766121
19,80041908	1552	0,686467	45	3	21,69750784	9,581053585
34,47067545	3881	0,685814	45	3	35,43274361	2,790975651
53,56960299	7762	0,685236	45	3	51,33554466	4,170384327
13,4151798	385	0,688781	60	3	10,31541879	23,10636946
14,94874461	776	0,687261	60	3	14,98226381	0,224227532
18,83430509	1552	0,68635	60	3	21,69362884	15,18146665
33,47647831	3881	0,685754	60	3	35,43006226	5,835691346
52,26322672	7762	0,68516	60	3	51,33009047	1,785454722
13,66588263	385	0,689752	15	3	10,33175916	24,39742508
15,68530167	776	0,687524	15	3	14,98705234	4,45161558
19,96759563	1552	0,68657	15	3	21,69890672	8,670603719
33,7997774	3881	0,685906	15	3	35,43432587	4,835974062
52,56159473	7762	0,685298	15	3	51,33505342	2,333531392
13,94923453	385	0,689528	30	3	10,32842627	25,95703912

15,84159553	776	0,687439	30	3	14,98591707	5,401466392
19,95641614	1552	0,686463	30	3	21,69638356	8,718837137
34,25355699	3881	0,685844	30	3	35,43307171	3,443480999
52,84665984	7762	0,685239	30	3	51,33348899	2,863323539
13,53690109	385	0,688949	45	3	10,31819125	23,77730192
15,36863493	776	0,687387	45	3	14,98517514	2,495080359
18,94654778	1552	0,68638	45	3	21,69412535	14,50173195
32,51419702	3881	0,685744	45	3	35,42826429	8,962445768
50,76994563	7762	0,685161	45	3	51,32862101	1,100405702
13,19504654	385	0,688728	60	3	10,31444464	21,83093398
14,79773128	776	0,687138	60	3	14,97897496	1,224807275
18,37278907	1552	0,686275	60	3	21,69070744	18,05887152
31,95236387	3881	0,6857	60	3	35,4266118	10,87321096
49,90681121	7762	0,685115	60	3	51,32598149	2,843640466
13,57083657	385	0,689432	15	3	10,32586513	23,9113589
15,47570435	776	0,687483	15	3	14,98595746	3,164617781
19,65859053	1552	0,686564	15	3	21,69866823	10,37753799
34,46370993	3881	0,685918	15	3	35,43508355	2,818540489
53,77004529	7762	0,685377	15	3	51,34229776	4,515055757
13,51726885	385	0,689095	30	3	10,3204316	23,65002341
15,23847806	776	0,687355	30	3	14,98366038	1,672199045
19,4228723	1552	0,686441	30	3	21,69553689	11,70097064
33,68863781	3881	0,685824	30	3	35,43177367	5,174254501
52,11925315	7762	0,685269	30	3	51,33625271	1,502324753
13,27225433	385	0,688898	45	3	10,31725908	22,26445621
14,81852486	776	0,687201	45	3	14,98019795	1,091020144
18,89095598	1552	0,686317	45	3	21,6916704	14,82568918
32,64648379	3881	0,68571	45	3	35,42611317	8,51433004
51,6342999	7762	0,685156	45	3	51,32811474	0,592987909
13,06395395	385	0,688537	60	3	10,31092913	21,07344254
14,46381046	776	0,687065	60	3	14,97701018	3,548164017
18,2894406	1552	0,686175	60	3	21,68684193	18,57575311
31,81268442	3881	0,685636	60	3	35,42254777	11,34724535
49,43774338	7762	0,685076	60	3	51,32242616	3,812234628
						ave.error
						9,713315111

APPENDIX B

numerical f	Re	alfa	n	correlated f	%error
0,16191646	385	15	2	0,169264587	4,538220885
0,113542081	776	15	2	0,131066512	15,4343051
0,087974837	1552	15	2	0,101776483	15,68817411
0,072311543	3881	15	2	0,072845098	0,737854616
0,067204832	7762	15	2	0,056566072	15,83034875
0,15199103	385	30	2	0,140611511	7,486967368
0,104951333	776	30	2	0,108879599	3,742940421
0,080581645	1552	30	2	0,08454778	4,921883816
0,065343496	3881	30	2	0,060513894	7,391098794
0,059128741	7762	30	2	0,046990579	20,52836145
0,144022898	385	45	2	0,126155136	12,40619484
0,095622994	776	45	2	0,097685606	2,157025072
0,070471253	1552	45	2	0,075855359	7,640145661
0,055926935	3881	45	2	0,054292415	2,922598234
0,045795798	7762	45	2	0,042159442	7,940370164
0,131936357	385	60	2	0,116808823	11,46578115
0,082769733	776	60	2	0,090448482	9,277243289
0,057798429	1552	60	2	0,070235549	21,5180941
0,04284751	3881	60	2	0,050270114	17,32330417
0,036347574	7762	60	2	0,039036023	7,396502882
0,16081722	385	15	2	0,169264587	5,252775332
0,115869105	776	15	2	0,131066512	13,11601359
0,088996689	1552	15	2	0,101776483	14,35985278
0,074247378	3881	15	2	0,072845098	1,88866012
0,063447699	7762	15	2	0,056566072	10,84614044
0,147635431	385	30	2	0,140611511	4,757611333
0,103162052	776	30	2	0,108879599	5,54229686
0,080142057	1552	30	2	0,08454778	5,49739211
0,065630048	3881	30	2	0,060513894	7,795445051
0,054449321	7762	30	2	0,046990579	13,69850312
0,132672864	385	45	2	0,126155136	4,912630655
0,087282514	776	45	2	0,097685606	11,91887269
0,066496954	1552	45	2	0,075855359	14,07343564
0,053036666	3881	45	2	0,054292415	2,367699305
0,043422335	7762	45	2	0,042159442	2,90839377
0,116317048	385	60	2	0,116808823	0,42278787
0,073578594	776	60	2	0,090448482	22,92771169

0,051537765	1552	60	2	0,070235549	36,27977269
0,039981318	3881	60	2	0,050270114	25,73401071
0,034414007	7762	60	2	0,039036023	13,43062497
0,170740175	385	15	2	0,169264587	0,864230129
0,118720033	776	15	2	0,131066512	10,39965936
0,092115295	1552	15	2	0,101776483	10,48814709
0,077599148	3881	15	2	0,072845098	6,126420999
0,072655773	7762	15	2	0,056566072	22,14510945
0,163598792	385	30	2	0,140611511	14,0510089
0,112670524	776	30	2	0,108879599	3,364610823
0,085103555	1552	30	2	0,08454778	0,653057538
0,066862714	3881	30	2	0,060513894	9,495307455
0,057337163	7762	30	2	0,046990579	18,04516175
0,147701619	385	45	2	0,126155136	14,58784478
0,097095879	776	45	2	0,097685606	0,607365838
0,070567507	1552	45	2	0,075855359	7,49332551
0,055529565	3881	45	2	0,054292415	2,22791258
0,047432633	7762	45	2	0,042159442	11,11722132
0,131232892	385	60	2	0,116808823	10,9911999
0,081923573	776	60	2	0,090448482	10,40592935
0,056649398	1552	60	2	0,070235549	23,98286836
0,043016076	3881	60	2	0,050270114	16,86355184
0,034778857	7762	60	2	0,039036023	12,24067231
0,179407936	385	15	2	0,169264587	5,653790785
0,12191778	776	15	2	0,131066512	7,504017877
0,095962843	1552	15	2	0,101776483	6,058219352
0,076704912	3881	15	2	0,072845098	5,032029968
0,070684779	7762	15	2	0,056566072	19,97418172
0,158349157	385	30	2	0,140611511	11,20160415
0,105660289	776	30	2	0,108879599	3,046849687
0,085210385	1552	30	2	0,08454778	0,777610374
0,069777743	3881	30	2	0,060513894	13,27622322
0,059959317	7762	30	2	0,046990579	21,62922963
0,142016901	385	45	2	0,126155136	11,16892754
0,093946343	776	45	2	0,097685606	3,980210774
0,068971383	1552	45	2	0,075855359	9,980916387
0,053108111	3881	45	2	0,054292415	2,229987489
0,046935485	7762	45	2	0,042159442	10,17576114
0,123737778	385	60	2	0,116808823	5,599708408
0,078202965	776	60	2	0,090448482	15,65863599
0,055612783	1552	60	2	0,070235549	26,29389375
0,042039338	3881	60	2	0,050270114	19,57874873
0,034887653	7762	60	2	0,039036023	11,89065563
0,180315464	385	15	3	0,199581656	10,68471431
0,128629563	776	15	3	0,154541904	20,14493419
0,101316241	1552	15	3	0,120005722	18,44667918

0,08614791	3881	15	3	0,085892421	0,296569318
0,076879308	7762	15	3	0,066697652	13,24368936
0,178022889	385	30	3	0,165796513	6,867867324
0,126532365	776	30	3	0,128381082	1,461061904
0,100665082	1552	30	3	0,099691178	0,9674698
0,085964173	3881	30	3	0,07135257	16,99731776
0,07547046	7762	30	3	0,055407086	26,58440607
0,165459016	385	45	3	0,14875085	10,0980694
0,113184786	776	45	3	0,115182126	1,764671749
0,085938713	1552	45	3	0,089441853	4,076323924
0,068807258	3881	45	3	0,064016758	6,962201379
0,058503904	7762	45	3	0,049710642	15,03021415
0,146467119	385	60	3	0,137730513	5,964892422
0,094259888	776	60	3	0,106648758	13,1433111
0,066225963	1552	60	3	0,082815475	25,04986166
0,050530499	3881	60	3	0,059274021	17,30345503
0,042222541	7762	60	3	0,046027786	9,012355142
0,196309226	385	15	3	0,199581656	1,666977566
0,144358637	776	15	3	0,154541904	7,054144736
0,112792577	1552	15	3	0,120005722	6,395053109
0,094700136	3881	15	3	0,085892421	9,300635478
0,08250502	7762	15	3	0,066697652	19,15928045
0,181944659	385	30	3	0,165796513	8,875306324
0,125900109	776	30	3	0,128381082	1,970587876
0,099740708	1552	30	3	0,099691178	0,049658685
0,081188232	3881	30	3	0,07135257	12,11464011
0,071979206	7762	30	3	0,055407086	23,02348224
0,150707474	385	45	3	0,14875085	1,298292794
0,102374821	776	45	3	0,115182126	12,51021066
0,080741432	1552	45	3	0,089441853	10,77565867
0,066161833	3881	45	3	0,064016758	3,242162951
0,056688861	7762	45	3	0,049710642	12,30968198
0,127275022	385	60	3	0,137730513	8,214879996
0,082043689	776	60	3	0,106648758	29,99020283
0,063775142	1552	60	3	0,082815475	29,85541556
0,049528796	3881	60	3	0,059274021	19,67587565
0,041131293	7762	60	3	0,046027786	11,90454536
0,184988858	385	15	3	0,199581656	7,888474053
0,132065765	776	15	3	0,154541904	17,01889932
0,105255775	1552	15	3	0,120005722	14,01343262
0,089241642	3881	15	3	0,085892421	3,752979344
0,080933635	7762	15	3	0,066697652	17,58970021
0,177422473	385	30	3	0,165796513	6,552698179
0,125501547	776	30	3	0,128381082	2,294421798
0,09946834	1552	30	3	0,099691178	0,224028693
0,08167971	3881	30	3	0,07135257	12,64345848

0,068383716	7762	30	3	0,055407086	18,97619838
0,158259514	385	45	3	0,14875085	6,00827334
0,107267998	776	45	3	0,115182126	7,377902903
0,080238528	1552	45	3	0,089441853	11,46995812
0,06386515	3881	45	3	0,064016758	0,237387803
0,055260372	7762	45	3	0,049710642	10,04287348
0,140002585	385	60	3	0,137730513	1,622878514
0,088535244	776	60	3	0,106648758	20,4590996
0,062903513	1552	60	3	0,082815475	31,65476881
0,048283204	3881	60	3	0,059274021	22,76323113
0,040303402	7762	60	3	0,046027786	14,2032283
0,222954828	385	15	3	0,199581656	10,48336662
0,160570594	776	15	3	0,154541904	3,7545417
0,123371057	1552	15	3	0,120005722	2,727815579
0,100242425	3881	15	3	0,085892421	14,31529954
0,088171317	7762	15	3	0,066697652	24,35447923
0,19830694	385	30	3	0,165796513	16,39399326
0,141188863	776	30	3	0,128381082	9,071381981
0,110024398	1552	30	3	0,099691178	9,391753623
0,089904099	3881	30	3	0,07135257	20,63479798
0,077850631	7762	30	3	0,055407086	28,82898179
0,158277875	385	45	3	0,14875085	6,019176675
0,115947768	776	45	3	0,115182126	0,6603335
0,086667547	1552	45	3	0,089441853	3,20109034
0,068693968	3881	45	3	0,064016758	6,808762849
0,060299506	7762	45	3	0,049710642	17,56044838
0,13948417	385	60	3	0,137730513	1,257244293
0,091637402	776	60	3	0,106648758	16,38125485
0,066847435	1552	60	3	0,082815475	23,88728919
0,052781485	3881	60	3	0,059274021	12,30078304
0,04427719	7762	60	3	0,046027786	3,953720025
					average error
					10,89504387

CURRICULUM VITAE

Name Surname **:Seyfi Girgin**

Place and Date of Birth **: Milas/MUĞLA 07.07.1990**

E-Mail **: seyfigirgin7@gmail.com**

EDUCATION

- **B.Sc.** **:** 2013, İzmir Institute of Technology, Engineering Faculty, Department of Mechanical Engineering

PROFESSIONAL EXPERIENCE AND REWARDS:

- 2016- Turkish Aerospace Industries
- 2015 the Von Karman Institute for Fluid Dynamics
- 2014 Robert Bosch Diesel Systems

PUBLICATIONS, PRESENTATIONS AND PATENTS ON THE THESIS:

- **Girgin S.** 2017: An Investigation of Heat Transfer Performance of Rectangular Plate – fin Heat Exchanger by Using Common Flow Up & Common Flow Down Confgurations with Different Wings Attack Angle, International Conference on Fluid Dynamics and Aerodynamics – October 19-20, 2007 Rome, Italy.

Girgin S. 2017: An Investigation of Heat Transfer Performance of Rectangular Plate – fin Heat Exchanger by Using Common Flow Up & Common Flow Down Confgurations with Different Wings Attack Angle, Journal of Applied Mechanical Engineering, Volume 6 Issue 5, 2168-9873